Exotic phases of interacting Majorana fermions and parafermions

Edward O'Brien

Magdalen College

University of Oxford

A thesis submitted for the degree of

Doctor of Philosophy

Hilary 2020

Acknowledgements

First and foremost I would like to thank my supervisor, Paul Fendley, for all his help and support during my DPhil. His enthusiasm and constant stream of new and exciting ideas has kept me motivated and committed to the subject throughout. I have learned a huge amount from him both in terms of physics itself, and in how to approach problems as a scientist.

I am also very grateful to my other collaborators, in particular Eric Vernier. His love of the subject and commitment to it, along with his sense of humour, made him a great person to work with and led to some very fruitful results. I have had many useful conversations with people in the Rudolf Peierls Centre leading to new insights, but I would like to thank Sid Parameswaran in particular, especially for his very illuminating comments regarding SPTs.

I am very thankful for the other graduate students I have had the privilege to get to know over the last few years. In particular, Emma, Henrik, Tunrayo and Yuri have kept me sane in the department, while Aaron, Alex, Alice, Josh, Leonie, Lucy, Scarlett and many others have always made Magdalen a really enjoyable place to live.

I would like to thank my parents, sister and grandfather for always being there and supporting me, through both my DPhil and everything else.

Finally, I would like to thank the EPSRC for funding me, without which I would not have had the opportunity to do this at all.

Abstract

In this thesis exotic phases of models preserving the symmetries of the one-dimensional quantum Ising and three-state Potts chains are considered, the natural habitats of Majorana fermions and parafermions, respectively. Along with numerical techniques, conformal field theory (CFT) is used to study the resulting physics.

Chapter 1 gives an introduction to the field and explains the basics of the numerical techniques to be used throughout the thesis. CFT is briefly introduced in Chapter 2 before the key results necessary for the thesis are given.

In Chapter 3, self-dual interactions are added to the critical Ising model, giving a range of different phases. A tricritical Ising point separates the Ising phase from an order-disorder coexistence phase on the chirally symmetric line, while a supersymmetric line provides the transition to an incommensurate phase in the general model. The model is solved exactly on a free-fermionic line giving insight into the points where only numerical analysis can be performed. This is supplemented by Appendix A, where the qualitative difference between similar perturbations is considered.

Chapters 4 and 5 consider models with the symmetries of the three-state Potts model. Various phases are found including an order-disorder coexistence phase, a second critical Potts phase, a "not-A" phase, and a representation symmetry protected topological phase. The effect of lattice momentum on the stability of phases and the connection with conformal field theory operators is studied. Lattice realizations of several CFTs are found, such as the tricritical Potts CFT and a CFT expressible in two different forms, either in terms of a boson and fermion, or Potts and tricritical Ising CFTs.

Contents

List of Abbreviations

ADP . . . . . Anti-disordered Potts.

AFP . . . . . Antiferromagnetic Potts.

AKLT . . . . . Affleck–Kennedy–Lieb–Tasaki.

APBC . . . . . Antiperiodic Boundary Conditions.

CFT . . . . . Conformal Field Theory.

DMRG . . . . Density Matrix Renormalization Group.

ED . . . . . Exact Diagonalization.

GS . . . . . Ground State.

h.c. . . . . . Hermitian Conjugate.

MERA . . . . Multiscale Entanglement Renormalization Ansatz.

MPS . . . . . Matrix Product State.

NS . . . . . Neveu–Schwarz.

OBC . . . . . Open Boundary Conditions.

PBC . . . . . Periodic Boundary Conditions.

PS . . . . . Product State.

RG . . . . . Renormalization Group.

SCFT . . . . . Superconformal Field Theory.

SVD . . . . . Singular Value Decomposition.

TCI . . . . . Tricritical Ising.

TCP . . . . . Tricritical Potts.

1 Introduction

Contents

1.1 Introduction

Since the advent of statistical mechanics, symmetries have been critical to the solution of problems in the field. When working out an effective model for a physical system, the first step is often to determine the underlying symmetries (both exact and approximate) to give a list of the possible interactions to be considered. Early developments in the field then considered only the shortest-range interactions consistent with the symmetries of the system to get a rough qualitative understanding of the physics of the system, such as the Ising and Heisenberg models [1–3].

These models are then typically split into *phases*, in which they behave qualitatively similarly, regardless of small changes in the coupling strengths or temperature. Most of even the simplest models have very different phases of matter depending

on the coupling strengths and temperature. To distinguish between phases, an *order parameter* is typically introduced, with qualitatively different values in the different phases. As an example, consider the classical Ising model in two spatial dimensions, taken to be the (x, y) plane. In this model there is a spin degree of freedom at each lattice site which can point in either the $+z$ or $-z$ direction, with a ferromagnetic interaction favouring spins on neighbouring sites aligning. The Ising model has an ordered phase at low temperature where energy considerations dominate and spins tend to align, even over long-distance scales, and a disordered phase at high temperature where entropy dominates and spins far away from each other are uncorrelated. The order parameter in this case is the magnetisation (the average value of the spin in the z-direction), with non-zero magnetisation in the ordered phase and vanishing magnetisation in the disordered phase.

An interesting question is then how and at what values of the couplings and temperature we transition from one phase to another. Most transitions can be split into two classes: first-order and second-order. First-order transitions have a latent heat and lead to phase coexistence as heat is added to a system at constant temperature, such as when ice melts to water. In these transitions correlation lengths remain finite, meaning that particles far apart in the system remain uncorrelated.

Second-order transitions are continuous phase transitions in which the correlation length diverges to infinity, meaning that correlators between particles obey a power-law, rather than exponential, decay with separation distance. An example of this occurs in the two-dimensional Ising model as it is tuned through its *critical temperature*. On one side of the second-order transition a symmetry is spontaneously broken, while on the other it is preserved.[1]

While the exact nature and location in parameter space of phase transitions are very important pieces of information in the study of physical systems, their determination is by no means trivial. In finding the location of the transition, *duality* has proved a key concept [7]. Duality corresponds to reparameterising

[1] Some transitions are also infinite-order, which are continuous but break no symmetries. The Berezinskii–Kosterlitz–Thouless transition in the two-dimensional XY and one-dimensional quantum XXZ models is the classic example of this [4–6].

variables to allow couplings to be exchanged in models. For example, in classical systems it often allows a mapping between the high- and low-temperature phases [7]. If such a duality exists, we know the transition must occur exactly at the point invariant under the duality transformation, known as the *self-dual* point, or we would necessarily have two transitions.

Duality may often help in determining the position of the transition, but it does not tell us what type of transition we have. One might naïvely imagine that the exact phase transitions would be completely different in different systems. Fortunately, nature is kinder than this and second-order transitions can be split into *universality classes* which have the same long-distance properties. The Landau theory of phase transitions [8] goes some of the way to explaining universality by writing the free energy of the system as a Taylor expansion of the order parameter involving only terms consistent with the symmetries of the model. Thus models with different order parameters can still have qualitatively similar expressions for their free energies if their underlying symmetries are the same.

Universality really became a key concept with the introduction of the Renormalization Group (RG) by Wilson in the 1970s [9–11]. In the RG formulation, perturbations away from a critical point are classified as *relevant*, *marginal* or *irrelevant*, and the long-distance behaviour of the model depends only on the relevant (and, possibly, the marginal) operators. Shorter-range interactions tend to be more relevant, and so many models can reduce to the same long-distance field theory. As we are typically concerned with physical systems with large numbers of particles and want to understand the mesoscopic and macroscopic phenomena, considering this long-distance behaviour is justified.

In the 1980s a further crucial development was made: the discovery of conformal field theory (CFT) [12]. Along with the normal Lorentz invariance of translations, boosts and rotations, CFTs also have *scale invariance*. This is a key feature of second-order transitions as, when the correlation length diverges, the system loses its sense of scale. Many second-order phase transitions are then described by CFTs. CFT is particularly powerful in two-dimensional classical systems (or

1+1-dimensional quantum systems) and this allows many continuum properties of models undergoing second-order transitions to be understood.

While CFT tells us a lot about the long-distance behaviour of lattice models, identifying the field theory in the first place is by no means a trivial task. Simple models such as the critical Ising and three-state Potts model may have been classified [12–16], but the behaviour as we perturb away is not necessarily fully understood. If there is a relevant operator obeying the symmetries of the model and perturbation, we know we will instantly transition to a different phase, but the CFT description will be stable for at least an infinitesimal perturbation if there are only irrelevant operators, giving extended critical phases. What these phases eventually transition to is then not a simple question and will be the focus of much of this thesis.

Landau theory has proved to be very useful in the classification of phases of matter, but it is by no means the end of the story. Topological order is also possible, where systems with the same symmetries can behave qualitatively differently [6]. There are two types of topological order with slightly different properties: *intrinsic topological order* and *symmetry protected topological order*. In systems with intrinsic topological order the ground-state degeneracy depends on the topology of the manifold on which it lives and this degeneracy is robust to any local perturbations [17], with one of the first examples of this being the fractional quantum Hall effect, discovered in 1982 [18, 19].

Intrinsic topological order is known not to exist in one dimension [20] and so, we will not consider it further in this thesis, but symmetry protected topological (SPT) order can. Here the topological phase is stable to any local perturbations obeying the symmetry protecting the phase and extra quantum numbers, such as the ground-state degeneracies with open boundary conditions or long-range "string" order parameters, are added to distinguish between the phases [17, 21]. The classic example of an SPT phase is the Haldane phase of the spin-1 antiferromagnetic Heisenberg model [22, 23], which is stable as long as a D_2, time-reversal, or spatial inversion symmetry is preserved.

A very important potential use of topological phases has emerged in the past 20 years in the field of quantum computation [24–27]. The potentially revolutionary importance of quantum computers was realised on the discovery of Shor's factoring algorithm (with serious implications for cyber security) and Grover's search algorithm [28–31]. A major issue with quantum computation is building stable memories and performing fault-tolerant computation. Unlike in classical systems where bits can be copied at will to help protect against errors, the no-cloning theorem prevents this for quantum bits (qubits) [32, 33]. This means that qubits have to be stable to perturbations to ensure accurate computation. As topological degrees of freedom cannot be changed by local perturbations, they offer the desired stability.

This then leads us full circle back to our example of the Ising model. As well as a description in terms of spin variables, the Ising model can be expressed as a model of *Majorana fermions* [34], in which language the ordered phase is topological [35]. Majorana modes appear in topological superconductors [35, 36] and Kitaev materials [37, 38] and there is hope that these may provide a means of building a quantum computer. In particular, the Kitaev material α-$RuCl_3$ [39, 40] has been touted as a promising candidate, with recent theoretical developments shedding further light on how it could be used [41].

Majorana fermions may be well known to most theoretical physicists, but their cousins, *parafermions* [42], are far less studied. As the Potts model is a generalisation of the Ising model to a case with more than two states per site [13, 43], so are parafermions a generalisation of Majoranas. This increased complexity makes them more difficult to construct in real materials, but also leads to increased versatility in what they could theoretically be used for [44–47].

The duality mentioned earlier in the Ising model becomes far more natural in terms of Majoranas, as is the Potts duality in terms of parafermions. Instead of corresponding to a mapping between couplings in the spin language, it becomes translation invariance in Majoranas/parafermions [48]. As Majoranas and

parafermions are currently a hot topic, this makes the self-dual Ising and Potts models natural objects to study, as well as their duality preserving perturbations.

Throughout most of this thesis we will be considering such self-dual interactions and discovering the various exotic phases. We start from the self-dual Ising or three-state Potts models and add in the shortest-range interactions consistent with their symmetries. By varying the relative strengths of the couplings, we find the different phases encountered by the spins (or, equivalently, the Majoranas and parafermions), discovering a wide-range of different physics, from order-disorder coexistence and "not-A" phases, to supersymmetry and incommensurability.

The rest of this chapter is split into two sections. Section 1.2 gives an introduction to the Ising Model. This will provide quantitative detail on the model, its phases, and the connection with Majorana fermions, setting up the rest of the thesis. Section 1.3 provides a brief rundown of the numerical techniques we will use in the subsequent chapters. As most models we discuss will not be analytically solvable except at very special points, these techniques will prove vital in our understanding of the physics.

Chapter 2 briefly introduces CFT and quickly moves on to explaining the main results we will need for our analysis. In Chapter 3 we consider the self-dual Ising model in the presence of other duality-preserving interactions. Appendix A explains a baffling result from Chapter 3, recently solved in Ref. [41].

Chapters 4 and 5 consider the self-dual three-state Potts model, and the shortest-range interactions with the same symmetries. In Chapter 4 we stick to the self-dual line, finding a host of phases with completely different physics. We then go off the self-dual line in Chapter 5, finding novel gapped phases in the first half, and explaining some of the mysteries of Chapter 4 in the second.

This thesis is based primarily on the publications [49, 50] (Chapters 3 and 5), along with the preprint [51] (Chapter 4). Refs. [52, 53] were also completed during this degree but will only be mentioned fleetingly.

1.2 The Ising Model

One of the oldest and most studied models in condensed matter physics is the Ising model [1, 2]. Its classical version involves a spin-$\frac{1}{2}$ at each site of a lattice with a nearest-neighbour interaction either favouring or disfavouring alignment:

$$E_{\{\sigma_j\}} = -J \sum_{\langle j,k \rangle} \delta_{\sigma_j,\sigma_k}, \tag{1.1}$$

where j and k label sites on the lattice, $\langle j,k \rangle$ indicates the sum is over nearest-neighbours only, and $\sigma_j = \pm 1$ gives the spin at site j.

The model is the simplest in which there are two possible states per site with an overall $\mathbb{Z}_2$ symmetry between the spin-up ($\sigma_j = 1$) and spin-down ($\sigma_j = -1$) directions. Even so, while the one-dimensional model is trivial using the transfer matrix method (see, for example, Ref. [54]), the two-dimensional version on the square lattice was not solved until 1944 in a groundbreaking paper by Onsager [55]. A full solution in three dimensions continues to elude all those who attempt to find it and remains one of the outstanding problems in statistical mechanics, although nearly exact results have been obtained using conformal bootstrap techniques [56].

In this thesis we will be concerned with the quantum Ising chain and perturbations around it. As the one-dimensional quantum Ising model is a limit of the two-dimensional classical model, it can be solved exactly, most easily using free fermions [55, 57, 58]. The model itself is given by

$$H_{\text{Ising}} = -\sum_j \left(J\sigma_j^z \sigma_{j+1}^z + f\sigma_j^x \right), \tag{1.2}$$

where σ_j^x and σ_j^z are the Pauli spin matrices acting on site j with identity operators acting everywhere else. Adding in the third Pauli matrix, σ^y, they satisfy the algebra

$$\left[\sigma^i, \sigma^j\right] = 2i\epsilon_{ijk}\sigma^k, \quad \left\{\sigma^i, \sigma^j\right\} = 2\delta_{i,j}. \tag{1.3}$$

The first term in H_{Ising} (1.2) favours aligning spins in the z-direction for $J > 0$ and anti-aligning them for $J < 0$, while the second term flips spins in the z-basis.

This model has a global $\mathbb{Z}_2$ symmetry given by the operator

$$\mathcal{F} = \prod_j \sigma_j^x, \tag{1.4}$$

which flips all spins in the z-basis. This $\mathbb{Z}_2$ is the crucial symmetry of the Ising model and physically corresponds to the absence of an external longitudinal field – spins are equally happy to point up or down as long as they are aligned with their neighbours. When we later perturb this model, we will ensure that this symmetry is preserved.

As we have said, the Ising model can be solved exactly for any couplings J and f, but the solution becomes particularly simple for $f = 0$ or $J = 0$. If $f = 0$, Equation 1.2 reduces to the completely ordered Ising Hamiltonian

$$H_{\text{order}} = -J \sum_j \sigma_j^z \sigma_{j+1}^z \tag{1.5}$$

and the eigenstates are the states with all spins having well defined spin in the z-direction. For $J > 0$ there are then two degenerate ground states consisting of all spins up and all spins down in the z-direction:

$$|\Psi_\uparrow\rangle = |\uparrow\uparrow\cdots\uparrow\cdots\rangle\,, \qquad |\Psi_\downarrow\rangle = |\downarrow\downarrow\cdots\downarrow\cdots\rangle\,, \tag{1.6}$$

where $\sigma_j^z |\uparrow\rangle_j = |\uparrow\rangle_j$ and $\sigma_j^z |\downarrow\rangle_j = -|\downarrow\rangle_j$. These are the completely ordered states in the z-basis. For periodic boundary conditions, where j takes the values 1 to L and we identify spins 1 and $L+1$, there is a finite gap of size $4J$ to the first excited states with two domain walls between up and down spins.

Taking $J = 0$ (and $f > 0$) instead, Equation 1.2 becomes the completely disordered Ising Hamiltonian

$$H_{\text{disorder}} = -f \sum_j \sigma_j^x. \tag{1.7}$$

This time there is a unique ground state given by

$$|\Psi_\updownarrow\rangle = |\updownarrow\updownarrow\cdots\updownarrow\cdots\rangle\,, \tag{1.8}$$

where $|\updownarrow\rangle = (|\uparrow\rangle + |\downarrow\rangle)/\sqrt{2}$ is the eigenstate of σ^x with eigenvalue 1. This state is completely disordered in the z-basis as all basis states have equal amplitude.

Just as for the completely ordered case, there is a finite gap to the first excited states, this time of size $2f$.

There are clear differences between the ground states of the completely ordered and disordered Ising Hamiltonians (1.5) and (1.7). Firstly, H_{order} (1.5) has two degenerate ground states, while H_{disorder} (1.7) has a single ground state. Secondly, if we know the spin in the z-direction at one site j, we immediately know the spin at any other site k in H_{order}, but in H_{disorder} we have no idea! This difference in long-range ordering between spins indicates that these two points are in distinct phases and that there must be a transition between the two at some point. The difference between these phases is expressed by the order parameter

$$C_\infty = \lim_{|k-j|\to\infty} C_{j,k}, \tag{1.9}$$

where

$$C_{j,k} = \left\langle \sigma_j^z \sigma_k^z \right\rangle . \tag{1.10}$$

In both the ordered and disordered Ising phases (surrounding the Hamiltonians 1.5 and 1.7, respectively), $C_{j,k}$ decays to a constant exponentially in $|k-j|$:

$$C_{j,k} \sim C_\infty + Ae^{-\frac{|k-j|}{\xi}} \tag{1.11}$$

for $|k-j| \gg \xi$, where ξ is the correlation length and A is a constant. The difference is that in the ordered Ising phase $C_\infty > 0$, whereas in the disordered Ising phase $C_\infty = 0$. ξ determines how quickly the correlator decays to its infinite limit and diverges as the transition point between the phases is approached.[2] To find this transition, we first introduce a concept which will prove essential throughout this thesis: *duality* [7]. Duality is generally a mapping between operators and is very useful in showing connections between different phases and the transitions between them. In the Ising case we define the following duality mapping:

$$\sigma_j^x \to \sigma_j^z \sigma_{j+1}^z, \qquad \sigma_j^z \sigma_{j+1}^z \to \sigma_{j+1}^x. \tag{1.12}$$

[2] Alternatively, we could consider the magnetisation order parameter $M_j = \langle \sigma_j^z \rangle$. This vanishes in the disordered phase, while in the ordered phase it is non-zero for a $\mathbb{Z}_2$ symmetry-breaking ground state. To ensure we have such a ground state, we can add an infinitesimal $\mathbb{Z}_2$ breaking field, $-\epsilon\sigma_k^z$, at a site k with $|k-j| \gg 1$ to select a preferred direction.

Substituting these into Equation 1.2, we find

$$H_{\text{Ising}} = -\sum_j \left(J\sigma_j^z\sigma_{j+1}^z + f\sigma_j^x\right) \to -\sum_j \left(f\sigma_j^z\sigma_{j+1}^z + J\sigma_{j+1}^x\right). \tag{1.13}$$

With periodic boundary conditions, the two models are the same except with $J \leftrightarrow f$. As the algebra is unchanged on switching $\sigma_j^z\sigma_{j+1}^z \leftrightarrow \sigma_j^x$, we have a mapping between the ordered and disordered phases! This immediately tells us that, if there is a single transition point between the ordered and disordered phases, it must occur at $J = f$ where duality maps the model onto itself: the *self-dual* point.

Duality is, in fact, made clearer by introducing *Majorana fermions*. Defining

$$\gamma_{2j-1} = \left(\prod_{k<j}\sigma_k^x\right)\sigma_j^z, \quad \gamma_{2j} = i\left(\prod_{k<j}\sigma_k^x\right)\sigma_j^z\sigma_j^x, \tag{1.14}$$

we see that

$$\sigma_j^x = -i\gamma_{2j-1}\gamma_{2j}, \quad \sigma_j^z\sigma_{j+1}^z = -i\gamma_{2j}\gamma_{2j+1}, \tag{1.15}$$

where we have ignored subtleties with boundary conditions. The Majorana fermions then obey the anticommutation relations

$$\{\gamma_a, \gamma_b\} = 2\delta_{a,b} \tag{1.16}$$

and Equation 1.2 can be rewritten as

$$H_{\text{Ising}} = i\sum_j \left(f\gamma_{2j-1}\gamma_{2j} + J\gamma_{2j}\gamma_{2j+1}\right). \tag{1.17}$$

It is then clear that self-duality at $J = f$ just corresponds to translation invariance in Majoranas (again, up to subtleties [48]). This connection between the Ising model and Majorana fermions will prove key both in helping our understanding of the physics and explaining its application to real world situations.

As the self-dual point is approached from either the side, the correlation length, ξ, diverges. Exactly at the self-dual point the correlation length becomes infinite and correlators decay algebraically rather than exponentially to 0. For example,

$$C_{j,k}^{J=f} \sim |k-j|^{-\frac{1}{4}} \tag{1.18}$$

for $|k-j| \gg 1$. The divergence of ξ removes a length scale from the model and allows the continuum limit of the model to be described by a Conformal Field Theory (CFT). The continuum CFT description explains the $-1/4$ power in Equation 1.18 and will be explained in Chapter 2.

1.3 Numerical Methods

Throughout this thesis we will depend heavily on numerical analysis. Numerics allow us not only to test our analytical predictions but also to find novel physics we would not even dream of being present. We will use two main techniques: Exact Diagonalization (ED) and the Density Matrix Renormalization Group (DMRG) [59–61].

1.3.1 Exact Diagonalization

Exact Diagonalization (ED) is one of the simplest and most brute force numerical methods. As the name suggests, it attempts to diagonalize the Hamiltonian directly and return the lowest n eigenvalues (and eigenvectors if required). The biggest issue with ED is the absolutely appalling scaling of the algorithms with the lattice size L. For a q-state per site system of length L, the Hamiltonian is of size $q^L \times q^L$. Even the most efficient algorithms for finding only the largest eigenvalue still scale with the size of the Hamiltonian and hence as q^L, giving them exponential complexity. We can slightly cut down on the size of our matrix by imposing symmetries, but this only buys us a few more sites at best. For example, using translation invariance for a periodic lattice cuts down the size of the matrix by a factor of roughly L, while if there is a $\mathbb{Z}_q$ symmetry this reduces it by a factor of q. Overall, the size of the matrix then scales as q^{L-1}/L, which is still exponential in L. On top of this, the matrix is now denser as we have removed a lot of zeros, so the speed up is not as significant as expected.

Despite the problems with scaling, ED does have some definite advantages. Symmetries are fairly simple to implement, whereas this is not always the case for DMRG, especially for momentum eigenstates. There is also not much cost

in calculating the lowest n eigenvalues rather than just the ground state – this will typically increase the computation time by a factor of n but not decrease the accuracy noticeably. These two factors make it particularly useful for calculating multiple excited states in different symmetry sectors. All ED used in this thesis was performed using MATLAB with either the *eig* or *eigs* functionality.

1.3.2 The Density Matrix Renormalization Group

In contrast to ED, the Density Matrix Renormalization Group (DMRG) is designed for use at large lattice lengths, L. Over the last 30 years, DMRG has emerged as the standout method for finding ground-state energies in one-dimensional quantum lattice systems. For a full introduction to the modern method, we refer the reader to Schollwöck's excellent review [61], while in the following we briefly explain the idea of the algorithm and its limitations.

DMRG is particularly strong at finding ground states for gapped systems with non-degenerate ground states. In these cases there is a finite correlation length, ξ, in the ground-state wavefunction and the entanglement entropy can be shown to obey an area law [62]. This essentially means that a site j does not really talk to sites k with $|k-j| \gg \xi$ and so the entanglement between these states is very low. DMRG abuses this by allowing each site only a finite amount of entanglement with the rest of the chain through the use of Matrix Product States.

A Matrix Product State (MPS) is a product of tensors designed to give an efficient but approximate estimate of a low-entanglement state. The state can be written as

$$|\Psi_{\mathrm{MPS}}\rangle = \sum_{\{\sigma\}} \sum_{\{\alpha\}} B^{\alpha_1}_{1,\sigma_1} A^{\alpha_1,\alpha_2}_{2,\sigma_2} ... A^{\alpha_{n-1},\alpha_n}_{n,\sigma_n} ... A^{\alpha_{L-2},\alpha_{L-1}}_{L-1,\sigma_{L-1}} B^{\alpha_{L-1}}_{L,\sigma_L} |\sigma_1 \sigma_2 ... \sigma_L\rangle \,, \qquad (1.19)$$

where the σ_i represent the "physical" indices and correspond to the states at each site and the α_j give the auxiliary indices to be summed over. The number of values α_j can take gives the *bond dimension* χ_j, where A_{j,σ_j} is a $\chi_{j-1} \times \chi_j$ matrix, and B_{1,σ_1} and B_{L,σ_L} are row and column vectors, respectively. For a q-state system per site, any state can be represented exactly by taking $\chi_1 = \chi_{L-1} = q$, $\chi_2 = \chi_{L-2} = q^2$, ..., $\chi_{L/2-1} = \chi_{L/2+1} = q^{L/2-1}$, $\chi_{L/2} = q^{L/2}$ (taking L even), but then the largest

tensors (at sites $L/2$ and $L/2+1$) have $q \times q^{L/2-1} \times q^{L/2} = q^L$ entries and we have to store just as much (and in fact slightly more) information than the actual state we are representing contains! The strength of the MPS formulation is that it allows us to get a good approximation of gapped states by fixing the maximum bond dimension to some χ, meaning that our largest tensor has $q\chi^2$ entries, regardless of L. To do this we use a singular value decomposition (SVD) to keep only the terms with the largest coefficients [61].

The DMRG algorithm then proceeds as follows. We consider one tensor at a time, treating the rest of the MPS as the environment, and minimise the energy by varying this tensor. We then multiply this by the adjacent tensor and perform an SVD to reduce the bond dimension back to a maximum of χ, before moving on to the next tensor in the chain and repeating the process. Sweeping up and down the chain we reduce the energy until it eventually converges. While it could converge to a local minimum in the Hilbert space rather than the global minimum, if χ is large enough, this is unlikely to happen and the agreement between DMRG and exact methods, such as ED, and other approximate methods, such as Monte Carlo, is typically very good.

Due to the finite entanglement for gapped systems, DMRG is very well suited to finding approximations to the ground-state energy and wavefunction. The computational complexity scales only with L and not exponentially in L as it did for ED, meaning that very large systems can be probed. Issues start to occur when the gap becomes very small and for gapless systems. For a CFT, for example, the entropy scales as $\log L$ and so the required bond dimension becomes linear in L, increasing the complexity. Despite this issue, it is still found that DMRG often provides the best estimates, even for gapless systems, although methods such as the Multiscale Entanglement Renormalization Ansatz (MERA) [63] have been developed specifically to address this problem.

A further issue with DMRG is its inability to split the Hamiltonian into momentum sectors. While it can deal with local symmetries such as $\mathbb{Z}_q$ or $U(1)$ invariance, it cannot make the most of translation invariance. Again, other methods

such as those based on periodic uniform Matrix Product States [64] are being developed to address this issue, but the publicly available codes are not yet sophisticated enough to compete with DMRG.

Throughout this thesis all DMRG calculations will be done using the ITensor C++ library [65]. We impose $\mathbb{Z}_q$ and $U(1)$ symmetries wherever possible and consider both open and periodic boundary conditions. While it is often stated that DMRG should be done with open rather than periodic boundary conditions wherever possible due to the lower entanglement entropy, when studying CFTs this cost is often offset by the increased speed of convergence of energy levels to their continuum predictions.

2

Conformal Field Theory Results

Contents

2.1 Introduction

Throughout this thesis we will find that a number of points and extended phases we encounter have a Conformal Field Theory [12, 15, 16] (CFT) as their thermodynamic limit. Two-dimensional CFTs have many beautiful properties but we will content ourselves with a brief outline of the results which will prove useful for our cause. We start by describing the most basic features of CFTs which will be essential before moving on to the more advanced and specific results to be used later in the thesis.

2.2 CFT in a few pages

A CFT has the normal rotational and translation invariance of a quantum field theory along with additional dilatation (scale) and "special conformal" invariance. The scale invariance explains the connection to many second-order phase transitions, as here the correlation length of the system diverges, removing scale from the problem. The special conformal transformation is required to ensure that the symmetry group is closed.

While the conformal group is a useful symmetry in any number of dimensions, it becomes particularly powerful in two dimensions. Here the conditions for conformal invariance of the coordinates x^μ under the infinitesimal transformation

$$x^\mu \to x^\mu + \epsilon^\mu \tag{2.1}$$

become equivalent to the Cauchy–Riemann equations [15]:

$$\partial_1 \epsilon_1 = \partial_2 \epsilon_2, \qquad \partial_1 \epsilon_2 = -\partial_2 \epsilon_1. \tag{2.2}$$

This equivalence allows us to use the powerful techniques of complex analysis and, defining

$$z = x_1 + i x_2, \quad \bar{z} = x_1 - i x_2, \tag{2.3}$$

the algebra splits into two separate parts – a *holomorphic* part depending on z and an *antiholomorphic* part depending on $\bar{z}$. In a two-dimensional classical theory x_1 and x_2 are the two spatial coordinates, while for a one-dimensional quantum system x_1 is the spatial and x_2 the time coordinate.

Defining the generators

$$l_n = -z^{n+1}\partial_z, \qquad \bar{l}_n = -\bar{z}^{n+1}\partial_{\bar{z}}, \tag{2.4}$$

the following algebras are obeyed:

$$[l_m, l_n] = (m-n) l_{m+n}, \qquad \left[\bar{l}_m, \bar{l}_n\right] = (m-n)\bar{l}_{m+n}. \tag{2.5}$$

In the quantum case, these commutation relations are complicated slightly by the presence of the *conformal anomaly*. The underlying algebra of two-dimensional CFT, the Virasoro algebra, can be then expressed as

$$\begin{aligned}[L_m, L_n] &= (m-n)L_{m+n} + \frac{c}{12}\left(m^3 - m\right)\delta_{m+n,0}, \\ \left[\bar{L}_m, \bar{L}_n\right] &= (m-n)\bar{L}_{m+n} + \frac{c}{12}\left(m^3 - m\right)\delta_{m+n,0},\end{aligned} \tag{2.6}$$

where L_n and $\bar{L}_n$ are the generators of the holomorphic and antiholomorphic algebras respectively and c is the *central charge* of the CFT.

As can be seen from Equation 2.6, the Virasoro algebra only depends on c. For the theory to be unitary and non-trivial, we require $c > 0$ and, while for $c \geq 1$ any value is allowed, for $0 < c < 1$ we can only have

$$c = 1 - \frac{6}{m(m+1)} \tag{2.7}$$

for $m = 3, 4, ...$ [66, 67]. The CFTs with $0 < c < 1$ are known as the *minimal models*. Minimal models corresponding to $m = 3$, 4, 5, and 6 will all be important in the remainder of the thesis, as well as CFTs with $c = 1$ and $c = 3/2$.

Although the Virasoro algebra only depends on c, fixing c is not necessarily enough to determine the CFT. The fields present also need to be specified to give a full description of all energy levels and correlators. For the minimal models on the torus, there are either one, two or three consistent CFTs for each allowed c. The number of minimal model CFTs and their form is given by the A-D-E classification [68], with A, D and E each corresponding to a series of CFTs. If $c \geq 1$, there is generally an infinite number of consistent CFTs.

We typically label a field by its *conformal weights*, defined by its eigenvalues under L_0 and $\bar{L}_0$. The field $\Phi_{h,\bar{h}}$ then obeys

$$L_0\Phi_{h,\bar{h}} = h\Phi_{h,\bar{h}}, \qquad \bar{L}_0\Phi_{h,\bar{h}} = \bar{h}\Phi_{h,\bar{h}}. \tag{2.8}$$

The *dimension*, Δ, and *spin*, s, of the operator are given by

$$\Delta = h + \bar{h} \quad \text{and} \quad s = h - \bar{h}, \tag{2.9}$$

respectively. As we will see, the dimension is related to the energy of eigenstates on the lattice. The spin gives the difference in weight between the holomorphic and antiholomorphic parts, corresponding to the right- and left-moving parts on the lattice. A spin s then corresponds to momentum $2\pi s/L$ on the lattice.[1]

The dimension of an operator describes how *relevant* it is in the sense of the Renormalization Group (RG) [9–11]. If $\Delta > 2$, the operator is *irrelevant* under an RG flow and so perturbing the CFT by this operator will not affect the long-distance behaviour of the system. If $\Delta < 2$, the operator is *relevant* and perturbing the CFT with it will change the long-range behaviour, leading to a phase transition. If $\Delta = 2$, the operator is *marginal* and further calculation is required to find the effect of perturbing by it. Determining which operators are relevant in a CFT is therefore essential in working out its stability to perturbations. We next discuss how fields can be rearranged into towers of increasing dimension, cutting down the number of operators we must consider.

By considering Equation 2.6, we see that

$$\begin{aligned} L_0 L_n \Phi_{h,\bar{h}} &= \left(L_n L_0 + [L_0, L_n]\right) \Phi_{h,\bar{h}} \\ &= \left(L_n h - n L_n\right) \Phi_{h,\bar{h}} \\ &= (h-n) L_n \Phi_{h,\bar{h}} \end{aligned} \tag{2.10}$$

and so $L_n \Phi_{h,\bar{h}}$ has holomorphic weight $h - n$ and dimension $\Delta = h + \bar{h} - n$. As an analogous relation holds for the antiholomorphic part, L_n and $\bar{L}_n$ each reduce the dimension by n. For the CFT to be unitary, we require $\Delta \geq 0$ for all fields and so there must exist a set of fields annihilated by all L_n and $\bar{L}_m$ for $n, m > 0$. These fields are known as the *primary* fields. Every other field can be obtained from these by applying some succession of *raising operators* L_n and $\bar{L}_m$ for $n, m < 0$. These other fields are then called *secondary* fields. The primary and set of all secondaries descended from it form the *conformal tower* of the primary. As the

[1] This is at least naïvely true. In fact, as we will see in Chapter 4, a spin $s = 0$ state does not always have lattice momentum 0, but a spin s' state in the same tower will still have momentum $\Delta k = 2\pi s'/L$ relative to this.

primary has the lowest dimension in its conformal tower, to look for the presence of relevant operators we can simply check the primaries.

2.2.1 The weights of the minimal models

A simple formula gives the weights for the minimal models. For a given m, the allowed weights are

$$h_{p,q}(m) = \frac{[(m+1)p - mq]^2 - 1}{4m(m+1)}, \tag{2.11}$$

where $1 \leq p \leq m-1$, $1 \leq q \leq p$. This, in fact, overcounts the primaries by a factor of 2 and all can be obtained by enforcing $p+q$ be even. Which combinations of the holomorphic and antiholomorphic parts are allowed and their degeneracies are determined by which series the minimal model is in (A, D or E). For example, in the A-series, $h_{p,q}$ is always combined with $h_{\bar{p},\bar{q}}$ and is non-degenerate. Every other field is then a descendant of one of these primaries.

To show how this works, we consider the simplest minimal model where $m = 3$. This theory in fact corresponds to the self-dual Ising model, given by $J = f$ in Equation 1.2. Here we have central charge

$$c_{\text{Ising}} = 1 - \frac{6}{3 \times 4} = \frac{1}{2} \tag{2.12}$$

and weights

$$h_{1,1} = 0, \quad h_{2,2} = \frac{1}{16}, \quad h_{1,3} = \frac{1}{2}. \tag{2.13}$$

The primary fields are then $\mathbb{1}$, σ and ϵ with weights $(h, \bar{h})$ of $(0,0)$, $(1/16, 1/16)$ and $(1/2, 1/2)$. These correspond to the identity operator, the spin field and the energy field, respectively.

2.3 Useful results

Having given a very quick summary of some of the most important elements of CFT, we now move on to the key results which will be used in this thesis. These are by no means the only useful signatures of CFTs, but they are the ones most easily tested in the lattice models studied here.

2.3.1 Correlators

For a gapped system, the connected two-point correlator of a local operator decays exponentially with the distance between the locations of the operators. For example, the spin-spin correlator in the off-critical Ising model decays as:

$$\langle \sigma_j^z \sigma_k^z \rangle_C \sim e^{-|j-k|/\xi} \tag{2.14}$$

for large separation $|j-k| \gg \xi$, where ξ is the correlation length of the system. As models approach criticality, their correlation lengths diverge and correlators decay more slowly.

Gapless systems have infinite correlation lengths and two-point correlators decay algebraically rather than exponentially with separation, e.g. the critical Ising model has the correlator

$$\langle \sigma_j^z \sigma_k^z \rangle \sim |j-k|^{-\frac{1}{4}} \tag{2.15}$$

for $|j-k| \gg 1$. In CFTs the decay with distance of a two-point correlator is given simply by the dimension of the operator:

$$\langle \Phi_j \Phi_k \rangle \sim |j-k|^{-2\Delta_\Phi}, \tag{2.16}$$

where Δ_Φ is the dimension of the operator Φ.

Generally, the continuum limit of lattice operators is given by a sum over all CFT operators with the same charges under the lattice symmetries as the lattice operator. The long-distance behaviour of the correlator is then determined by the most relevant operator in this sum. For the critical Ising model, the most relevant operator in the CFT with the same charges as σ^z is the σ operator of dimension $\Delta_\sigma = 1/16 + 1/16 = 1/8$, showing the agreement between Equations 2.15 and 2.16.

By finding where correlation lengths diverge, we can investigate transitions between gapped and gapless regions or between gapped regions separated by a gapless point. The scaling of the algebraic decay of the correlators within these gapless regions then gives hints of the CFT operators present and hence the CFT itself.

2.3.2 Lattice energy levels

One of the techniques we will use to investigate the phases of our models is based on ratios of low-lying energy levels. In a CFT the energies of low-lying levels on a finite lattice of length L with periodic boundary conditions are given by the following beautiful formula:

$$E_{h,\bar{h}} = \epsilon_0 L + \frac{2\pi v}{L}\left(h + \bar{h} - \frac{c}{12}\right) + \mathcal{O}(1/L^2), \tag{2.17}$$

where h and $\bar{h}$ are the holomorphic and anti-holomorphic weights of the operator acting on the ground-state to get the energy level, $\Phi_{h,\bar{h}}$, ϵ_0 is the ground-state energy density in the thermodynamic limit, v is the Fermi velocity, and c is the central charge of the CFT [69, 70]. For a given lattice model, v and ϵ_0 are both proportional to the global constant multiplying the Hamiltonian, while ϵ_0 is also affected by the addition of the identity operator at each site. As neither of these changes affects the eigenstates of the Hamiltonian, they do not alter the CFT description of the model.

To remove the effects of ϵ_0 and v, we consider *ratios* of energy levels, giving the formula

$$\frac{E_\alpha - E_\beta}{E_\gamma - E_\delta} = \frac{\Delta_\alpha - \Delta_\beta}{\Delta_\gamma - \Delta_\delta} \tag{2.18}$$

to leading order in $1/L$, where $\Delta_\alpha = h_\alpha + \bar{h}_\alpha$ is the dimension of the operator $\Phi_{h_\alpha,\bar{h}_\alpha}$. Which states on the lattice correspond to which operators in the CFT can be deduced by considering the symmetries of both as will be explained later.

Returning to our example of the critical Ising model, we first need to identify the levels in our lattice model. Taking periodic boundary conditions, we can split our states into momentum eigenstates. As the Ising Hamiltonian (1.2) commutes with the spin flip operator (1.4), we can split the model into $\mathbb{Z}_2$ sectors too. Considering the primary fields of the Ising CFT, all have spin $s = h - \bar{h} = 0$ and so are in the momentum $k = 0$ sector. While the identity and energy operators, $\mathbb{1}$ and ϵ, are even under the $\mathbb{Z}_2$, the spin operator, σ is odd. Considering just the $k = 0$ sector, the lowest lying states in the $\mathbb{Z}_2$ even sector are then those corresponding to $\mathbb{1}$ and

ϵ, whereas in the $\mathbb{Z}_2$ odd sector it is σ. Defining $E^j_{k,r}$ to be the j^{th} excited state in the sector with momentum k and $\mathbb{Z}_2$ charge r, we find the CFT prediction

$$\frac{E^0_{0,1} - E^0_{0,0}}{E^1_{0,0} - E^0_{0,0}} = \frac{\Delta_\sigma - \Delta_{\mathbb{1}}}{\Delta_\epsilon - \Delta_{\mathbb{1}}} = \frac{\frac{1}{8} - 0}{1 - 0} = \frac{1}{8}. \tag{2.19}$$

We can then find this ratio numerically for a range of lattice lengths, L. If it converges to the CFT prediction with increasing L, this is strong evidence that the continuum limit of the lattice model is indeed described by this CFT. Repeating this for different ratios then provides further evidence.

2.3.3 Probing the central charge

As mentioned earlier, the value of the central charge, c, is the only thing affecting the Virasoro algebra (2.6). We also noted that, for $c < 1$, identifying the value of c cuts down the number of possible CFTs to a maximum of three. Even for $c \geq 1$, the value is still essential information in identifying the underlying theory.

The easiest way of finding c numerically in a $1+1$-dimensional lattice model is to consider the von Neumann entanglement entropy as shown by Calabrese and Cardy [71]. The von Neumann entanglement entropy between a subsystem A and its environment is defined as

$$S_A = -\operatorname{Tr} \rho_A \log \rho_A, \tag{2.20}$$

where ρ_A is the reduced density matrix of subsystem A. Calabrese and Cardy demonstrated that, for a chain of length L with periodic boundary conditions, the von Neumann entanglement entropy between a subchain of length l and the rest of the chain is given by

$$S = \frac{c}{3} \log\left((L/\pi)\sin(\pi l/L)\right) + c_1, \tag{2.21}$$

where the lattice spacing has been set to 1 and c_1 is a constant. Typically we will consider the bipartite entanglement with $l = L/2$, simplifying Equation 2.21 to

$$S_{L/2} = \frac{c}{3} \log L + c_2. \tag{2.22}$$

This entanglement entropy is extracted easily when using DMRG [59–61].

Although the entanglement entropy can be used to distinguish between different CFTs, the distinction between the behaviours of the entanglement entropy of gapped and gapless systems is even clearer. As shown by Hastings [62], the ground states of all gapped systems in one-dimensional quantum systems obey an "area-law" and so have entanglement entropy tending to a constant in the thermodynamic limit:

$$\lim_{L\to\infty} S_{\text{gapped}} = \text{const.} \tag{2.23}$$

This is consistent with the entanglement entropy of a CFT diverging as $S \sim \log L$ due to the $1/L$ splitting of energy levels giving a gapless system, as described in Subsection 2.3.2. Investigating the scaling of the entanglement entropy thus gives us a strong distinguishing characteristic between gapped systems and CFTs as there is a clear qualitative difference between tending to a constant and diverging as a logarithm with system size.

Returning to our faithful example of the Ising CFT, we have a central charge of $c = 1/2$. Working out the half-chain entanglement entropy for a model with periodic boundary conditions and described by the Ising CFT in the continuum limit should give entropy scaling of

$$S_{\text{Ising},L/2} = \frac{1}{6}\log L + c_2 \tag{2.24}$$

for large L.

2.4 Superconformal Field Theory

Supersymmetry, to be explained in Section 3.4, can be incorporated into CFTs, giving superconformal field theories (SCFTs) [72]. In SCFTs, there are further conserved currents of dimension $(3/2, 0)$ and $(0, 3/2)$, corresponding to the supercharges. For $N = 1$ supersymmetry (with one supercharge), the Virasoro

algebra gets extended to the super Virasoro algebra [73, 74]:

$$[L_m, L_n] = (m-n)L_{m+n} + \frac{\hat{c}}{8}\left(m^3 - m\right)\delta_{m+n,0}, \tag{2.25}$$

$$\{G_m, G_n\} = 2L_{m+n} + \frac{\hat{c}}{2}\left(m^2 - \frac{1}{4}\right)\delta_{m+n}, \tag{2.26}$$

$$[L_m, G_n] = \left(\frac{m}{2} - n\right)G_{m+n}, \tag{2.27}$$

with analogous relations holding for the antiholomorphic algebra.

The L_m operators are the same as those of Equation 2.6, while the G_m are the new fermionic operators extending the algebra. As SCFTs still have the same symmetry group as CFTs, along with supersymmetry, they must still be CFTs and hence Equations 2.6 and 2.25 should be equivalent. The only difference between the two is the change of $c/12$ to $\hat{c}/8$, showing that $\hat{c} = 3c/2$.

There are, in fact, two different SCFT algebras: Ramond and Neveu–Schwarz (NS) [73, 74]. The distinction corresponds to the allowed values of m in G_m: Ramond has $m \in \mathbb{Z}$, while NS has $m \in \mathbb{Z} + 1/2$. As with the normal Virasoro algebra, L_m and G_n with $m, n > 0$ are lowering operators, while those with $m, n < 0$ are raising operators. Our superconformal primary fields are thus those fields annihilated by all L_m and G_n with $m, n > 0$. Note that there are states that are conformal primaries but not superconformal primaries as they are annihilated by all L_m with $m > 0$, but not by all G_n with $n > 0$. We will see an example of this when we consider the Tricritical Ising CFT shortly in Subsection 2.4.1.

The super Virasoro algebra, once the Ramond or NS sector is chosen, is determined just from $\hat{c}$, just as the Virasoro algebra was from c. Analogously, for $\hat{c} < 1$, only certain values are allowed [72]. These lead to the superconformal minimal models with

$$\hat{c} = 1 - \frac{8}{\hat{m}(\hat{m}+2)}, \tag{2.28}$$

where $\hat{m} = 3, 4, \ldots$. The allowed weights of superconformal primaries are then given by

$$h_{p,q} = \frac{\left[(\hat{m}+2)p - \hat{m}q\right]^2 - 4}{8\hat{m}(\hat{m}+2)} + \frac{1}{32}\left(1 - (-1)^{p-q}\right), \tag{2.29}$$

where $1 \leq p < \hat{m}$, $1 \leq q < \hat{m} + 2$ and for the NS sector $p - q$ is even, while for the Ramond sector it is odd.

2.4.1 The Tricritical Ising CFT

The first SCFT minimal model is the tricritical Ising (TCI) CFT, corresponding to $\hat{m} = 3$. This has $\hat{c} = 7/15$ and so $c = 7/10$, meaning that it is also a CFT minimal model. In fact, this is the only model which is both a CFT and SCFT minimal model, as the next SCFT minimal model has $\hat{c} = 2/3$ and hence $c = 1$.

Using Equation 2.29, we see that the distinct primary weights are 0 and 1/10 in the NS sector and 3/80 and 7/16 in the Ramond sector, where we have ignored double counting. Every state in the SCFT can then be found by applying the super Virasoro raising operators to these primaries.

As we noted above, the TCI CFT is also a CFT minimal model and so we can use Equation 2.11 to find the CFT primaries, giving chiral dimensions 0, 1/10, 3/5, 3/2, 3/80 and 7/16. There then appear to be two extra primary fields in the CFT minimal model! This is resolved by noting that

$$G_{1/2} \left|1/10\right\rangle = \left|3/5\right\rangle , \qquad G_{3/2} \left|0\right\rangle = \left|3/2\right\rangle , \tag{2.30}$$

where $|h\rangle$ represents the holomorphic part of the field with weight h, showing that $|3/5\rangle$ and $|3/2\rangle$ are descendants of $|1/10\rangle$ and $|0\rangle$, respectively, under the super Virasoro algebra, but not under the Virasoro algebra.

2.5 Free boson CFTs

In Section 2.2 we mentioned that, for central charges $c < 1$, only specific values of c are allowed and each of these has a finite (1, 2 or 3) number of possible CFTs. For $c > 1$, any value of c is allowed and there are, generically, an infinite number of possible CFTs for each c. $c = 1$ is the boundary case in which there are an infinite number of CFTs, but they can all be written down [75]. The simplest $c = 1$ CFTs are free boson CFTs, with the infinite number of theories given by different compactification radii, i.e. changing the radius of the circle on which the

boson lives. All other CFTs at $c = 1$ can be found by "modding out" subgroups of the $U(1)$ symmetry of the boson, giving *orbifold* theories [75–77], although for now we will focus on the circle (free boson) theories. Throughout this thesis we will follow the conventions of Ginsparg [15, 75].

To write down the free boson partition function on the torus, we begin by introducing the *modular parameter* of a torus, τ. Taking z as our complex coordinate on the plane from Equation 2.3, we first go to the cylinder by defining $z \equiv \exp(iw)$, where the period of the cylinder is $w \equiv w + 2\pi$. Here $\mathrm{Im}(w)$ corresponds to the imaginary time coordinate, while $\mathrm{Re}(w)$ corresponds to the spatial part. To turn the cylinder into a torus, we then identify $w \equiv w + 2\pi\tau$, where $\tau = \tau_1 + i\tau_2$ and τ_1 and τ_2 are real.

The free boson partition function on the torus at a compactification radius R can be written as [15, 75]

$$Z(R) = \frac{1}{\eta\bar{\eta}} \sum_{m,n\in\mathbb{Z}} q^{\frac{1}{8R^2}\left(m+2R^2n\right)^2} \bar{q}^{\frac{1}{8R^2}\left(m-2R^2n\right)^2}, \tag{2.31}$$

where $q \equiv \exp(2\pi i\tau)$ and

$$\eta = q^{\frac{1}{24}} \prod_{n=1}^{\infty} (1 - q^n) \tag{2.32}$$

is the Dedekind eta function and accounts for the descendant fields. Each term $q^{h-1/24}\bar{q}^{\bar{h}-1/24}$ corresponds to a field in the CFT with weights $(h, \bar{h})$.

m and n are the eigenvalues of two $U(1)$ charges dual to each other, and are often referred to as the electric and magnetic charges. As the sums over m and n are over all integers, we see that there are an infinite number of primary fields. For special radii, this infinite sum can be rewritten as a finite sum of primary fields of some extended algebra. These radii obey $R = \sqrt{p'/(2p)}$, where p' and p are integers [16].

We will see that lattice symmetries often allow us to cut down this infinite number of theories to a single consistent one. Specifically, Section 4.7 will show how a combination of S_3 symmetry and self-duality fixes the boson radius to $R = \sqrt{3/2}$.

3

The $\mathbb{Z}_2$ invariant model

Contents

3.1 Introduction

The $1+1$-dimensional critical Ising model has long been studied in condensed matter physics. In terms of theory, it has the distinct advantage of being exactly solvable [55], most easily in terms of free fermions as mentioned in Chapter 1 [57, 58]. Perturbing by a duality-breaking interaction gaps the system, taking it to either the ordered or disordered Ising phase, depending on the sign of the interaction. In

2010 Coldea *et al.* exhibited the transition between the ordered and disordered phases experimentally using cobalt niobate in a transverse magnetic field [78]. Their experiment considered weakly coupled chains of cobalt niobate, each of which gives a good approximation to an Ising chain, with an externally applied field providing the transverse "spin-flipping" term. In the ordered phase, the $\mathbb{Z}_2$ symmetry in a given chain is spontaneously broken, giving a non-zero expectation to the magnetisation of that chain which then, using a mean field theory approach, provides a weak longitudinal magnetic field for the nearby chains. This longitudinal field vanishes at the transition to the paramagnetic phase (where the $\mathbb{Z}_2$ symmetry is no longer spontaneously broken), at which point the ratios of the energies of low-lying states are known from theory [79]. The energies in the ordered and disordered phases, along with those at the transition, were found to agree with predictions for the Ising model, using neutron scattering measurements.

In fact, recently Majoranas (1.14) have sparked far more interest in the condensed matter community than the spin version of the Ising model due to their connection to non-Abelian topological quantum computation [26, 27]. Topological superconductors have been proposed as one way in which Majorana modes could appear [35, 36] and be used in quantum computation (for a review of experimental efforts in this area see, e.g., Ref. [80]). "Kitaev materials" [37, 38], such as α-$RuCl_3$, have been the focus of other experimental groups [39, 40], providing another possible avenue. As self-duality (more or less) corresponds to translation invariance of Majoranas [48] and these are often the particles of interest, rather than spins, imposing self-duality seems a natural constraint on our physical system.

While CFT gives us a clear prediction of the behaviour expected when the critical Ising model is perturbed by a duality-breaking perturbation, it is less clear what happens when a self-dual (and $\mathbb{Z}_2$ invariant) interaction is added. In this case there are no relevant interactions, as stated in Chapter 2, and so the system remains in the critical Ising phase, at least for infinitesimally small perturbations.

One way in which this phase can end is through a transition to a gapped region via a point in the universality class of the tricritical Ising (TCI) CFT [66, 81]. The

TCI CFT is the minimal model with $m = 4$, corresponding to a central charge of $c = 7/10$, as given by Equation 2.7. While it is the second minimal model in the series after the Ising model, it has by no means as natural a lattice realisation.

It is known to correspond to the termination of the Ising critical line in the Blume–Capel model [81–84], given by the spin-1 Hamiltonian

$$H_{\mathrm{BC}} = -\sum_j \left(S_j^z S_{j+1}^z - \gamma S_j^x - \delta S_j^{z\,2} \right), \tag{3.1}$$

where we follow the notation of Ref. [85]. For $\delta = -\infty$, this reduces to the quantum Ising model and hence there is a critical Ising transition between ordered and disordered phases, while at $\gamma = 0$ the model is fully classical and there is a first-order transition between the ferromagnetic "Ising" ordered states and the state with all $S_j^z = 0$. These lines of second- and first-order transitions terminate as they hit each other via a point in universality class of the TCI CFT, occurring at $\lambda \approx 0.42$, $\delta \approx 0.91$ [84].

While this model does indeed display a TCI point, there are several drawbacks. Firstly, and arguably most importantly, this model requires fine tuning to get to its TCI point, as the values of both γ and λ must be set just right. Thus this transition is just a single point in the phase diagram which can easily be avoided (or missed). Secondly, it occurs in a spin-1 chain – effectively an Ising model with vacancies allowed – making numerics more challenging. Finally, there is no obvious link to supersymmetry in the lattice model which, as we have seen in Section 2.4.1, is one of the fascinating features of the TCI CFT [72].

More recently, other models have been proposed in which TCI points occur [85–87]. The Rahmani model [85, 86] is built out of explicitly self-dual operators and hence does not require fine tuning – there is only one free parameter in the Hamiltonian and so varying this necessarily takes the system through its TCI point. Secondly, like the Ising model, it is based on a spin-$\frac{1}{2}$ Hamiltonian and so has two states per site, rather than the three of the Blume–Capel model.

There are some potential issues with the Rahmani model though. Firstly, the term added to perturb the Ising model must be tuned at a strength of $\sim$

250 times the Ising interaction before the TCI point is reached. This intriguing feature was not understood until a recent work by Aasen *et al.* provided an explanation based on renormalization of the kinetic energy with interaction strength [41]. As well as this, the Rahmani model still has no obvious connection with the supersymmetry of the continuum CFT.

Turning to the second model mentioned above, introduced by Grover *et al.* [87], a TCI point was again found without fine tuning. They considered topological superconductors in both two and three dimensions, but we mention only the two dimensional case here as it aligns more closely with our work. The topological superconductor is protected by time-reversal symmetry, which naturally has a pair of counterpropagating Majorana edge modes. Introducing an Ising field that changes sign under time-reversal to describe the magnetic instability of the edge, the action then acquires a bosonic degree of freedom as well.

The presence of both bosons and fermions indicates the possibility of emergent supersymmetry, which is indeed found to occur in the low energy limit of the model, when the boson is described by an Ising degree of freedom. The coupling between the boson and fermion leads to an effective mass term for the Majorana, with the mass given by the expectation of the the Ising order parameter, $\langle \sigma_j^z \rangle$. At large transverse magnetic fields, this expectation value vanishes, giving a massless Majorana model and hence a $c = 1/2$ CFT, while at small fields, the $\mathbb{Z}_2$ symmetry of the Ising model is spontaneously broken and the order parameter becomes non-zero, gapping out the Majorana degree of freedom. The natural transition point between these two is given by a point in the universality class of the Tricritical Ising CFT, which is confirmed numerically.

Supersymmetry thus emerges at the symmetry breaking phase transition between the ordered and disordered Ising phases, where the Majorana chain acquires an effective mass. While this presence of emergent supersymmetry was natural in the boson plus Majorana language, in terms of the Ising and Majorana chains it seems less clear why it should occur. Numercially, the introduction of a Ising chain in addition to the Majorana chain also makes the analysis more difficult, as

did the presence of a three-state per site rather than two-state per site system in the Blume–Capel model.

It could be thought that, perhaps, the lack of explicit supersymmetry in any of the models mentioned so far indicates that it is always simply an emergent property in the field theory limit. This is not necessarily the case though, as can be seen from a number of models with explicit lattice supersymmetry that correspond to supersymmetric field theories in their continuum limits [88–91].

In our model we will see that all of the above desired features align. It is once again a model requiring no fine tuning (other than self-duality, which is just translation invariance in terms of Majoranas) for a system with two states per site. The ratio of couplings for which the TCI point occurs is $\mathcal{O}(1)$ and throughout the phase diagram the Hamiltonian can be expressed as the sum of two supersymmetric theories. While this is not quite supersymmetric on its own, it at least makes the connection far clearer. Moreover, we discuss an explicitly supersymmetric line, also studied in Ref. [92], which will prove to be a line of phase transitions to an incommensurate region.

The remainder of this chapter is set out as follows. Section 3.2 recaps the basics of the Ising model and shows its stability to self-dual perturbations, as well as explaining the Rahmani perturbation [85, 86]. Section 3.3 introduces our non-chiral model and details its phase diagram, including the order-disorder coexistence phase and TCI point. In Section 3.4 lattice supersymmetry is introduced, while in Section 3.5 we generalise our model to allow chirality and show how supersymmetry fits into the picture. In Section 3.6 we summarise the results and explain some of the extensions to the model other groups have investigated. This chapter is largely based on Ref. [49].

3.2 The stability of the critical Ising phase

As mentioned in Chapter 1, the Ising model has Hamiltonian

$$\begin{aligned} H_{\text{Ising}}(J,f) &= -\sum_{j=1}^{L}\left(J\sigma_j^z\sigma_{j+1}^z + f\sigma_j^x\right) \\ &= i\sum_{j=1}^{L}\left(J\gamma_{2j}\gamma_{2j+1} + f\gamma_{2j-1}\gamma_{2j}\right), \end{aligned} \tag{3.2}$$

where γ_a operators represent Majoranas as given in Equation 1.14, L is the lattice length, and we have ignored subtleties with boundary conditions. This has a $\mathbb{Z}_2$ symmetry characterised by the spin-flip operator

$$\mathcal{F} = \prod_{j=1}^{L}\sigma_j^x, \tag{3.3}$$

which flips all spins in the z-direction. As $[H_{\text{Ising}}, \mathcal{F}] = 0$, we can pick a basis of eigenstates of H_{Ising} with well-defined eigenvalue under $\mathcal{F}$. Because σ^x has eigenvalues ± 1, so does $\mathcal{F}$, with these two eigenvalues giving the $\mathbb{Z}_2$ symmetry. As well as this $\mathbb{Z}_2$ symmetry, we have imposed spatial parity symmetry (the Hamiltonian is invariant under relabelling $j \to L+1-j$) and we additionally have translation invariance, at least in the bulk.

In this chapter we will focus on perturbing from the self-dual Ising model:

$$H_I = -\sum_{j=1}^{L}\left(\sigma_j^z\sigma_{j+1}^z + \sigma_j^x\right). \tag{3.4}$$

As stated previously, the continuum limit of this model is described by the Ising CFT with central charge $c = 1/2$ and primary fields

$$\mathbb{1} = \left(0,0\right), \qquad \sigma = \left(\frac{1}{16},\frac{1}{16}\right), \qquad \epsilon = \left(\frac{1}{2},\frac{1}{2}\right), \tag{3.5}$$

named the identity, spin and energy fields, respectively, [12]. The identity and energy fields are even under the spin-flip operator $\mathcal{F} = \prod_j \sigma_j^x$, while the spin field is odd. If we perturb our lattice model by a coupling invariant under $\mathcal{F}$, this remains a symmetry and hence the spin field cannot be part of this operator. If

we also maintain translation invariance and spatial parity, the simplest perturbing operator we can construct is

$$H_\epsilon = \sum_{j=1}^{L} \left(\sigma_j^z \sigma_{j+1}^z - \sigma_j^x\right). \tag{3.6}$$

Adding $\lambda_\epsilon H_\epsilon$ to H_I (3.4) and rescaling gives any Ising Hamiltonian (3.2). This perturbation contains, among other fields, the energy field $\epsilon = (1/2, 1/2)$. As $\Delta_\epsilon = 1/2 + 1/2 = 1 < 2$, this operator is relevant and so it gaps the system, explaining the phase transition to either the ordered or disordered Ising phase, depending on the sign of λ_ϵ.

As lattice operators generally consist of a superposition of all operators in the CFT obeying the same symmetries, it may appear that, whatever lattice term we add, we will always have at least one of the spin and energy fields and so will gap the system. In fact, we can use self-duality to escape this problem. The energy operator is anti-self-dual [93, 94] and so, if we perturb by a self-dual $\mathbb{Z}_2$ invariant perturbation, this will have to be in the identity tower and so will be irrelevant, having dimension $\Delta = 4$ [93]. Hence perturbing with this operator should preserve the critical Ising line, at least for some range of couplings!

There are no single-site or nearest-neighbour interactions which preserve every symmetry of Ising as well as self-duality, other than H_I itself, so we have to go to next-nearest-neighbour interactions. At this stage, several possibilities occur. Considering Majoranas, the simplest option is

$$H_{\text{ff}} = i \sum_{a=1}^{2L} \gamma_a \gamma_{a+3}, \tag{3.7}$$

corresponding to

$$H_{\text{ff}} = \sum_{j=1}^{L} \sigma_j^y \sigma_{j+1}^y - \sigma_j^z \sigma_{j+1}^x \sigma_{j+2}^z. \tag{3.8}$$

Ignoring Ising for the moment, H_{ff} can be written as

$$H_{\text{ff}} = \sum_{n=1}^{3} \left(i \sum_{m=0}^{2L/3-1} \gamma_{3m+n} \gamma_{3(m+1)+n} \right) \tag{3.9}$$

and hence it decomposes into three copies of the critical Ising model, albeit with non-trivial selection rules on the allowed combinations of states due to the boundary conditions. As this model is free-fermionic, it can be solved exactly, as can any combination of it and the Ising Hamiltonian. Thus we will not consider this further but instead investigate interacting models.

The shortest range interaction beyond simple free fermions was investigated by Rahmani, Zhu, Franz and Affleck in 2015 [85, 86] and consists of Majoranas on four consecutive sites. Combining this with the Ising model we get

$$H_{\mathrm{R}} = it\sum_{a=1}^{2L}\gamma_a\gamma_{a+1} + g\sum_{a=1}^{2L}\gamma_a\gamma_{a+1}\gamma_{a+2}\gamma_{a+3}, \tag{3.10}$$

where the ferromagnetic Ising model corresponds to $t > 0$, $g = 0$. Rahmani *et al.* found that the critical Ising phase is extremely stable to increasing g from 0, with the phase surviving until $g/t \approx 250$. At this point there is a phase transition via a point in the universality class of the TCI CFT [66, 72] to a gapped phase.

This transition is very interesting for a number of reasons. Firstly, why is the ratio of couplings at which the transition occurs so astronomically large? This question remained unanswered in the literature until recently, when Aasen *et al.* presented a beautiful explanation to be described later [41]. Secondly, as mentioned in Chapter 2, the TCI CFT is not just a CFT, it is a superconformal field theory (SCFT), meaning that it has supersymmetry in addition to conformal invariance [72, 95]. There is, however, no obvious supersymmetry on the lattice [96]. We will see that in our model to be studied next the connection to supersymmetry is far clearer.

3.3 Our non-chiral model

We now come to the model we studied and the focus for this chapter of the thesis. The next simplest interacting model that can be studied has Hamiltonian

$$H(\lambda_I, \lambda_3) = 2\lambda_I H_I + \lambda_3 H_3 + E_0, \tag{3.11}$$

where

$$H_I = -\sum_{j=1}^{L} \left(\sigma_j^x + \sigma_j^z \sigma_{j+1}^z\right) = i \sum_{a=1}^{2L} \gamma_a \gamma_{a+1}, \tag{3.12}$$

$$H_3 = \sum_{j=1}^{L} \left(\sigma_j^x \sigma_{j+1}^z \sigma_{j+2}^z + \sigma_j^z \sigma_{j+1}^z \sigma_{j+2}^x\right) = -\sum_{a=1}^{2L} \gamma_{a-2} \gamma_{a-1} \gamma_{a+1} \gamma_{a+2}, \tag{3.13}$$

and $E_0 = L(\lambda_I^2 + \lambda_3^2)/\lambda_3$ is an energy shift to make the link with supersymmetry clearer, as will be explained later. We will assume $\lambda_3 > 0$, $\lambda_I > 0$ as this is the region of interest – indeed, Ref. [41] recently showed the model remains in the critical Ising phase up to large negative values of λ_3/λ_I and the unitary $U = \sigma_1^y \sigma_2^z \sigma_3^y \sigma_4^z \cdots \sigma_{L-1}^y \sigma_L^z$ maps $\lambda_I \to -\lambda_I$, $\lambda_3 \to \lambda_3$ (at least for even L), meaning that the full phase diagram can be understood by setting $\lambda_I \geq 0$.

3.3.1 The frustration-free point

We will start our analysis by looking at the specific point $H(1,1)$. At this point the Hamiltonian can be rewritten in the illuminating form

$$\begin{aligned} H(1,1) &= \sum_{j=1}^{L} \Big[\left(\mathbb{1}_j - \sigma_j^x\right) \left(\mathbb{1}_{j+1,j+2} - \sigma_{j+1}^z \sigma_{j+2}^z\right) \\ &\qquad + \left(\mathbb{1}_{j,j+1} - \sigma_j^z \sigma_{j+1}^z\right) \left(\mathbb{1}_{j+2} - \sigma_{j+2}^x\right) \Big] \\ &\equiv \sum_{j=1}^{L} H_{j,j+1,j+2}. \end{aligned} \tag{3.14}$$

Both terms have been factorized into two parts, each of which acts on different sites. Taking the single-site basis $\{|\uparrow\rangle, |\downarrow\rangle\}$, where

$$\sigma_j^z |\uparrow\rangle_j = |\uparrow\rangle_j, \qquad \sigma_j^z |\downarrow\rangle_j = -|\downarrow\rangle_j, \tag{3.15}$$

we see that $\mathbb{1}_j - \sigma_j^x$ projects onto the state $(|\uparrow\rangle_j - |\downarrow\rangle_j)/\sqrt{2}$ and so annihilates the state $|\updownarrow\rangle_j \equiv (|\uparrow\rangle_j + |\downarrow\rangle_j)/\sqrt{2}$, while $\mathbb{1}_{j,j+1} - \sigma_j^z \sigma_{j+1}^z$ projects onto $|\uparrow\downarrow\rangle_{j,j+1}$ and $|\downarrow\uparrow\rangle_{j,j+1}$, and so annihilates $|\uparrow\uparrow\rangle_{j,j+1}$ and $|\downarrow\downarrow\rangle_{j,j+1}$. As each term in the Hamiltonian is a product of commuting projectors, the terms themselves are projectors. This

means that the smallest possible eigenvalue of the Hamiltonian itself is 0 and so any state annihilated by the Hamiltonian must be a ground state. The three states

$$|\mathcal{G}_\uparrow\rangle = |\uparrow\uparrow\cdots\uparrow\cdots\rangle\,, \qquad |\mathcal{G}_\downarrow\rangle = |\downarrow\downarrow\cdots\downarrow\cdots\rangle\,, \qquad \left|\mathcal{G}_\updownarrow\right\rangle = |\updownarrow\updownarrow\cdots\updownarrow\cdots\rangle\,, \quad (3.16)$$

are hence ground states. These are, in fact, the only linearly independent ground states as we will now show.

We start by considering $H_{j,j+1,j+2}$ from Equation 3.14. Of the eight basis states of sites $j, j+1, j+2$, four are annihilated by $H_{j,j+1,j+2}$:

$$\left|\mathcal{G}^{(3)}_{j,\uparrow}\right\rangle = |\uparrow\uparrow\uparrow\rangle\,, \quad \left|\mathcal{G}^{(3)}_{j,\downarrow}\right\rangle = |\downarrow\downarrow\downarrow\rangle\,, \quad \left|\mathcal{G}^{(3)}_{j,\updownarrow}\right\rangle = |\updownarrow\updownarrow\updownarrow\rangle\,, \quad (3.17)$$

$$\left|\mathcal{G}^{(3)}_{j,s}\right\rangle = |\uparrow\uparrow\downarrow\rangle + |\downarrow\uparrow\uparrow\rangle + |\downarrow\uparrow\downarrow\rangle - |\uparrow\downarrow\uparrow\rangle - |\uparrow\downarrow\downarrow\rangle - |\downarrow\downarrow\uparrow\rangle\,. \quad (3.18)$$

$\left|\mathcal{G}^{(3)}_{j,\updownarrow}\right\rangle$ is not orthogonal to $\left|\mathcal{G}^{(3)}_{j,\uparrow}\right\rangle$ or $\left|\mathcal{G}^{(3)}_{j,\downarrow}\right\rangle$, but they are linearly independent and are all orthogonal to $\left|\mathcal{G}^{(3)}_{j,s}\right\rangle$. It is then immediately clear that $|\mathcal{G}_\uparrow\rangle$, $|\mathcal{G}_\downarrow\rangle$ and $\left|\mathcal{G}_\updownarrow\right\rangle$ from Equations 3.16 are indeed ground states.

To work out if there are any other ground states, we consider the four sites $j-1, j, j+1, j+2$. Any state annihilated by $H_{j-1,j,j+1} + H_{j,j+1,j+2}$ must be a linear combination of the eight states $\left|\uparrow \mathcal{G}^{(3)}_{j,r}\right\rangle$, $\left|\downarrow \mathcal{G}^{(3)}_{j,r}\right\rangle$, where r is one of $\uparrow, \downarrow, \updownarrow$, or s. It must also be expressible as a linear combination of $\left|\mathcal{G}^{(3)}_{j-1,r'} \uparrow\right\rangle$, $\left|\mathcal{G}^{(3)}_{j-1,r'} \downarrow\right\rangle$, and so we need to find non-zero coefficients $\alpha_{\uparrow,r}$, $\alpha_{\downarrow,r}$, $\beta_{r',\uparrow}$, $\beta_{r',\downarrow}$ obeying

$$\sum_r \left(\alpha_{\uparrow,r}\left|\uparrow \mathcal{G}^{(3)}_{j,r}\right\rangle + \alpha_{\downarrow,r}\left|\downarrow \mathcal{G}^{(3)}_{j,r}\right\rangle\right) = \sum_{r'}\left(\beta_{r',\uparrow}\left|\mathcal{G}^{(3)}_{j-1,r'} \uparrow\right\rangle + \beta_{r',\downarrow}\left|\mathcal{G}^{(3)}_{j-1,r'} \downarrow\right\rangle\right). \quad (3.19)$$

Considering the 16 basis states, we see that all must have the same coefficient other than $|\uparrow\uparrow\uparrow\uparrow\rangle$ and $|\downarrow\downarrow\downarrow\downarrow\rangle$, the coefficients for which are unconstrained. Thus

$$|\uparrow\uparrow\uparrow\uparrow\rangle\,, \quad |\downarrow\downarrow\downarrow\downarrow\rangle\,, \quad |\updownarrow\updownarrow\updownarrow\updownarrow\rangle\,, \quad (3.20)$$

are the only linearly independent solutions. Repeating this along the chain, we see that the states in Equations 3.16 are the only ground states.

We find numerically that there is a finite gap from these ground states to the first excited state, meaning that $H(1,1)$ is gapped. As $H(1,0)$ is gapless and is

in the universality class of the Ising CFT, we must have a phase transition for some $H(1, \lambda_{\text{PT}})$, where $0 < \lambda_{\text{PT}} \leq 1$.

Before finding the location and nature of this phase transition, we first discuss the ground states given in Equations 3.16 in more detail. $|\mathcal{G}_\uparrow\rangle$ and $|\mathcal{G}_\downarrow\rangle$ are completely ordered in the σ^z-diagonal basis and are the ground states of the completely ordered Ising model: $H_{\text{order}} \equiv H_{\text{Ising}}(1, 0)$ from Equation 3.2, whereas $\left|\mathcal{G}_\updownarrow\right\rangle$ is completely disordered in the σ^z-diagonal basis and is the ground state of the completely disordered Ising model: $H_{\text{disorder}} \equiv H_{\text{Ising}}(0, 1)$. As the dual of H_{order} is H_{disorder} and our Hamiltonian $H(1, 1)$ is self-dual, if $|\mathcal{G}_\uparrow\rangle$ and $|\mathcal{G}_\downarrow\rangle$ are ground states, this automatically forces $\left|\mathcal{G}_\updownarrow\right\rangle$ to be a ground state too.

In fact, by combining H_{order} and $H(1, 1)$ as

$$H_o = \lambda_o H_{\text{order}} + \lambda_1 H(1, 1) \tag{3.21}$$

we have, for $\lambda_o, \lambda_1 \geq 0$, a line of Hamiltonians where $|\mathcal{G}_\uparrow\rangle$ and $|\mathcal{G}_\downarrow\rangle$ are ground states. $H(1, 1)$ is just where this line hits the self-dual line and so we require $\left|\mathcal{G}_\updownarrow\right\rangle$ to be a ground state too. Keeping $\lambda_1 > 0$ and now taking λ_o negative, we now see that $|\mathcal{G}_\uparrow\rangle$ and $|\mathcal{G}_\downarrow\rangle$ remain exact eigenstates, but they are no longer necessarily ground states.

3.3.2 The TCI transition

We know that, for $\lambda_I > 0$, a transition from the critical Ising phase to a gapped phase with three degenerate ground states occurs for some $0 < \lambda_3 \leq 1$ in $H(1, \lambda_3)$ (3.11). To find the location and nature of the transition, we use the methods described in Section 1.3. To get a rough idea of the type of transition and its location, we fix $\lambda_I = 1$ and find the half-chain entanglement entropy for the model at different λ_3 and lattice lengths L with periodic boundary conditions, as approximated by DMRG. Using Equation 2.22, along with the Ising and TCI CFTs having $m = 3$ and $m = 4$ in Equation 2.7, respectively, giving central charges

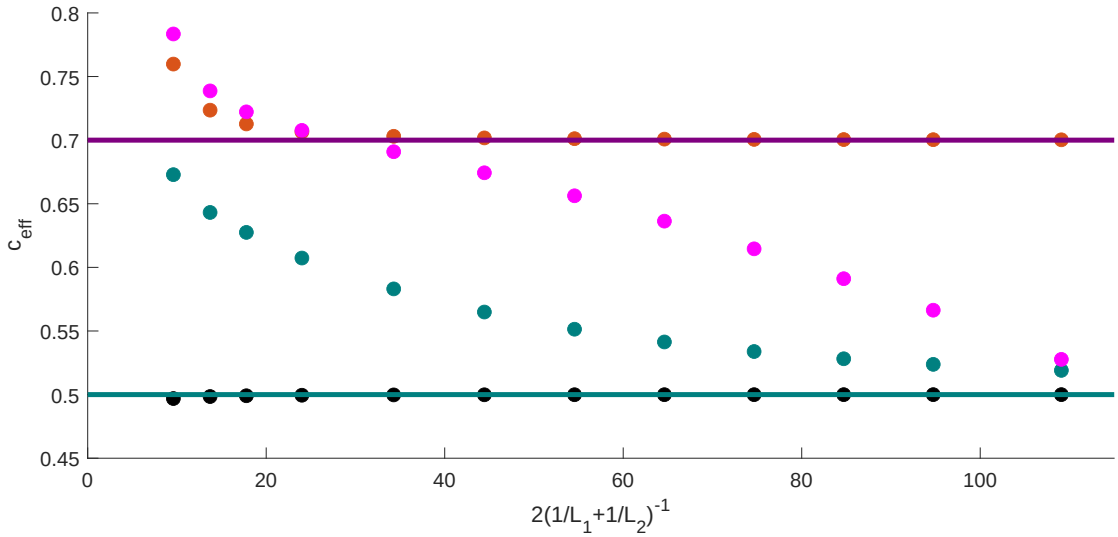

Figure 3.1: The effective central charge versus L. L_1 and L_2 are the two lattice lengths used to calculate c_{eff}. The black, green, red and mauve dots correspond to $\lambda_3/\lambda_I = 0,\ 0.8,\ 0.856,\ 0.87$ respectively, while the green and purple lines give the Ising and TCI predictions.

$c = 1/2$ and $c = 7/10$, we have that the entropy tends to

$$S_{\text{I}} = \frac{1}{6}\log L + C_{\text{I}}, \tag{3.22}$$

$$S_{\text{TCI}} = \frac{7}{20}\log L + C_{\text{TCI}}, \tag{3.23}$$

$$S_{\text{gapped}} = C_{\text{g}}, \tag{3.24}$$

for large L, where C_{I}, C_{TCI} and C_{g} are constants that depend on the exact lattice couplings. By considering two different lattice lengths L_1 and L_2, we find

$$c_{\text{eff}} = 3\,\frac{S(L_2) - S(L_1)}{\log \frac{L_1}{L_2}}, \tag{3.25}$$

where c_{eff} is the effective central charge.

In Figure 3.1 we plot c_{eff} versus L for $\lambda_3/\lambda_I = 0,\ 0.8,\ 0.856,\ 0.87$ in black, green, red and mauve respectively. The Ising and TCI predictions of 0.5 and 0.7 are given by the green and purple lines. c_{eff} seems to converge to the Ising line for $\lambda_3/\lambda_I = 0,\ 0.8$ as $L \to \infty$, while it approaches the TCI line for $\lambda_3/\lambda_I = 0.856$. As L increases, c_{eff} plummets for $\lambda_3/\lambda_I = 0.87$. This suggests that there may be a transition from an Ising phase to a gapped phase via a point in the universality class of the TCI model at $\lambda_3/\lambda_I \approx 0.856$.

CFT	c	$R_1 = \frac{A_0^- - P_0^+}{P_1^+ - P_0^+}$	$R_2 = \frac{P_0^- - P_0^+}{P_1^+ - P_0^+}$	$R_3 = \frac{P_1^- - P_0^+}{P_1^+ - P_0^+}$
Ising	1/2	1/2	1/8	9/8
TCI	7/10	7/2	3/8	35/8

Table 3.1: The central charge and three ratios for energy levels as predicted by the Ising and TCI CFTs.

The second test we do concerns the energy levels. Reproducing Equation 2.18, we have

$$\frac{E_\alpha - E_\beta}{E_\gamma - E_\delta} = \frac{\Delta_\alpha - \Delta_\beta}{\Delta_\gamma - \Delta_\delta}, \tag{3.26}$$

where Δ_α is the conformal dimension of the state in the CFT corresponding to the energy level E_α on the lattice. We consider both the positive and negative spin-flip sectors (denoted by $+$ and $-$), defined as the eigenvalue of the eigenstate under $\mathcal{F}$ (3.3), as well as both periodic and antiperiodic boundary conditions (P and A), where in antiperiodic boundary conditions any term in the Hamiltonian involving $\sigma_L^z\sigma_1^z$ picks up an extra minus sign. Finally, we consider the j^{th} excited state in each sector (j). For example, the first excited state with an eigenvalue of -1 under the spin-flip operator and with periodic boundary conditions is denoted by P_1^-.

The conformal dimensions of each of these have been worked out previously, (see e.g. [72, 85]) and from these we find the three ratios given in Table 3.1. These ratios were found using DMRG and are plotted against L for $\lambda_3 = 0$, 0.8, 0.856 and 0.87 in Figure 3.2. The green and purple lines give the theoretical values for the Ising and TCI CFTs respectively, while the ratio should diverge for the gapped region as P_0^+ and P_1^+ are degenerate in the continuum limit here. Subfigure (d) shows the ratio R_1 plotted against L for $\lambda_3 = 0.855$, $\lambda_3 = 0.856$, and $\lambda_3 = 0.857$.

Figure 3.2 shows the convergence to the predicted Ising ratios with increasing L for $\lambda_3/\lambda_I \lessapprox 0.856$ and diverging for $\lambda_3/\lambda_I \gtrapprox 0.856$, in agreement with a gapped region with degenerate ground states. At $\lambda_3/\lambda_I \approx 0.856$, the ratios approach the prediction of the TCI CFT, giving strong evidence that the transition is indeed in this universality class.

Continuing to increase the strength of λ_3 beyond the frustration-free point at $\lambda_I = \lambda_3$, the system remains in a phase of order-disorder coexistence, as confirmed by

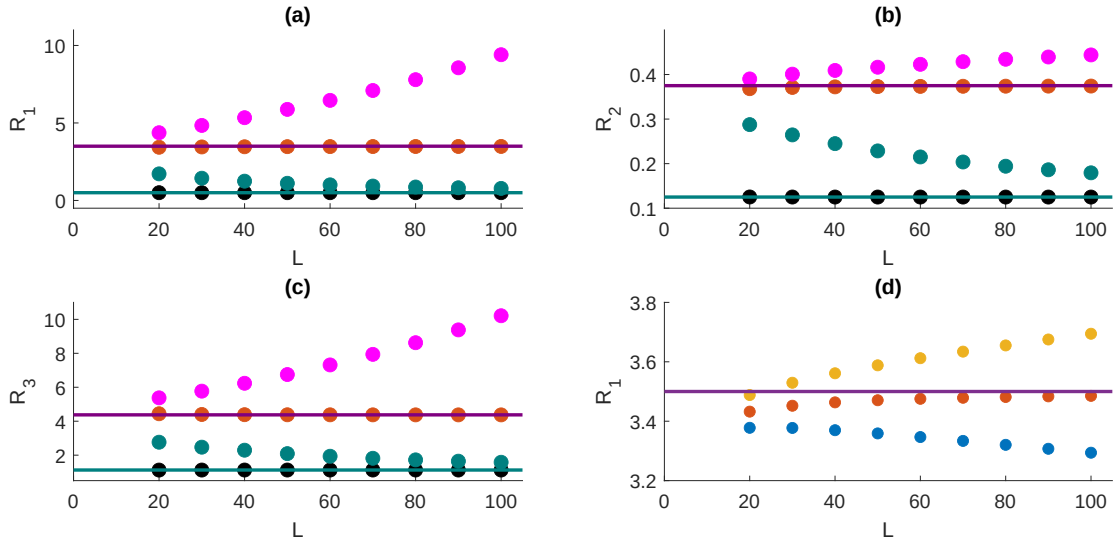

Figure 3.2: The three ratios R_1, R_2 and R_3 as defined in Table 3.1 are plotted against L in (a), (b) and (c) respectively. $\lambda_I = 1$ and λ_3 takes the values 0 (black), 0.8 (green), 0.856 (red) and 0.87 (mauve). In (d), R_1 is plotted against L for $\lambda_I = 1$ and λ_3 taking the values 0.855 (blue), 0.856 (red) and 0.857 (yellow).

Aasen *et al.* [41]. This phase survives until the extreme point $\lambda_I = 0$, $\lambda_3 > 0$, where the model in fact becomes free-fermionic [97]. This fascinating point has a ground state degeneracy exponentially large in the system size and is supersymmetric.

We have now shown several nice features of our model. We have a TCI point at a relative coupling strength of $\mathcal{O}(1)$ and the gapped region has a frustration-free prototypical point within it. There is one aspect that was mentioned earlier which has not yet been addressed though: supersymmetry. In the rest of this chapter we will explain the connection of our model to supersymmetry and extend it so that we find a line of exact supersymmetry.

3.4 Lattice supersymmetry

Before moving onto our lattice model, we first explain precisely what we mean by lattice supersymmetry [96]. Supersymmetry [98–100] is often considered in the context of high-energy physics as a means of extending beyond the standard model and solving the hierarchy problem [101–103]. It is normally thought of as associating a fundamental fermionic particle to each fundamental boson and vice versa. For example, each fermionic quark has a corresponding bosonic "squark".

We will define lattice supersymmetry with a similar link between bosonic and fermionic excitations. We call a Hamiltonian supersymmetric if it can be written in the form

$$H_{\mathrm{S}} = \mathcal{Q}^2 \tag{3.27}$$

for some fermionic and Hermitian operator $\mathcal{Q}$ [96]. This form has some immediate consequences. Firstly, the Hamiltonian is positive semi-definite. This can be seen by taking the expectation of the Hamiltonian in any state:

$$\langle\psi|H|\psi\rangle = \langle\psi|\mathcal{Q}\mathcal{Q}|\psi\rangle = |\mathcal{Q}\,|\psi\rangle|^2 \geq 0. \tag{3.28}$$

Secondly, $[H, \mathcal{Q}] = 0$ and so applying $\mathcal{Q}$ to any eigenstate of the Hamiltonian $|E\rangle$ with energy E necessarily either gives another state of energy E or annihilates the state:

$$H\left(\mathcal{Q}\,|E\rangle\right) = \mathcal{Q}H\,|E\rangle = \mathcal{Q}E\,|E\rangle = E\left(\mathcal{Q}\,|E\rangle\right). \tag{3.29}$$

Acting with $\mathcal{Q}$ again then brings the state back to its original form other than a factor of E ($\mathcal{Q}(\mathcal{Q}\,|E\rangle) = \mathcal{Q}^2\,|E\rangle = E\,|E\rangle$) and so we see that all states appear in doublets ($|E\rangle$ and $\mathcal{Q}\,|E\rangle$), other than zero energy states. As applying a fermionic operator, $\mathcal{Q}$, turns a state from bosonic to fermionic and vice versa, we can view these doublets as boson-fermion pairs.

3.4.1 A fermionic example

As an example of a supersymmetric lattice model, we turn to the model studied recently by Sannomiya, Katsura and Nakayama [104], an extension of a system first investigated by Nicolai [105]. In this model the Hamiltonian is taken to be

$$H = \left\{\mathcal{Q}, \mathcal{Q}^\dagger\right\}, \tag{3.30}$$

where

$$\mathcal{Q} = \sum_{k=1}^{N/2} g c_{2k-1} + c_{2k-1} c_{2k}^\dagger c_{2k+1} \tag{3.31}$$

and the c_k are fermionic operators obeying

$$\{c_i, c_j^\dagger\} = \delta_{i,j}, \qquad \{c_i, c_j\} = \{c_i^\dagger, c_j^\dagger\} = 0. \tag{3.32}$$

(In Nicolai's original model there was no single fermion term in $\mathcal{Q}$ and so $g = 0$.)

As $\mathcal{Q}^2 = 0$, we see that the Hamiltonian can be rewritten as

$$H = \left(\mathcal{Q} + \mathcal{Q}^\dagger\right)^2 \tag{3.33}$$

and so, the Hamiltonian is supersymmetric.

Sannomiya *et al.* found that, for $g > 0$, there is a non-degenerate ground state and the long-range behaviour of the model is described by a CFT with central charge $c = 1$, to be contrasted with the case $g = 0$ where there is an exponentially large number of ground states. This is similar to the free-fermion point in our model mentioned above [97] and the connection between the Hamiltonians will soon become clear!

Before moving on to the supersymmetric version of our model, we briefly mention a second model based on fermions studied by Sannomiya *et al.* In this case the Hamiltonian takes the same form as Equation 3.30, but with $\mathcal{Q}$ replaced by

$$\mathcal{Q} = \sum_{j=1}^{N} g c_j + c_{j-1} c_j c_{j+1}. \tag{3.34}$$

In this model, again, there is an exponentially large number of ground states for $g = 0$, but the behaviour is subtly different for $g \neq 0$. While there is a finite number of ground states, the dispersion relation is not linear in momentum as it was for the previous case, but is instead cubic – i.e. $E(k) \propto k^3$ for low-lying states [106]. This dispersion relation breaks Lorentz invariance and means that the system cannot be described by a CFT. Interestingly, we will find that our supersymmetric line also has a cubic dispersion relation [92].

3.5 Our chiral model

The Sannomiya Hamiltonians (3.30 and 3.31 or 3.34) were built from fermionic operators with canonical anticommutation relations, but we have seen that our Hamiltonian (3.11) is more naturally expressed in terms of Majorana fermions. Majoranas in fact have an advantage over conventional fermions in constructing supercharges, Q: $\gamma_a^\dagger = \gamma_a$ and so to get an hermitian supercharge we can just consider a single sum over γ_a, rather than sums over both c_k and $c_k^\dagger$. The $\mathcal{Q}$ analogous to Equation 3.34 in terms of Majoranas is

$$\mathcal{Q}^+(\lambda_I, \lambda_3) = \frac{1}{2\sqrt{\lambda_3}} \sum_{a=1}^{2L} \left(\lambda_I \gamma_a + i\lambda_3 \gamma_{a-1}\gamma_a\gamma_{a+1}\right), \tag{3.35}$$

where the i in the second term is required for $\mathcal{Q}^+$ to be hermitian.

A supersymmetric Hamiltonian can then be constructed as

$$H_{\mathrm{S}}^+(\lambda_I, \lambda_3) = \left(\mathcal{Q}^+(\lambda_I, \lambda_3)\right)^2, \tag{3.36}$$

which we will now discuss and was the subject of Ref. [92]. Calculating $H_{\mathrm{S}}^+(\lambda_I, \lambda_3)$ explicitly, we find

$$H_{\mathrm{S}}^+(\lambda_I, \lambda_3) = L\frac{\lambda_I^2 + \lambda_3^2}{2\lambda_3} + \sum_{b=1}^{2L}\left[i\lambda_I\left(\gamma_b\gamma_{b+1} - \frac{1}{2}\gamma_{b-1}\gamma_{b+1}\right) - \frac{1}{2}\lambda_3\gamma_{b-2}\gamma_{b-1}\gamma_{b+1}\gamma_{b+2}\right], \tag{3.37}$$

where the constant in front assumes periodic boundary conditions in Majoranas. Going to the spin basis, and again sweeping the boundary conditions under the carpet, we find that, up to a constant,

$$H_{\mathrm{S}}^+(\lambda_I, \lambda_3) = \lambda_I H_I + \frac{1}{2}\lambda_3 H_3 + \frac{1}{2}\lambda_c H_c, \tag{3.38}$$

where

$$H_c = \sum_{j=1}^{L}\left(\sigma_j^y\sigma_{j+1}^z - \sigma_j^z\sigma_{j+1}^y\right). \tag{3.39}$$

Up to this H_c term, Equations 3.38 and 3.11 are the same! The extra term given by H_c is clearly chiral due to the minus sign – supersymmetry has come at the price of breaking spatial parity.

3.5.1 Supersymmetry operators in the non-chiral model

Before studying this supersymmetric model in detail, we first consider a similar Hamiltonian, built from the supercharge

$$\mathcal{Q}^-(\lambda_I,\lambda_3)=\frac{1}{2\sqrt{\lambda_3}}\sum_{a=1}^{2L}(-1)^a\left(\lambda_I\gamma_a-i\lambda_3\gamma_{a-1}\gamma_a\gamma_{a+1}\right), \tag{3.40}$$

giving

$$\begin{aligned} H_S^-(\lambda_I,\lambda_3)&=\left(\mathcal{Q}^-(\lambda_I,\lambda_3)\right)^2, \\ &=L\frac{\lambda_I^2+\lambda_3^2}{2\lambda_3}+\sum_{b=1}^{2L}\left[i\lambda_I\left(\gamma_b\gamma_{b+1}+\frac{1}{2}\gamma_{b-1}\gamma_{b+1}\right)-\frac{1}{2}\lambda_3\gamma_{b-2}\gamma_{b-1}\gamma_{b+1}\gamma_{b+2}\right]. \end{aligned} \tag{3.41}$$

We then see that Equation 3.11 can be written as

$$H(\lambda_I,\lambda_3)=\left(\mathcal{Q}^+(\lambda_I,\lambda_3)\right)^2+\left(\mathcal{Q}^-(\lambda_I,\lambda_3)\right)^2 \tag{3.42}$$

and so our original non-chiral line can be written as the sum of two chiral supersymmetric Hamiltonians. Note that, as the anticommutator $\{\mathcal{Q}^+,\mathcal{Q}^-\}$ is non-trivial, the Hamiltonian itself is not supersymmetric.

As mentioned in Chapter 2, an SCFT has supercurrents G and $\bar{G}$ corresponding to operators of weights $(3/2,0)$ and $(0,3/2)$ respectively [72]. The Hamiltonian of the field theory can then be written as

$$H_{\text{field theory}}=\left(\int dx\, G\right)^2+\left(\int dx\,\bar{G}\right)^2. \tag{3.43}$$

As this form is very similar to $H(\lambda_I,\lambda_3)$ (3.42), it is tempting to make the identification

$$\mathcal{Q}^+\to\int G,\qquad \mathcal{Q}^-\to\int\bar{G}, \tag{3.44}$$

as we take the continuum limit. We would then hope that we could find $Q^+=\sum_j G_j$, where G_j are local operators and have the same correlation functions as the CFT operators in the long-distance limit. The most obvious identification is

$$\mathcal{G}_j\equiv\lambda_I\gamma_{2j}+i\lambda_3\gamma_{2j-1}\gamma_{2j}\gamma_{2j+1}, \tag{3.45}$$

but this turns out to be slightly wrong. The issue is that, in the TCI CFT, there are other fermionic fields more relevant than G and $\bar{G}$: ψ and $\bar{\psi}$ with weights $(3/5, 1/10)$ and $(1/10, 3/5)$ respectively. Generically, a lattice operator will contain every field obeying its symmetries, as happens, for example, in the identification of the parafermion field in the three-state Potts model [107]. Thus, the correlator at long distances is dominated by the most relevant allowed operator and so,

$$\langle \mathcal{G}_j \mathcal{G}_k \rangle \sim |j-k|^{-7/5} \tag{3.46}$$

in the limit $|j-k| \gg 1$.

Following the method of Ref. [107], the correct way to remove the unwanted ψ and $\bar{\psi}$ fields from the lattice operators is to consider duality. G, Q^+ and $\bar{\psi}$ are even under duality, while $\bar{G}$, Q^- and ψ are odd [93, 94]. This leads to the identifications

$$G_j = \lambda_I \left(\gamma_{2j-1} + \gamma_{2j}\right) + i\lambda_3 \left(\gamma_{2j-2}\gamma_{2j-1}\gamma_{2j} + \gamma_{2j-1}\gamma_{2j}\gamma_{2j+1}\right), \tag{3.47}$$

$$\bar{G}_j = \lambda_I \left(\gamma_{2j-1} - \gamma_{2j}\right) - i\lambda_3 \left(\gamma_{2j-2}\gamma_{2j-1}\gamma_{2j} - \gamma_{2j-1}\gamma_{2j}\gamma_{2j+1}\right), \tag{3.48}$$

$$\psi_j = \lambda_I \left(\gamma_{2j-1} - \gamma_{2j}\right) + i\lambda_3 \left(\gamma_{2j-2}\gamma_{2j-1}\gamma_{2j} - \gamma_{2j-1}\gamma_{2j}\gamma_{2j+1}\right), \tag{3.49}$$

$$\bar{\psi}_j = \lambda_I \left(\gamma_{2j-1} + \gamma_{2j}\right) - i\lambda_3 \left(\gamma_{2j-2}\gamma_{2j-1}\gamma_{2j} + \gamma_{2j-1}\gamma_{2j}\gamma_{2j+1}\right). \tag{3.50}$$

These were checked by finding the two-point functions at the TCI point, with the results shown in Figure 3.3. These were calculated using DMRG on a lattice with open boundary conditions and length $L = 400$. As can be seen, the correlators converge nicely to the values expected from Equation 2.16 of

$$\langle G_j G_k \rangle \sim |j-k|^{-2\Delta_G} \sim |j-k|^{-3}, \quad \langle \psi_j \psi_k \rangle \sim |j-k|^{-2\Delta_\psi} \sim |j-k|^{-1.4}. \tag{3.51}$$

Now that we have seen the supersymmetry generators on the non-chiral line, we define the more general Hamiltonian

$$\begin{aligned} \tilde{H}(\lambda_I, \lambda_3, \lambda_c) &= \left(1 + \frac{\lambda_c}{\lambda_I}\right) {Q^+}^2(\lambda_I, \lambda_3) + \left(1 - \frac{\lambda_c}{\lambda_I}\right) \mathcal{Q}^{-2}(\lambda_I, \lambda_3) \\ &= 2\lambda_I H_I + \lambda_3 H_3 + \lambda_c H_c + E_0. \end{aligned} \tag{3.52}$$

The non-chiral line given by Equation 3.11 corresponds to $\tilde{H}(\lambda_I, \lambda_3, 0)$, while the supersymmetric line given by Equation 3.38 is $\tilde{H}(\lambda_I, \lambda_3, \lambda_I)$.

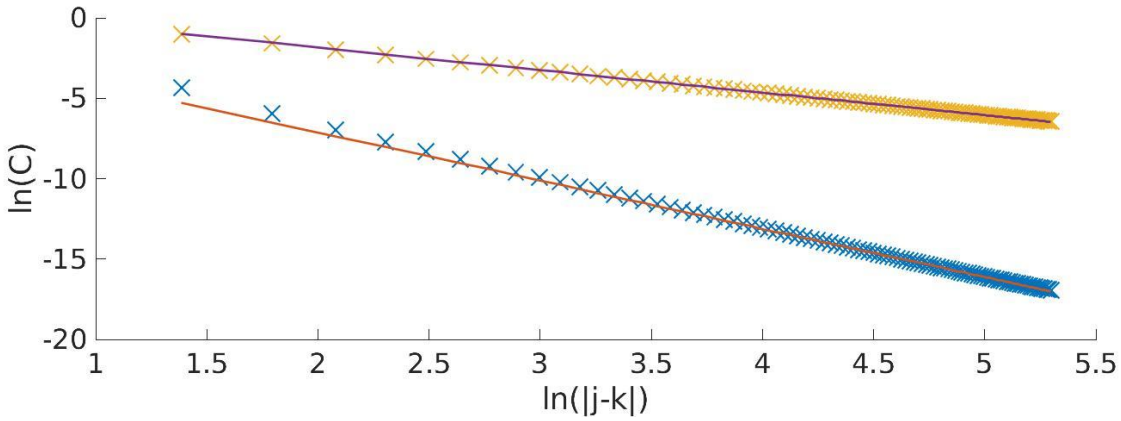

Figure 3.3: The two point correlators $C_{jk} = \langle G_j G_k \rangle$ (blue crosses) and $\langle \psi_j \psi_k \rangle$ (yellow crosses), from Equations 3.47 and 3.49, are plotted against $|j-k|$ at the tricritical point $\lambda_3/\lambda_I = 0.856$. The red and purple lines correspond to $A|j-k|^{-3}$ and $B|j-k|^{-1.4}$, respectively, where A and B are fitting parameters.

3.5.2 The free-fermionic line

Before looking at this model generally, we will focus on the special case $\lambda_3 = 0$. Here the Hamiltonian reduces to

$$\tilde{H}(\lambda_I, 0, \lambda_c) = i \sum_{a=1}^{2L} (2\lambda_I \gamma_a \gamma_{a+1} - \lambda_c \gamma_a \gamma_{a+2}) \tag{3.53}$$

and is free-fermionic, meaning that we can solve it exactly. In this case we will have to be careful about boundary conditions to get the exact spectra and so we define a new Hamiltonian

$$H_{I,c} = i \sum_{a=1}^{2L} (2\lambda_a \gamma_a \gamma_{a+1} - \kappa_a \gamma_{a-1} \gamma_{a+1}), \tag{3.54}$$

where we have made the coupling site dependent to make boundary conditions easier to deal with. L is the length of the lattice of spins and hence the Majorana lattice extends to $2L$.

To solve this, we first construct raising and lowering operators, designed to obey

$$[H_{I,c}, \Psi] = 2\epsilon\Psi, \tag{3.55}$$

as then, if $|E\rangle$ is an eigenstate of H obeying $H|E\rangle = E|E\rangle$, $\Psi|E\rangle$ will either be an eigenstate obeying $H(\Psi|E\rangle) = (E + 2\epsilon)\Psi|E\rangle$ or will be a null vector. Defining

$$\Psi = \sum_{a=1}^{2L} \mu_a \gamma_a, \tag{3.56}$$

where μ_j is arbitrary, and using

$$[\gamma_a\gamma_b, \gamma_c] = \gamma_a\delta_{bc} - \gamma_b\delta_{ac}, \tag{3.57}$$

we arrive at

$$[H, \Psi] = \sum_{a=1}^{2L} \mu'_a\gamma_a, \tag{3.58}$$

where

$$\mu'_a = i\left(2\lambda_a\mu_{a+1} - 2\lambda_{a-1}\mu_{a-1} - \kappa_{a+1}\mu_{a+2} + \kappa_{a-1}\mu_{a-2}\right). \tag{3.59}$$

For a given set of λ_a and κ_a we can now find every creation and annihilation operator. The ground state must be the state annihilated by all operators which lower the energy but not annihilated by any of those which raise it.

For the self-dual and translation invariant model with periodic boundary conditions (in terms of Majoranas), we set $\lambda_a = \lambda_I$ and $\kappa_a = \lambda_c\ \forall a$. We can then solve Equations 3.56, 3.58 and 3.59 using the Ansatz

$$\mu_a = \mu e^{ika}, \tag{3.60}$$

where $k = n\pi/L$, $n = -L+1, -L+2, ..., -1, 0, 1, ..., L-1, L$. These give the energies

$$2\epsilon_k = -4\sin(k)\left(\lambda_I - \lambda_c\cos(k)\right). \tag{3.61}$$

From this it is clear that $\epsilon_{-k} = -\epsilon_k$ and from Equations 3.56 and 3.60 we see that

$$\Psi_{-k} = \Psi_k^\dagger, \qquad \{\Psi_k, \Psi'_k\} = 2\delta_{k',-k}, \tag{3.62}$$

where we have taken $\mu = 1/\sqrt{2L}$, allowing us to identify Ψ_k with an annihilation operator for $0 < k < \pi$ and Ψ_{-k} the corresponding creation operator, assuming $\lambda_c \leq \lambda_I$.

The above construction is clear unless $k = 0$ or $k = \pi$, where $\epsilon_k = 0$ and the creation and annihilation operators coincide. We see that, if Ψ_0 is an allowed operator in terms of boundary conditions and number of states, then Ψ_π must be too and vice versa. We therefore take the combinations

$$\Psi_+ = \frac{1}{\sqrt{2}}\left(\Psi_0 + i\Psi_\pi\right), \qquad \Psi_- = \frac{1}{\sqrt{2}}\left(\Psi_0 - i\Psi_\pi\right), \tag{3.63}$$

which then satisfy $\{\Psi_+, \Psi_+\} = \{\Psi_-, \Psi_-\} = 0$ and $\{\Psi_+, \Psi_-\} = 2$, along with $[H, \Psi_+] = [H, \Psi_-] = 0$. We make the arbitrary choice that Ψ_+ is a creation operator, while Ψ_- is an annihilation operator. We now have L independent creation operators, each with a corresponding annihilation operator, and so have spanned the whole space.

Before declaring victory, we pause to consider the above result. With periodic boundary conditions we have a creation operator that does not change the energy. Applying this to the ground state should then give a second state of zero energy, but we know that there is a single identity operator in a CFT and so, for periodic boundary conditions in terms of spins, there should be a unique ground state, at least at the point $\lambda_c = 0$ where we know the model to be described by the Ising CFT. This is resolved by considering the various boundary conditions for spins and Majoranas – periodic in one does not necessarily correspond to periodic in the other!

To see how the boundary conditions should transform, we consider the explicit Hamiltonian in terms of spins with periodic boundary conditions:

$$H_{\text{spins}} = -\sum_{j=1}^{L}\Big[\lambda_I\left(\sigma_j^x + \sigma_j^z\sigma_{j+1}^z\right) + \lambda_3\left(\sigma_j^z\sigma_{j+1}^y - \sigma_j^y\sigma_{j+1}^z\right)\Big], \tag{3.64}$$

where $\sigma_{L+1}^{x,y,z} \equiv \sigma_1^{x,y,z}$, so the Hamiltonian is periodic. To rewrite this Hamiltonian in terms of Majoranas, we reproduce Equations 1.15:

$$\sigma_j^x = -i\gamma_{2j-1}\gamma_{2j}, \qquad \sigma_j^z\sigma_{j+1}^z = -i\gamma_{2j}\gamma_{2j+1}, \tag{3.65}$$

which allows us to write

$$\sigma_j^z\sigma_{j+1}^y = -i\sigma_j^z\sigma_{j+1}^z\sigma_{j+1}^x = i\gamma_{2j}\gamma_{2j+2}, \tag{3.66}$$

and, similarly, $\sigma_j^y\sigma_{j+1}^z = -i\gamma_{2j-1}\gamma_{2j+1}$. These expressions, along with those for σ_j^x and $\sigma_j^z\sigma_{j+1}^z$ (3.65), are perfectly sensible unless $j = L$, in which case γ_{2j+1} and γ_{2j+2} are not yet defined. To work out what these should be, we consider the specific offending terms in Equation 3.64:

$$H_{\text{offending}} = -\lambda_I\sigma_1^z\sigma_L^z + \lambda_3\left(\sigma_1^z\sigma_L^y - \sigma_1^y\sigma_L^z\right). \tag{3.67}$$

We will deal with the first of these terms explicitly, with the treatments of the others following analogously. We can write $-\lambda_I \sigma_1^z \sigma_L^z$ as

$$\begin{aligned} -\lambda_I \sigma_1^z \sigma_L^z &= -\lambda_I \sigma_1^z \left(\prod_{j=2}^{L-1} \sigma_j^z \sigma_j^z \right) \sigma_L^z \\ &= -\lambda_I \prod_{j=1}^{L-1} \left(\sigma_j^z \sigma_{j+1}^z \right) \\ &= -\lambda_I \prod_{j=1}^{L-1} \left(-i \gamma_{2j} \gamma_{2j+1} \right) \\ &= -(-i)^{L-1} \lambda_I \prod_{a=2}^{2L-1} \gamma_a . \end{aligned} \tag{3.68}$$

All we seem to have done is expressed our operator in terms of a long chain of Majoranas! Fortunately, the symmetry of the model comes to our aid. We know that the spin-flip operator, $\mathcal{F}$ (3.3), is a symmetry. Rewriting this in terms of Majoranas we get

$$\begin{aligned} \mathcal{F} &= \prod_{j=1}^{L} \sigma_j^x \\ &= \prod_{j=1}^{L} \left(-i \gamma_{2j-1} \gamma_{2j} \right) \\ &= (-i)^L \prod_{a=1}^{2L} \gamma_a . \end{aligned} \tag{3.69}$$

We can then rewrite Equation 3.68 as

$$\begin{aligned} -\lambda_I \sigma_1^z \sigma_L^z &= -i \lambda_I \gamma_1 \mathcal{F} \gamma_L \\ &= -i \lambda_I \gamma_L \gamma_1 \mathcal{F}, \end{aligned} \tag{3.70}$$

and so we see that the sign of this term depends on the eigenvalue of the state under $\mathcal{F}$. The same holds for the other two offending terms and we find that we have periodic boundary conditions ($\gamma_{2L+1} = \gamma_1$, $\gamma_{2L+2} = \gamma_2$) for states with an eigenvalue of -1 under $\mathcal{F}$, while we have antiperiodic boundary conditions ($\gamma_{2L+1} = -\gamma_1$, $\gamma_{2L+2} = -\gamma_2$) for states with an eigenvalue of $+1$ under $\mathcal{F}$.

We now see how to proceed: split the Hamiltonian into sectors odd and even under $\mathcal{F}$, then solve the model with the appropriate boundary conditions in terms

of Majoranas. The only difference for antiperiodic boundary conditions is the values k can take in Equation 3.60 – now $k = (n - 1/2)\pi/L$ for $n = -L + 1, -L + 2, ..., -1, 0, 1, ..., L - 1, L$.

Starting in the $\mathcal{F} = 1$ sector, we need antiperiodic boundary conditions. Our ground state (for $\lambda_c \leq \lambda_I$) is then annihilated by all Ψ_k with $k < 0$ and by none of those with $k > 0$, giving an energy of

$$\begin{aligned} E^{(0)}_{\mathcal{F}=1} &= -4\sum_{n=0}^{L-1} \sin\left(\frac{(2n+1)\pi}{2L}\right)\left(\lambda_I - \lambda_c \cos\left(\frac{(2n+1)\pi}{2L}\right)\right) \\ &= -4\lambda_I \sum_{n=0}^{L-1} \sin\left(\frac{(2n+1)\pi}{2L}\right) \\ &= -4\lambda_I \text{cosec}\left(\frac{\pi}{2L}\right), \end{aligned} \tag{3.71}$$

where the second term in the first line vanishes as it reduces to summing sine functions symmetrically over a whole period. This shows that, for $|\lambda_c| \leq \lambda_I$, the ground-state energy is independent of λ_I!

As all states must have the same value of $\mathcal{F}$ within a sector, we can only get between them by applying an even number of Ψ_k operators. The first excited state must then be the state obtained by acting with the two lowest energy creation operators: $\Psi_{-\pi/L}$ and $\Psi_{-\pi+\pi/L}$, giving

$$E^{(1)}_{\mathcal{F}=1} = E^{(0)}_{\mathcal{F}=1} + 8\sin\left(\frac{\pi}{2L}\right)\left(\lambda_I - \lambda_c \cos\left(\frac{\pi}{2L}\right)\right). \tag{3.72}$$

Further excited states are found by applying further creation operators, but always in pairs.

Going next to the case with $\mathcal{F} = -1$, we require periodic boundary conditions. As we had L Ψ_k operators annihilating the ground state in the $\mathcal{F} = 1$ sector, here $L - 1$ must annihilate it so that $\mathcal{F} = -1$. This gives an energy of

$$\begin{aligned} E^{(0)}_{\mathcal{F}=-1} &= -4\sum_{n=1}^{L-1} \sin\left(\frac{n\pi}{L}\right)\left(\lambda_I - \lambda_c \cos\left(\frac{n\pi}{L}\right)\right) \\ &= -4\lambda_I \sum_{n=1}^{L-1} \sin\left(\frac{n\pi}{L}\right) \\ &= -4\lambda_I \text{cot}\left(\frac{\pi}{L}\right). \end{aligned} \tag{3.73}$$

Again, to get the first excited state we must now act with two creation operators. One of these will be Ψ_+ as it has zero energy, but there are two choices for the second: $\Psi_{-\pi/L}$ and $\Psi_{-\pi+\pi/L}$. We then have two degenerate first excited states of energy

$$E^{(1)}_{\mathcal{F}=-1} = E^{(0)}_{\mathcal{F}=-1} + 4\sin\left(\frac{\pi}{L}\right)\left(\lambda_I - \lambda_c \cos\left(\frac{\pi}{L}\right)\right). \tag{3.74}$$

To do a sanity check on our results before moving on, we consider the pure Ising model ($\lambda_c = 0$). Taking the limit $L \to \infty$ we find

$$E^{(0)}_{\mathcal{F}=1} = -\frac{2v}{\pi}L + \frac{2\pi v}{L}\left(-\frac{1/2}{12} + 0 + 0\right) + \mathcal{O}\left(\frac{1}{L^3}\right), \tag{3.75}$$

$$E^{(1)}_{\mathcal{F}=1} = -\frac{2v}{\pi}L + \frac{2\pi v}{L}\left(-\frac{1/2}{12} + \frac{1}{2} + \frac{1}{2}\right) + \mathcal{O}\left(\frac{1}{L^3}\right), \tag{3.76}$$

$$E^{(0)}_{\mathcal{F}=-1} = -\frac{2v}{\pi}L + \frac{2\pi v}{L}\left(-\frac{1/2}{12} + \frac{1}{16} + \frac{1}{16}\right) + \mathcal{O}\left(\frac{1}{L^3}\right), \tag{3.77}$$

$$E^{(1)}_{\mathcal{F}=-1} = -\frac{2v}{\pi}L + \frac{2\pi v}{L}\left(-\frac{1/2}{12} + \frac{17}{16} + \frac{1}{16}\right) + \mathcal{O}\left(\frac{1}{L^3}\right), \tag{3.78}$$

where $v = 4\lambda_I$ is the Fermi velocity. We see that the gaps are in agreement with the CFT predictions of the dimensions from Equation 2.17: for $\mathcal{F} = 1$ the ground state is the identity operator with $(h, \bar{h}) = (0, 0)$, while the first excited state is the energy operator with weights $(1/2, 1/2)$. In the $\mathcal{F} = -1$ sector, the lowest energy state is the spin operator with weights $(1/16, 1/16)$, while the two degenerate first excited states have weights $(17/16, 1/16)$ and $(1/16, 17/16)$.

3.5.3 The chiral free-fermionic model

Now that we have checked that the results of the Ising CFT are correctly reproduced at $\lambda_c = 0$, we move on to consider general λ_c (for $\lambda_I \geq 0$). Reproducing the energy of the operator Ψ_k from Equation 3.61,

$$2\epsilon_k = -4\sin(k)\left(\lambda_I - \lambda_c \cos(k)\right), \tag{3.79}$$

we see that for $|\lambda_c| < \lambda_I$, Ψ_k with $-\pi < k < 0$ continue to have positive energy and those with $0 < k < \pi$ continue to have negative energy, meaning that our creation and annihilation operators remain the same. This means that, although the energies in the spectrum change, the ground state remains the same throughout

this region. There is an important change though: ϵ_k is no longer equal to $\epsilon_{\pi-k}$ due to the effect of the $\cos(k)$ factor. This makes the model chiral and leads to different Fermi velocities for the left- and right-moving eigenstates.

At $\lambda_c = \lambda_I$, something more significant happens though. At this point the energies become

$$\begin{aligned} 2\epsilon_k^S &= -4\lambda_I \sin k \,(1 - \cos k) \\ &= -4 \sin k + 2 \sin (2k) \,. \end{aligned} \tag{3.80}$$

Expanding this for small k we find

$$2\epsilon_k^S = -2k^3 + \mathcal{O}\left(k^5\right), \tag{3.81}$$

showing that the model now has cubic dispersion within each sector. Note that around $k = \pi$, the dispersion is still linear though and, as we have seen that the gap between the $\mathcal{F}$ sectors is independent of λ_c for $|\lambda_c| \leq \lambda_I$, the gap between the sectors remains $\sim 1/L$.

Taking $\lambda_c > \lambda_I$, we see that which Ψ_k are creation operators and which are annihilation operators now begins to change. The critical values of k where the energies are 0 are $k = 0$, π, $\operatorname{acos}(\lambda_I/\lambda_c)$, $-\operatorname{acos}(\lambda_I/\lambda_c)$. In Figure 3.4, $2\epsilon_k$ is plotted against k for 5 different pairs of λ_I and λ_c. The blue, red, yellow and purple lines correspond to $\lambda_I = 1$ and $\lambda_c = 0$, 0.8, 1, and 1.2 respectively, while the green line is $\lambda_I = 0$, $\lambda_c = 1$. As can be seen, for $\lambda_c < \lambda_I$, there are zeros at $k = 0, \pi$, while for $\lambda_c > \lambda_I$ a further pair of zeros occur at $k = \pm \operatorname{acos}(\lambda_I/\lambda_c)$. The yellow line, corresponding to $\lambda_c = \lambda_I$ is flat at the $k = 0$, indicating the k^3 dispersion here.

For $\lambda_c < \lambda_I$, the model is still in an Ising phase, just with different Fermi velocities for the left- and right-moving parts. For $\lambda_c > \lambda_I$ the phase is completely different and is in fact incommensurate. Changing either λ_c or L changes the Ψ_k operators with negative energy, meaning that the ground state jumps between momentum sectors. As we will see later, this behaviour continues as λ_3 is added and the model is no longer exactly solvable.

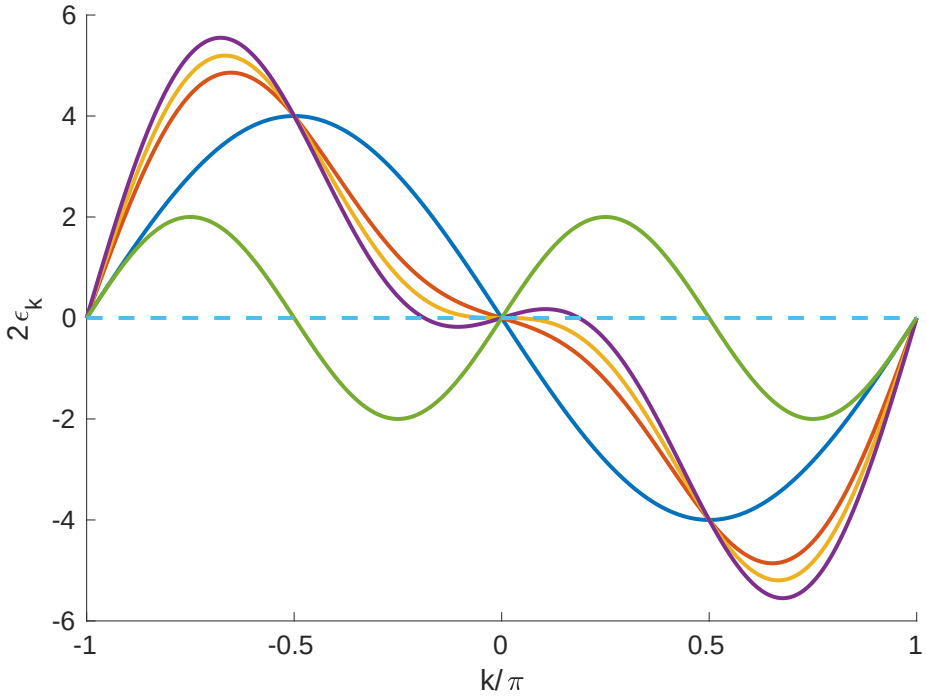

Figure 3.4: $2\epsilon_k$ is plotted against k using Equation 3.61 for $\lambda_I = 1$, $\lambda_c = 0$ (blue), 0.8 (red), 1 (yellow), and 1.2 (purple) and for $\lambda_I = 0$, $\lambda_c = 1$ (green).

Before investigating this general case, we first consider the extreme point given by $\lambda_I = \lambda_3 = 0$, $\lambda_c = 1$, corresponding to the green line in Figure 3.4. Here the Hamiltonian is simply

$$\begin{aligned} H_{c=1} &= -i \sum_{a=1}^{2L} \gamma_a \gamma_{a+2} \\ &= -i \sum_{j=1}^{L} \gamma_{2j-1}\gamma_{2j+1} + \gamma_{2j}\gamma_{2j+2}, \end{aligned} \tag{3.82}$$

and so it turns into two copies of the Ising model, albeit with non-trivial boundary conditions. This point is thus a CFT of central charge $c = 1$.

3.5.4 The general chiral model

We now turn to the general case with $\lambda_3 \neq 0$. This model is interacting and so cannot be solved exactly, but we will see that many of the qualitative features remain the same. Returning to $\tilde{H}(\lambda_I, \lambda_3, \lambda_c)$ (3.52), we see that, for $|\lambda_c| < \lambda_I$, the

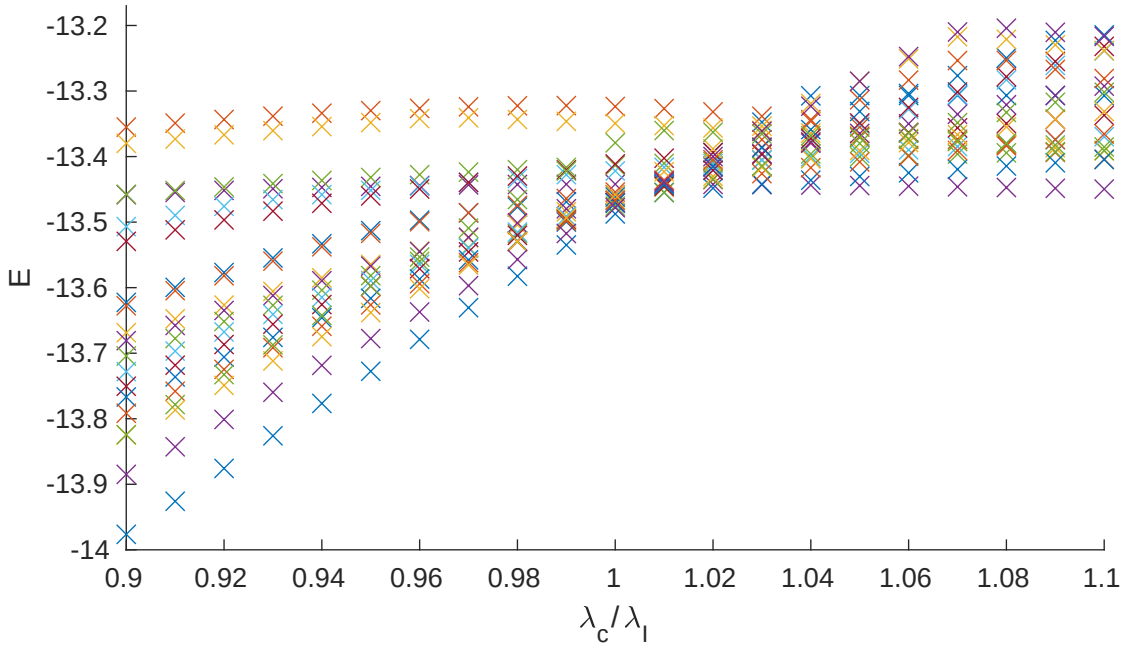

Figure 3.5: The incommensurate transition for $\lambda_3/\lambda_I = 0.856$ and $L = 19$. The crosses give the lowest energy levels in each momentum sector, with $k = 0$ in blue.

coefficients of both $(Q^+)^2$ and $(Q^-)^2$ are positive, while for $\lambda_c > \lambda_I$, the coefficient of $(Q^-)^2$ is negative. This has a profound effect on the physics as we will now explain.

As $(Q^+)^2$ is the square of an hermitian operator, its eigenvalues are positive semi-definite and so the eigenvalues of $\tilde{H}(\lambda_I, \lambda_3, \lambda_c)$ are bounded from below by 0 for $|\lambda_c| < \lambda_I$. There is no bound on the maximum eigenvalue of $(Q^+)^2$ though (at least in the thermodynamic limit), so for $\lambda_c > \lambda_I$ the ground state can change rapidly with both L and the coupling strengths, leading to incommensurate behaviour. This incommensurability is demonstrated in Figure 3.5, where the lowest energy levels in each momentum sector are plotted against λ_c/λ_I for $\lambda_3/\lambda_I = 0.856$ and $L = 19$. The blue crosses are the $k = 0$ states and remain the ground states until $\lambda_c/\lambda_I \approx 1$ when the levels start crossing frequently, indicating the beginning of the incommensurate phase.

The Ising and gapped phases are found to survive up to the supersymmetric line as has been confirmed both by us and recently in Ref. [41]. The TCI point in the non-chiral model becomes a line when H_c is added and is found to remain at the same λ_3/λ_I to within about 5% up to $\lambda_c = \lambda_I$. Moreover, as the three exact ground

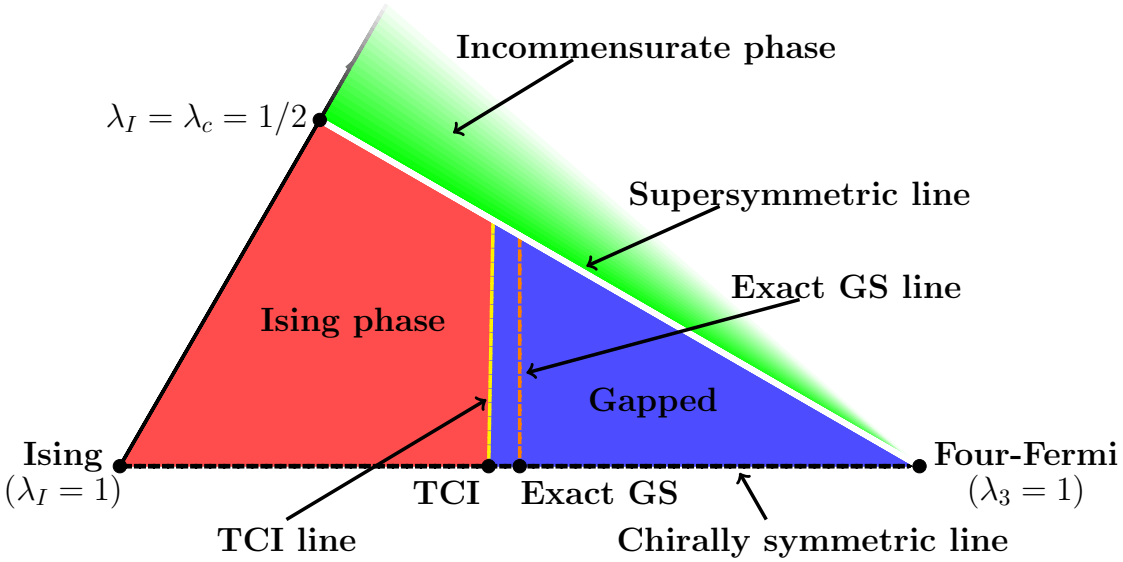

Figure 3.6: The full phase diagram of the perturbed Ising model in our region of interest, setting $\lambda_I + \lambda_3 + \lambda_c = 1$ and $\lambda_I, \lambda_c, \lambda_3 \geq 0$. Changing $\lambda_c \to -\lambda_c$ leaves the diagram invariant.

states at $\lambda_I = \lambda_3$, $\lambda_c = 0$ have zero energy, they must be annihilated by both $(Q^+)^2$ and $(Q^-)^2$ and so remain exact ground states along the line $\lambda_I = \lambda_3$, $-\lambda_I \leq \lambda_c \leq \lambda_I$.

We now present the full phase diagram in Fig 3.6. The red, blue and green areas indicate the three phases: Ising, gapped and incommensurate. The chirally symmetric line is the dashed horizontal line linking the Ising and Four-Fermi point, while the black line on the left-hand side is $\lambda_3 = 0$, corresponding to the exactly solvable free-fermionic models. The TCI, exact ground-state and supersymmetric lines are indicated in yellow, orange and white respectively.

The only area of the diagram requiring more description is the supersymmetric line. This was studied by Sannomiya *et al.* in Ref. [92]. They showed that supersymmetry is spontaneously broken for small λ_3 and the dispersion relation remains $E \propto k^3$ away from the exactly solvable point $\lambda_I = \lambda_c$, $\lambda_3 = 0$. This line has proved to be extremely difficult to study numerically due to the multitude of very low-lying states and so we have been unable to determine how far this k^3 dispersion survives and what happens at the multicritical point when the TCI and supersymmetric lines meet.

The final point in the phase diagram worthy of discussion is the Four-Fermi point [97]. This is the point with $\lambda_I = \lambda_c = 0$ and is the only place at which the

model is both supersymmetric and non-chiral. Here the model is exactly solved thanks to a hidden free-fermion structure and is found to have a dispersion relation $E \propto k^{3/2}$ for open boundary conditions.

3.6 Conclusions and outlook

We have shown that the critical Ising model perturbed by a self-dual, non-chiral interaction can lead to a TCI transition at a ratio of couplings of $\mathcal{O}(1)$. After this, we encounter an order-disorder coexistence phase with three degenerate ground states, including a frustration-free point, where the ground states are exactly degenerate for any lattice length and correspond to the completely ordered and disordered Ising states. Continuing to the extreme point where the Ising coupling vanishes, we encounter a point with a hidden free-fermion structure [97]. Breaking chirality, we see that the Ising and gapped phases survive until they hit a supersymmetric line, after which the model becomes incommensurate. The TCI transition also survives all the way to this line, as does the line of frustration free ground states.

Since the completion of our paper a number of other groups have explored different areas related to the content. Li, Lantagne-Hurtubise and Franz have constructed a similar model on the kagome lattice which also exhibits lattice supersymmetry [108, 109]. Other interacting Majorana models have also recently been considered on the honeycomb lattice [110] and on two- and four-leg chains [109]. In addition, our model been used as a check for benchmarking numerical tests, such as periodic uniform matrix product states [64, 111] and for testing the extraction of conformal data from lattice models.

Recently, Aasen *et al.* posted a paper investigating the non-Abelian spin liquid phase in α-$RuCl_3$, a Kitaev material [37, 39–41]. This compound, and Kitaev materials more generally, are of great interest in the field of quantum computing, where the production of fault-tolerant qubits remains a key problem [26, 27, 38]. Aasen *et al.* investigated ways of detecting emergent Majorana fermions and anyons along with their statistics. In their paper they make use of our self-dual perturbed Ising model (3.11) to gain insights into their emergent Majoranas, showing its

potential significance to the highly important field of quantum computing. As well as this, they solved the mystery mentioned earlier of why our model has its TCI point at a ratio of couplings of $\mathcal{O}(1)$ while the Rahmani model (3.10) needs an interaction strength almost three orders of magnitude larger. They argue that the four-fermion interactions can be split into two parts, one which effectively boosts the Ising term for low-energy excitations, and a second which remains a four-Majorana term [41]. In the Rahmani case, this boost is large and occurs linearly in the momentum, k, of quasiparticles, while in our case the linear term vanishes and the lowest order term is cubic. For the low energy excitations, which have small k, the effective Ising interaction gets renormalised strongly in the Rahmani case but only weakly in ours, explaining why a far stronger Rahmani perturbation is needed. The details of the underlying calculation are given in Appendix A, or can be found in Ref. [41].

4

The S_3 invariant model

Contents

4.1 Introduction

In Chapter 3 we considered the critical Ising model perturbed by a self-dual interaction. The q-state Potts model is a generalisation of the Ising model to a system with q states per site [13, 43]. The $\mathbb{Z}_2$ symmetry between the two possible spin directions becomes an S_q symmetry (the permutation group of q elements). Just as in the Ising model, for $q = 3$ there is a second-order transition between an ordered region and a disordered region, which has a continuum limit again described

by a CFT, this time with central charge $c = 4/5$ [14].

As with the Ising model, the Potts model has attracted renewed interest in recent times due to its connection with *parafermions* [42]. Just as the Potts model is a generalisation of the Ising model, so is the parafermion a generalisation of the Majorana fermion, albeit with a more complicated algebra. In fact, this very complication allows for new possibilities in terms of topological phases of matter and quantum computation [47]. Similarly to Ising, a self-dual model in spins corresponds to translation invariance in parafermions, hence motivating the study of such spin models.

Due to the increased complexity of parafermions compared to Majoranas and the larger Hilbert space, the number of available interactions is also greater. Whereas in the Ising case there were no self-dual nearest-neighbour interactions with the symmetries of Ising other than the critical Ising Hamiltonian itself, this is no longer the case for Potts. Specialising to three states, just imposing the S_3 symmetry is still not enough to limit us to a unique perturbation, but adding in spatial parity and time-reversal (to be explained in Section 4.2) is, giving the Hamiltonian H_1, as will be defined in Equation 4.34. It is worth noting that this is parity in terms of spins, which is a different condition from parity in parafermions – Li *et al.* studied a model with parafermion parity but not spin parity and found completely different, but still very interesting, phases of matter [112].

In Chapter 3 we found an order-disorder coexistence phase separated from the critical Ising phase by a TCI CFT. One might hope that perturbing the Potts model in a similar way would give another order-disorder coexistence phase separated from the Potts phase by the analogous CFT, the tricritical Potts (TCP) CFT [113]. This order-disorder coexistence phase proved to be of practical importance in terms of quantum computation in the Ising case [41] and so, we might also hope a parafermionic equivalent could be of use.

One of the key features of the perturbed Ising model was its link with supersymmetry [96], especially when perturbing from the TCI point. In the 3-state case supersymmetry has a generalisation to "fractional supersymmetry" based on the

presence of spin 4/3 rather than spin 3/2 operators [113, 114]. Again, the effect of this in the CFT is known, but its presence in lattice models is more unclear [114, 115].

Unlike the Ising model, taking the negative of the critical 3-state Potts Hamiltonian does not lead to the same field theory and is given by a $c = 1$ CFT [116, 117]. While the corresponding classical model is unstable to perturbations [117], the quantum version stays in the same phase. This surprising behaviour will be explained in Chapter 5.

While the critical ferromagnetic Potts and, to a lesser extent, the antiferromagnetic Potts models have been well-studied, the same is not true for the second symmetry preserving Hamiltonian, H_1. This Hamiltonian is fascinating in its own right though and has many intriguing features, such as integrability and a connection with the Onsager algebra and quantum groups [52]. Once again, the continuum field theory depends on the sign of this Hamiltonian. One sign gives the same CFT as the critical antiferromagnetic Potts model, and has a flow to the critical ferromagnetic Potts model [52, 118, 119], while the other is supersymmetric and has been studied less in the literature [52, 120].

In this chapter we will investigate in detail the whole phase diagram, as given in Figure 4.1. We start by summarising the Potts model, its connection to parafermions, and the critical ferromagnetic and antiferromagnetic points in Section 4.2, before introducing the second symmetry-preserving Hamiltonian in Section 4.3. The remainder of the chapter then plots out the phase diagram, with Sections 4.4 and 4.5 going through the order-disorder coexistence and TCP phases, while Section 4.6 looks at the connection to fractional supersymmetry. Section 4.7 explains the region around $-H_1$, while Sections 4.8 and 4.9 do the same around the antiferromagnetic point and H_1, respectively. The phase diagram in this chapter focuses entirely on the self-dual line, with duality-breaking behaviour deferred to Chapter 5. This chapter is based predominantly on Ref. [51].

4.2 The Potts model

The one-dimensional 3-state quantum Potts model on L sites has Hamiltonian

$$H_{\mathrm{P}}(J,f) = -\sum_{j=1}^{L}\left[J\left(\sigma_j^\dagger\sigma_{j+1}+\sigma_j\sigma_{j+1}^\dagger\right)+f\left(\tau_j+\tau_j^\dagger\right)\right], \tag{4.1}$$

where the operators σ_j and τ_j act non-trivially only on site j and σ and τ obey the algebra

$$\sigma^2=\sigma^\dagger, \quad \tau^2=\tau^\dagger=1, \quad \sigma^3=\tau^3=1, \quad \sigma\tau=\omega\tau\sigma, \tag{4.2}$$

where $\omega \equiv \exp(2\pi i/3)$.

We will consider two main bases: the σ- and τ-diagonal bases. In the σ-diagonal basis

$$\sigma=\begin{pmatrix}1&0&0\\0&\omega&0\\0&0&\omega^2\end{pmatrix}, \qquad \tau=\begin{pmatrix}0&0&1\\1&0&0\\0&1&0\end{pmatrix}, \tag{4.3}$$

while in the τ-diagonal basis

$$\sigma=\begin{pmatrix}0&1&0\\0&0&1\\1&0&0\end{pmatrix}, \qquad \tau=\begin{pmatrix}1&0&0\\0&\omega&0\\0&0&\omega^2\end{pmatrix}. \tag{4.4}$$

For periodic boundary conditions, as we will generally consider unless stated otherwise, we define $\sigma_{L+1} \equiv \sigma_1$, $\tau_{L+1} \equiv \tau_1$.

The Potts model has a number of symmetries. Firstly, there is an S_3 symmetry of relabelling the spin directions in the σ-diagonal basis. This comprises a non-commuting $\mathbb{Z}_3$ and $\mathbb{Z}_2$ pair of symmetries. The $\mathbb{Z}_3$ consists of cyclic permutations of the spins generated by

$$\mathcal{S}=\prod_{j=1}^{L}\tau_j, \tag{4.5}$$

such that $\mathcal{S}^\dagger\sigma_j\mathcal{S} = \omega\sigma_j$ and $\mathcal{S}^\dagger\tau_j\mathcal{S} = \tau_j$. In the τ-diagonal basis (4.4) this permutation acts diagonally, while in the σ-diagonal basis (4.3) the spins are shifted. As $\mathcal{S}^3=1$, $\mathcal{S}$ has eigenvalues ω^r for $r=0,\pm1$. The $\mathbb{Z}_2$ in the S_3 is charge conjugation, $\mathcal{C}$, and conjugates both σ_j and τ_j: $\mathcal{C}\sigma_j\mathcal{C}=\sigma_j^\dagger$, $\mathcal{C}\tau_j\mathcal{C}=\tau_j^\dagger$.

We can express the $\mathbb{Z}_3$ generator as $\mathcal{S} = \omega^Q$, where

$$Q = \sum_{j=1}^{L} S_j^z, \qquad S_j^z = \frac{i}{\sqrt{3}} \left(\tau_j^\dagger - \tau_j \right). \tag{4.6}$$

For the Potts model itself, the $U(1)$ generated by Q is not a symmetry, but we will see that it is at special points in our phases diagram to be discussed later.

Along with translation invariance, the Potts model has two further symmetries. Parity symmetry requires invariance under exchange of operators at sites j and $L+1-j$, meaning that the chain looks the same "in whichever direction you look at it". The second is time-reversal symmetry, which changes $\sigma_j \leftrightarrow \sigma_j^\dagger$ but leaves τ_j invariant. As it is anti-unitary, it also complex conjugates any constants (e.g. $\omega \leftrightarrow \omega^2$).

Now that we have described the symmetries of the Potts model, we move onto its phase diagram. We focus on the ferromagnetic Potts model with $J, f \geq 0$. From Equation 4.1, $H_{\mathrm{P}}(J, 0)$ is an exactly solvable point. We consider the σ-diagonal basis, where it is clear that all terms in the Hamiltonian commute. The three ground states can then be read off immediately as the three states in which all spins align in the σ-direction:

$$|\Psi_{\mathrm{o}}\rangle = |AA\cdots A\rangle\,, \tag{4.7}$$

for $A = 0, 1, 2$ and $\sigma_j |A\rangle_j = \omega^A |A\rangle_j$. These are the completely ordered states in the σ basis. For periodic boundary conditions, there is then a gap of $6J$ to the first-excited states, where there are two points with adjacent spins not in the same direction.

Taking $H_{\mathrm{P}}(0, f)$ instead, we find another exactly solvable point, this time with all operators diagonal in the τ basis. Here there is a unique ground state

$$|\Psi_{\mathrm{d}}\rangle = \left|\hat{0}\hat{0}\cdots\hat{0}\right\rangle, \tag{4.8}$$

where $\tau_j \left|\hat{0}\right\rangle_j = \left|\hat{0}\right\rangle_j$. In the τ basis this is completely ordered, while in the σ basis there is an equal amplitude for every basis state and so it is called the completely disordered state: $\left|\hat{0}\right\rangle = (|0\rangle + |1\rangle + |2\rangle)/\sqrt{3}$. There is then a finite gap of $3f$ to the first excited states with one site not in the $\left|\hat{0}\right\rangle$ state.

The Ising model also had completely ordered ground states and a completely disordered ground state at its solvable points (1.6 and 1.8). In the Ising case we saw that the ordered and disordered points were surrounded by ordered and disordered phases which were related to each other by duality [7]. Perhaps unsurprisingly, an analogous duality can be found in the Potts case [121]. Taking

$$\tau_j \to \sigma_j^\dagger \sigma_{j+1}, \qquad \sigma_j^\dagger \sigma_{j+1} \to \tau_{j+1}, \tag{4.9}$$

we see that, with periodic boundary conditions, $H_{\mathrm{P}}(J, f)$ maps to itself, just with $J \leftrightarrow f$. We see that there is a self-dual point at $J = f$, as there was in the Ising case. This point is described by a CFT with $c = 4/5$ and is the transition between ordered and disordered phases, just as in the Ising case [14, 121].

4.2.1 Parafermions

The similarities between the Ising model and the 3-state Potts model may lead to some hope that it can be solved exactly for all couplings, but unfortunately this is not the case. The Ising model was solved by transforming to Majorana fermions (1.14) obeying the algebra $\{\gamma_a, \gamma_b\} = 2\delta_{a,b}$ and this simple anticommutation relation allowed the model to be solved. In the Potts case the analog of the Majorana fermion is the parafermion [42], where

$$\psi_{2j-1} = \sigma_j \prod_{k=1}^{j-1} \tau_k, \qquad \psi_{2j} = \omega \sigma_j \prod_{k=1}^{j} \tau_k. \tag{4.10}$$

Here the algebra $\psi_a^3 = 1$, $\psi_a \psi_b = \omega \psi_b \psi_a$ for $a < b$ is obeyed. This more complicated commutation relation means the model can no longer be solved generally.

We can still get some useful insights by looking at the model in terms of parafermions though. From Equations 4.10, we see that

$$\tau_j = \omega^2 \psi_{2j-1}^\dagger \psi_{2j}, \qquad \sigma_j^\dagger \sigma_{j+1} = \omega^2 \psi_{2j}^\dagger \psi_{2j+1}, \tag{4.11}$$

and so, up to boundary conditions, Equation 4.1 can be rewritten as

$$H_{\mathrm{P}}(J, f) = -\omega^2 \sum_{j=1}^{L} \left(J \psi_{2j}^\dagger \psi_{2j+1} + f \psi_{2j-1}^\dagger \psi_{2j} + \text{h.c.} \right). \tag{4.12}$$

As in the Ising case, the self-dual point $J = f$ is translation invariant in terms of parafermions. When we consider perturbing the Potts model later, we will see that the shortest-range couplings are also clearer in the parafermion language than in terms of spins due to the simpler behaviour under duality.

Before moving on, we should note that parafermions can be defined for a q-state system. In this case Equation 4.10 is unchanged, but ω is replaced by $\omega_q = \exp(2\pi i/q)$ and σ and τ obey the relations

$$\sigma^q = \tau^q = 1, \qquad \sigma_q \tau_q = \omega_q \tau_q \sigma_q \tag{4.13}$$

leading to $\psi_a^q = 1$, $\psi_a \psi_b = \omega_q \psi_b \psi_a$ for $a < b$. We see that Majorana fermions and 3-state parafermions are special cases with $q = 2$, 3 respectively.

Parafermionic operators also appear in CFTs [113, 122]. The property of needing q parafermions to return to the identity can be seen from an operator with fractional spin. In fact, similarly to the CFT minimal models, there is a family of parafermionic CFTs, each of which has a field ψ with weights

$$\left(h, \bar{h}\right) = \left(\frac{q-1}{q}, 0\right). \tag{4.14}$$

This series has central charge

$$c = 2\,\frac{q-1}{q+2} \tag{4.15}$$

and will prove to be useful in our analysis later. For now, we note that the Ising and Potts CFTs correspond to the $q = 2, 3$ models in this series.

4.2.2 The ferromagnetic and antiferromagnetic Potts CFTs

As mentioned above, the second-order transition between the ordered and disordered Potts models occurs at the self-dual point $J = f > 0$ and is in the universality class of a CFT with central charge $c = 4/5$ [14, 66]. While the Ising model is part of the A-series of minimal models, the Potts model is in the D-series, meaning it has a non-diagonal partition function [14, 68, 123, 124]:

$$Z_{\mathrm{P}} = (\chi_0 + \chi_3)(\bar{\chi}_0 + \bar{\chi}_3) + (\chi_{\frac{2}{5}} + \chi_{\frac{7}{5}})(\bar{\chi}_{\frac{2}{5}} + \bar{\chi}_{\frac{7}{5}}) + 2\,\chi_{\frac{1}{15}}\bar{\chi}_{\frac{1}{15}} + 2\,\chi_{\frac{2}{3}}\bar{\chi}_{\frac{2}{3}}. \tag{4.16}$$

Here χ_h is the holomorphic *character* of the primary field with holomorphic weight h, consisting of the contributions of the primary and all its descendent fields, i.e. the entire conformal tower, to the partition function, while $\bar{\chi}_{\bar{h}}$ is the equivalent for the antiholomorphic part [16]. The 1/15 and 2/3 operators are charged under the $\mathbb{Z}_3$ and so cannot be present in any perturbation neutral under it. Thus the most relevant operator is the $(2/5, 2/5)$ energy operator and this drives the transition to the ordered or disordered Potts model, depending on the sign of the perturbation.

In the Ising case, the energy operator was odd under duality and so could be neglected from self-dual perturbations. The same happens in the Potts model, meaning that the $(2/5, 2/5)$ operator is not present in self-dual perturbations [107]. The least irrelevant operator obeying every symmetry of the self-dual Potts model is then the $(7/5, 7/5)$ operator [125], with dimension $7/5 + 7/5 = 14/5 > 2$, showing that the critical Potts model is stable to self-dual perturbations.

For Ising, the antiferromagnetic model was equivalent to the ferromagnetic model up to a unitary transformation, but this no longer holds in the three-state Potts model. To understand this difference, we consider the purely disordered points. In the Ising model this is

$$H_{\text{Ising,d}} = -f \sum_{j=1}^{L} \sigma_j^x, \tag{4.17}$$

where $f > 0$ for the "ferromagnetic" point and $f < 0$ for the "antiferromagnetic" point. At the ferromagnetic point, the spins want to align in the state with eigenvalue 1 under σ^x, while for the antiferromagnetic case they want eigenvalue -1. Both of these just give a single choice of the preferred state.

For the Potts model we get instead

$$H_{\text{Potts,d}} = -f \sum_{j=1}^{L} \left(\tau_j + \tau_j^\dagger \right). \tag{4.18}$$

In the τ-diagonal basis,

$$T \equiv \tau + \tau^\dagger = \begin{pmatrix} 2 & 0 & 0 \\ 0 & -1 & 0 \\ 0 & 0 & -1 \end{pmatrix}, \tag{4.19}$$

and so, we see that the spins want to be in the state with eigenvalue 2 under T for the ferromagnetic case. For the antiferromagnetic case though, there is no longer a single preferred direction – there are two states with eigenvalue -1. This difference has a profound effect and means there are 2^L degenerate ground states for $f < 0$, rather than the unique ground state for $f > 0$.

The inequivalence between a single favoured direction and a single disfavoured direction will reappear and play an important role as we perturb our model. For now, we use it as justification that the antiferromagnetic Potts model is not necessarily the same as the ferromagnetic Potts model. In fact, the antiferromagnetic self-dual point is a CFT with central charge $c = 1$ [116, 117]. The CFT for the antiferromagnetic Potts model is on the circle line of bosonic theories and has radius $R = \sqrt{3/2}$ in the conventions of Ginsparg [15, 75] and as given in Section 2.5, resulting in a partition function of

$$Z_{\text{AFP}} = \frac{1}{\eta\bar{\eta}} \sum_{m,n\in\mathbb{Z}} q^{\frac{1}{12}(m+3n)^2} \bar{q}^{\frac{1}{12}(m-3n)^2}. \tag{4.20}$$

We will leave a discussion of this partition function to later in our analysis.

4.3 The second symmetry-preserving interaction

We now introduce the unique nearest-neighbour Hamiltonian which preserves all the symmetries of the Potts model, other than the Potts Hamiltonian itself. The next shortest range terms obeying the $\mathbb{Z}_3$ symmetry take the form of a nearest neighbour $\sigma_j^\dagger\sigma_{j+1}$ (or its conjugate) operator combined with a τ or $\tau^\dagger$ operator at site j or $j+1$, giving eight possible terms. To find the allowed interactions made from these terms, we consider the action of each of the symmetries of the Potts model. Taking the first term to be $e^{i\alpha}\tau_j\sigma_j^\dagger\sigma_{j+1}$ for some real α, we see the action of charge conjugation (C), time-reversal (T), parity (P), and hermiticity (h) on this term:

$$e^{i\alpha}\tau_j\sigma_j^\dagger\sigma_{j+1} \xrightarrow{C} e^{i\alpha}\tau_j^\dagger\sigma_j\sigma_{j+1}^\dagger; \tag{4.21}$$

$$e^{i\alpha}\tau_j\sigma_j^\dagger\sigma_{j+1} \xrightarrow{T} e^{-i\alpha}\tau_j\sigma_j\sigma_{j+1}^\dagger; \tag{4.22}$$

$$e^{i\alpha}\tau_j\sigma_j^\dagger\sigma_{j+1} \xrightarrow{P} e^{i\alpha}\omega\sigma_j\sigma_{j+1}^\dagger\tau_{j+1}; \tag{4.23}$$

$$e^{i\alpha}\tau_j\sigma_j^\dagger\sigma_{j+1} \xrightarrow{h} e^{-i\alpha}\omega^2\tau_j^\dagger\sigma_j\sigma_{j+1}^\dagger. \tag{4.24}$$

As can be seen, C, T, and P each transform $e^{i\alpha}\tau_j\sigma_j^\dagger\sigma_{j+1}$ to a different term. By applying these three all eight terms can be generated. The constant $e^{i\alpha}$ is then set to $\omega \equiv \exp(2\pi i/3)$ for consistency between charge conjugation and hermiticity. Requiring the symmetries above has fully specified the Hamiltonian (up to a real multiplying constant), giving

$$\begin{aligned} H_2 = -\sum_{j=1}^{L}\Big[&\omega\left(\tau_j\sigma_j^\dagger\sigma_{j+1} + \sigma_j^\dagger\sigma_{j+1}\tau_{j+1} + \tau_j^\dagger\sigma_j\sigma_{j+1}^\dagger + \sigma_j\sigma_{j+1}^\dagger\tau_{j+1}^\dagger\right) \\ &+ \omega^2\left(\tau_j^\dagger\sigma_j^\dagger\sigma_{j+1} + \sigma_j^\dagger\sigma_{j+1}\tau_{j+1}^\dagger + \tau_j\sigma_j\sigma_{j+1}^\dagger + \sigma_j\sigma_{j+1}^\dagger\tau_{j+1}\right)\Big]. \end{aligned} \tag{4.25}$$

Note that we did not impose self-duality, but in fact get it for free!

The only other nearest-neighbour terms we could hope to add would involve terms containing both τ_j and τ_{j+1} operators. We disallow these as they can be thought of as longer range, as can be seen in two ways. Firstly, the dual of $\tau_j\tau_{j+1}$ is $\sigma_j^\dagger\sigma_{j+2}$, which is a next-nearest-neighbour term. The second way is to reexpress the terms using parafermions, as described in Subsection 4.2.1. In terms of parafermions, the original Potts model has only nearest-neighbour terms, whereas our perturbation has parafermion terms ranging three sites and any terms involving τ_j and τ_{j+1} have parafermions ranging four sites.

This interaction has, in fact, been studied in terms of the Temperley–Lieb algebra [126, 127]. The Temperley–Lieb algebra is generated by the operators e_a obeying the relations

$$\begin{aligned} &e_a^2 = ne_a, \\ &e_a e_{a\pm1} e_a = e_a, \\ &e_a e_{a'} = e_{a'} e_a, \qquad |a - a'| > 1, \end{aligned} \tag{4.26}$$

for $a = 1, 2, ..., 2L$, where n is a parameter determining the algebra. Ikhlef *et al.* then defined the Hamiltonian

$$H_{\text{Ikhlef}} = -n\cos(\theta)\sum_{a=1}^{2L} P^{(0)}_{a,a+1} - \left(n^2-1\right)\sin(\theta)\sum_{a=1}^{2L}\left(P^{(\frac{3}{2})}_{a,a+1,a+2} - 1\right), \tag{4.27}$$

where

$$P^{(0)}_{a,a+1} \equiv \frac{e_a}{n}, \tag{4.28}$$

$$P^{(\frac{3}{2})}_{a,a+1,a+2} \equiv 1 + \frac{(e_a e_{a+1} + e_{a+1}e_a) - n\,(e_a + e_{a+1})}{n^2-1}, \tag{4.29}$$

are projection operators, and θ is the parameter determining the couplings [127].

The physics described by this model depends on which representation of the Temperley–Lieb algebra is used. Ikhlef *et al.* mainly study the XXZ representation, but for $n = \sqrt{q}$, the q-state Potts model is also a representation [128]. For $n = \sqrt{3}$ in the Potts representation,

$$e_{2j-1} = \frac{1}{\sqrt{3}}\left(1 + \tau_j + \tau_j^\dagger\right), \tag{4.30}$$

$$e_{2j} = \frac{1}{\sqrt{3}}\left(1 + \sigma_j^\dagger\sigma_{j+1} + \sigma_j\sigma_{j+1}^\dagger\right), \tag{4.31}$$

and H_{Ikhlef} (4.27) is equivalent to the self-dual Potts model perturbed by our interaction, H_2 (4.25).

Equivalent Hamiltonians can be found for any q-state Potts model with $q \geq 3$. For $q = 2$, the Ising model, the representation of the Temperley–Lieb algebra is given by

$$e_{2j-1} = \frac{1}{\sqrt{2}}\left(1 + \sigma_j^x\right), \tag{4.32}$$

$$e_{2j} = \frac{1}{\sqrt{2}}\left(1 + \sigma_j^z\sigma_{j+1}^z\right), \tag{4.33}$$

and $P^{(\frac{3}{2})}_{j,j+1,j+2}$ vanishes. This is consistent with there being no nearest-neighbour interaction obeying every symmetry of the Ising model, other than Ising itself.

Rather than adding H_2 (4.25) to H_{P} (4.1), we will instead consider

$$H_1 = \sum_{j=1}^{L}\left(3S_j^+S_{j+1}^- - 3{S_j^+}^2{S_{j+1}^-}^2 + \tau_j + \text{h.c.}\right), \tag{4.34}$$

where $S_j^+ = (2 - \omega\tau_j - \omega^2\tau_j^\dagger)\sigma_j/3$ and $S_j^- = S_j^+$. Although not immediately obvious, $H_1 = -H_P(1,1) + H_2$.

In fact H_1 has even more symmetry than the Potts model. In the τ-diagonal basis

$$S^+ = \begin{pmatrix} 0 & 0 & 1 \\ 1 & 0 & 0 \\ 0 & 0 & 0 \end{pmatrix}, \qquad S^- = \begin{pmatrix} 0 & 1 & 0 \\ 0 & 0 & 0 \\ 1 & 0 & 0 \end{pmatrix}, \tag{4.35}$$

and so the $\mathbb{Z}_3$ symmetry $\mathcal{S} = \prod_j \tau_j$ is promoted to a full $U(1)$ symmetry generated by

$$Q = \sum_{j=1}^{L} S_j^z, \qquad S_j^z \equiv \frac{i}{\sqrt{3}}\left(\tau_j^\dagger - \tau_j\right) = \begin{pmatrix} 0 & 0 & 0 \\ 0 & 1 & 0 \\ 0 & 0 & -1 \end{pmatrix}. \tag{4.36}$$

As H_1 is self-dual, it has a second $U(1)$ symmetry, dual to the first:

$$\hat{Q} = \sum_{j=1}^{L} \frac{i}{\sqrt{3}}\left(\sigma_j\sigma_{j+1}^\dagger - \sigma_j^\dagger\sigma_{j+1}\right). \tag{4.37}$$

While $[H_1, Q] = [H_1, \hat{Q}] = 0$, $[Q, \hat{Q}] \neq 0$ and so large degeneracies are generated in the spectrum [52]. In fact, the degeneracies arise from Q and $\hat{Q}$ obeying the Dolan–Grady relations [129] and hence generate the full Onsager algebra [55, 130, 131].

Both H_1 and $-H_1$ have been studied before and are known to correspond to special cases of the integrable spin-1 XXZ chain [52, 132, 133]. Along with the Onsager algebra, both of these models have a connection with quantum groups [52], although this is beyond the scope of this thesis. H_1 has the additional fascinating property of supersymmetry [96, 120], the significance of which will be explained later.

Throughout the rest of this chapter we will focus on the Hamiltonian

$$H(\theta) = \cos(\theta)H_{\mathrm{P}}(1,1) + \sin(\theta)H_1, \tag{4.38}$$

where we will sometimes label $\lambda_{\mathrm{P}} \equiv \cos(\theta)$, $\lambda_1 \equiv \sin(\theta)$. This reduces to the ferromagnetic Potts model for $\theta = 0$ and to H_1 for $\theta = \pi/2$. The phase diagram explored in this chapter is given in Figure 4.1.

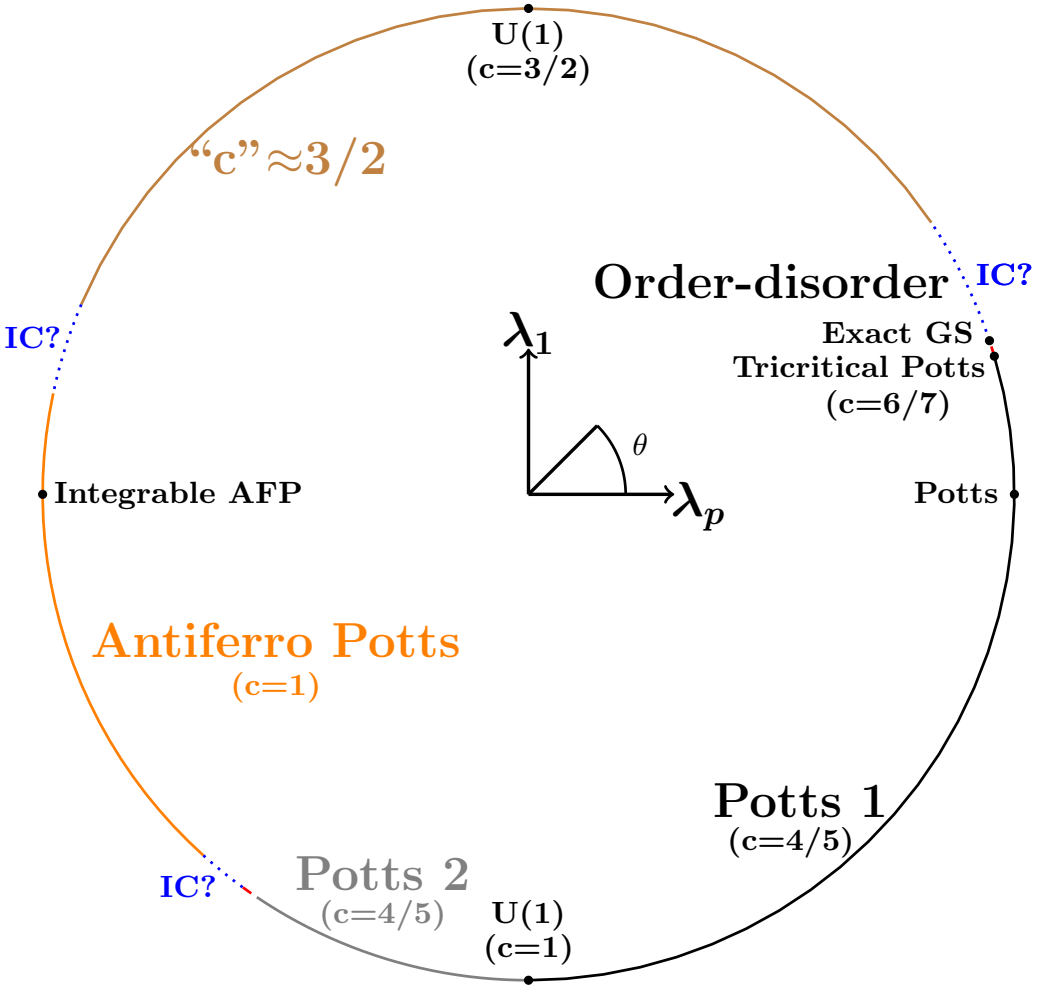

Figure 4.1: The phase diagram associated with $H(\theta)$ (4.38). The angle around the diagram corresponds to θ, with the ferromagnetic Potts point (H_{P}) at $\theta = 0$ on the right-hand side and H_1 at $\theta = \pi/2$ on the top. The solid lines correspond to gapless regions, while the blue "IC?" sections are believed to be incommensurate phases. The special points discussed in this chapter are marked with black dots.

4.4 The order-disorder coexistence phase

As we saw in Subsection 4.2.2, there are no relevant self-dual operators obeying every symmetry of the Potts model in the Potts CFT, meaning that the critical Potts point extends to a finite phase when perturbed by H_1. We also found that the ferromagnetic and antiferromagnetic self-dual Potts models were described by two different CFTs in their continuum limits, meaning that there must be at least

one phase transition in each of the ranges $0 < \theta \leq \pi$ and $-\pi \leq \theta < 0$.

To locate our first phase transition, we begin by considering the point $H(\theta_{\text{ff}})$, where $\sin(\theta) = 1/\sqrt{10}$, $\cos(\theta) = 3/\sqrt{10}$, giving $\lambda_1/\lambda_{\text{P}} = 1/3$. This point has four exact frustration-free ground states, given by the three ground states of the completely ordered Potts model $|AA...A\rangle$ (4.7) and the ground state of the completely disordered Potts model $|00...0\rangle$ (4.8), analogously to the frustration-free point in the perturbed Ising model (3.14).

To see this, we first rewrite $H(\theta_{\text{ff}})$ as a sum of projectors:

$$H(\theta_{\text{ff}}) = -\sum_j \left(B_j + C_j\right), \tag{4.39}$$

where

$$\begin{aligned}
B_j &= \sigma_j^\dagger \sigma_{j+1} + \sigma_j \sigma_{j+1}^\dagger + \tau_j + \tau_j^\dagger + \omega^2 \tau_j \sigma_j \sigma_{j+1}^\dagger \\
&\quad + \omega \tau_j \sigma_j^\dagger \sigma_{j+1} + \omega \tau_j^\dagger \sigma_j \sigma_{j+1}^\dagger + \omega^2 \tau_j^\dagger \sigma_j^\dagger \sigma_{j+1}, \\
C_j &= \sigma_j^\dagger \sigma_{j+1} + \sigma_j \sigma_{j+1}^\dagger + \tau_{j+1} + \tau_{j+1}^\dagger + \omega \sigma_j^\dagger \sigma_{j+1} \tau_{j+1} \\
&\quad + \omega^2 \sigma_j^\dagger \sigma_{j+1} \tau_{j+1}^\dagger + \omega^2 \sigma_j \sigma_{j+1}^\dagger \tau_{j+1} + \omega \sigma_j \sigma_{j+1}^\dagger \tau_{j+1}^\dagger.
\end{aligned}$$

While it may appear that we have just rewritten the Hamiltonian in a more complicated and opaque form, B_j and C_j can each be expressed as a rescaled projector offset by a constant: $B_j = 2 - 6P_B(j)$ and $C_j = 2 - 6P_C(j)$. $P_B(j)$ and $P_C(j)$ are two-site projectors acting on site j and $j+1$ given by

$$\begin{aligned}
P_B(j) &= \frac{1}{2}\Big[\left(|\hat{1}\hat{0}\rangle - |\hat{2}\hat{2}\rangle\right)\left(\langle\hat{1}\hat{0}| - \langle\hat{2}\hat{2}|\right) + \left(|\hat{2}\hat{0}\rangle - |\hat{1}\hat{1}\rangle\right)\left(\langle\hat{2}\hat{0}| - \langle\hat{1}\hat{1}|\right) \\
&\quad + \left(|\hat{1}\hat{2}\rangle - |\hat{2}\hat{1}\rangle\right)\left(\langle\hat{1}\hat{2}| - \langle\hat{2}\hat{1}|\right)\Big], \\
P_C(j) &= \frac{1}{2}\Big[\left(|\hat{0}\hat{1}\rangle - |\hat{2}\hat{2}\rangle\right)\left(\langle\hat{0}\hat{1}| - \langle\hat{2}\hat{2}|\right) + \left(|\hat{0}\hat{2}\rangle - |\hat{1}\hat{1}\rangle\right)\left(\langle\hat{0}\hat{2}| - \langle\hat{1}\hat{1}|\right) \\
&\quad + \left(|\hat{1}\hat{2}\rangle - |\hat{2}\hat{1}\rangle\right)\left(\langle\hat{1}\hat{2}| - \langle\hat{2}\hat{1}|\right)\Big],
\end{aligned}$$

where $|\hat{n}\rangle$ obeys $\tau\,|\hat{n}\rangle = \omega^{\hat{n}}\,|\hat{n}\rangle$. As $|\hat{0}\hat{0}\rangle$ is annihilated by both projectors, $|\hat{0}\hat{0}...\hat{0}\rangle$ must be a ground state of the whole Hamiltonian. Using

$$|A\rangle = \frac{1}{\sqrt{3}}\left(|\hat{0}\rangle + \omega^A\,|\hat{1}\rangle + \omega^{2A}\,|\hat{2}\rangle\right),$$

where, as before, $\sigma|A\rangle = \omega^A|A\rangle$, we see that $|AA\rangle$ is also annihilated by both P_B and P_C. Analogously to our method in Subsection 3.3.1, by considering three consecutive sites we can show that the only states annihilated by every two-site projector are $|\hat{0}\hat{0}...\hat{0}\rangle$ and $|AA...A\rangle$.

Before moving on, we note that there are analogous points for the general q-state Potts model with $q \geq 3$, as found by the Temperley–Lieb formulation [127, 134]. Each of these has $q+1$ degenerate ground states – the q ordered ground states of the completely ordered Potts model and the one disordered ground state.

4.5 The tricritical Potts transition

Now that we have found a point with four exact ground states at $\theta = \text{atan}\,(1/3) \approx 0.102\pi$, we know there must be a phase transition in the range $0 < \theta \lessapprox 0.102\pi$, as the Potts point at $\theta = 0$ has a unique ground state and is gapless. In the Ising case, the analogous transition occured via a point in the universality class of the tricritical Ising model, as shown in Subsection 3.3.2. In the 3-state Potts case, the expected analogue is then the tricritical Potts (TCP) model [135], a CFT with central charge $c = 6/7$ [113].

To find the location and check the nature of the transition, we consider ratios of energy levels, as described in Subsection 2.3.2. Defining E_r^j as the j^{th} excited state in the $\mathbb{Z}_3 = r$ sector, we plot the ratios $(E_0^2 - E_0^0)/(E_0^1 - E_0^0)$ and $(E_1^1 - E_0^0)/(E_0^1 - E_0^0)$ against lattice length L for different $\lambda_1/\lambda_{\text{P}}$ (as given in the caption) in Figure 4.2. The dashed red and solid blue lines give the predictions of the Potts and TCP models, respectively. To find these values, we first consider the partition functions of the Potts and TCP CFTs:

$$Z_{\text{P}} = (\chi_0 + \chi_3)(\bar{\chi}_0 + \bar{\chi}_3) + (\chi_{\frac{2}{5}} + \chi_{\frac{7}{5}})(\bar{\chi}_{\frac{2}{5}} + \bar{\chi}_{\frac{7}{5}}) + 2\,\chi_{\frac{1}{15}}\bar{\chi}_{\frac{1}{15}} + 2\,\chi_{\frac{2}{3}}\bar{\chi}_{\frac{2}{3}}, \quad (4.40)$$

$$\begin{aligned} Z_{\text{TCP}} = {} & (\chi_0 + \chi_5)(\bar{\chi}_0 + \bar{\chi}_5) + (\chi_{\frac{1}{7}} + \chi_{\frac{22}{7}})(\bar{\chi}_{\frac{1}{7}} + \bar{\chi}_{\frac{22}{7}}) + (\chi_{\frac{5}{7}} + \chi_{\frac{12}{7}})(\bar{\chi}_{\frac{5}{7}} + \bar{\chi}_{\frac{12}{7}}) \\ & + 2\,\chi_{\frac{1}{21}}\bar{\chi}_{\frac{1}{21}} + 2\,\chi_{\frac{10}{21}}\bar{\chi}_{\frac{10}{21}} + 2\,\chi_{\frac{4}{3}}\bar{\chi}_{\frac{4}{3}}. \end{aligned} \quad (4.41)$$

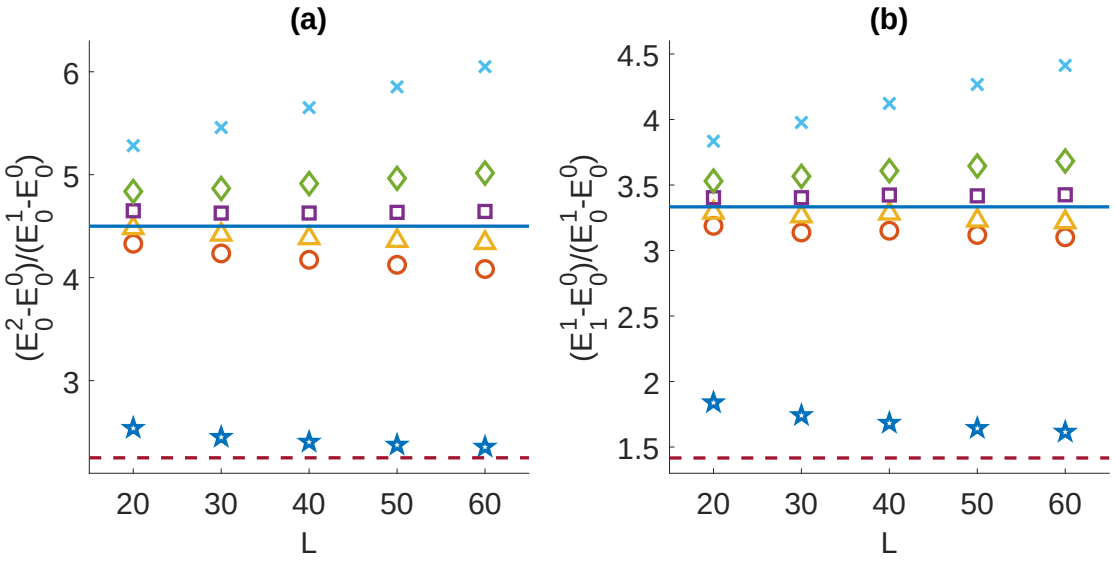

Figure 4.2: The ratios $(E_0^2 - E_0^0)/(E_0^1 - E_0^0)$ and $(E_1^1 - E_0^0)/(E_0^1 - E_0^0)$ are plotted against L for different values of λ_1/λ_P in subfigures (a) and (b), respectively. Values for $\lambda_P = 1$, $\lambda_1 = 0.25$ (blue stars), 0.295 (red circles), 0.296 (yellow triangles), 0.297 (purple squares), 0.298 (green diamonds) and 0.3 (teal crosses) are shown. The Potts and TCP lines are plotted in dashed red and solid blue at 9/4 and 9/2 in (a), and at 17/12 and 10/3 in (b), respectively.

The terms premultiplied by 2 all have $\mathbb{Z}_3$ charge of $r = 1, 2$, while the others have charge 0. In the Potts and TCP cases, we then get the following correspondences:

$$\text{Potts}: \frac{E_0^2 - E_0^0}{E_0^1 - E_0^0} \to \frac{\frac{7}{5}+\frac{2}{5}}{\frac{2}{5}+\frac{2}{5}} = \frac{9}{4}, \quad \frac{E_1^1 - E_0^0}{E_0^1 - E_0^0} \to \frac{\frac{16}{15}+\frac{1}{15}}{\frac{2}{5}+\frac{2}{5}} = \frac{17}{12}; \tag{4.42}$$

$$\text{TCP}: \frac{E_0^2 - E_0^0}{E_0^1 - E_0^0} \to \frac{\frac{8}{7}+\frac{1}{7}}{\frac{1}{7}+\frac{1}{7}} = \frac{9}{2}, \quad \frac{E_1^1 - E_0^0}{E_0^1 - E_0^0} \to \frac{\frac{10}{21}+\frac{10}{21}}{\frac{1}{7}+\frac{1}{7}} = \frac{10}{3}. \tag{4.43}$$

For the order-disorder coexistence phase, the two-lowest energy levels in the $r = 0$ sector are degenerate up to exponentially small splitting in L (for the frustration-free point these correspond to $|\hat{0}\hat{0}...\hat{0}\rangle$ and $(|00..0\rangle + |11...1\rangle + |22...2\rangle)/\sqrt{3}$, respectively). The ratios thus diverge with lattice length in this phase, as shown in Figure 4.2. We see that for $\lambda_1/\lambda_P \approx 0.297$ ($\theta \approx 0.092\pi$), we get good convergence to the TCP predictions, while for smaller θ the ratios head to the Potts predictions and for larger θ they diverge, as expected for the order-disorder coexistence phase.

In the TCP partition function, the $(1/7, 1/7)$ primary field is the most relevant neutral under the $\mathbb{Z}_3$. As for the $(2/5, 2/5)$ field in the Potts model, this field is odd under duality and so is a forbidden perturbation along our self-dual line, leaving

$(5/7, 5/7)$ as the most relevant field. As $5/7 + 5/7 = 10/7 < 2$, this operator is relevant and so the TCP point is unstable [114, 136], as found by our numerics.

4.6 The $\mathcal{Q}^3$ connection

Before continuing with the phase diagram, we investigate an intriguing connection to supersymmetry. In Section 3.5, we saw that our non-chiral perturbed Ising model could be written as the sum of two supersymmetric Hamiltonians. This made sense as we were perturbing from the TCI CFT, which is itself supersymmetric, with $(3/2, 0)$ and $(0, 3/2)$ supersymmetry operators. In the 3-state case we instead perturb from the TCP CFT, where the supersymmetry operators are replaced by $(4/3, 0)$ and $(0, 4/3)$ operators, which remain symmetry generators away from the TCP point [113], giving an emergent "fractional supersymmetry" [114]. We can then write the effective field theory in the order-disorder coexistence phase as the sum of two cubes of parafermionic operators [114, 115]. On the lattice, we find

$$H(\theta_{\text{ff}}) = \mathcal{Q}_{\text{ff}}^3 + {\mathcal{Q}_{\text{ff}}^\dagger}^3 + \text{longer range terms}, \tag{4.44}$$

where $\mathcal{Q}_{\text{ff}}$ is the parafermionic operator defined as

$$\mathcal{Q}_{\text{ff}} \equiv -\sum_{a=1}^{2L} \left(2\omega^2 \psi_a + \psi_a^\dagger \psi_{a+1}^\dagger\right) \tag{4.45}$$

and the ψ_a operators are defined as in Equation 4.10.

Taking the more general form

$$\mathcal{Q} = \sum_{a=1}^{2L} \left(\alpha \psi_a + \beta \psi_a^\dagger \psi_{a+1}^\dagger\right), \tag{4.46}$$

to make $\mathcal{Q}^3 + {\mathcal{Q}^\dagger}^3$ hermitian and invariant under charge conjugation, parity and time-reversal symmetry, we require $\beta^3 \in \mathbb{R}$ and $\alpha = 2\omega^2\beta$. This then leads to

$$\begin{aligned}
\mathcal{Q}^3 + {\mathcal{Q}^\dagger}^3 = 3\beta^3 \sum_{j=1}^{L} \Big[& 4\left(\tau_j + \tau_j^\dagger + \sigma_j^\dagger \sigma_{j+1} + \sigma_j \sigma_{j+1}^\dagger\right) \\
& + 2\omega\left(\tau_j \sigma_j^\dagger \sigma_{j+1} + \sigma_j^\dagger \sigma_{j+1} \tau_{j+1} + \tau_j^\dagger \sigma_j \sigma_{j+1}^\dagger + \sigma_j \sigma_{j+1}^\dagger \tau_{j+1}^\dagger\right) \\
& + 2\omega^2\left(\tau_j^\dagger \sigma_j^\dagger \sigma_{j+1} + \sigma_j^\dagger \sigma_{j+1} \tau_{j+1}^\dagger + \tau_j \sigma_j \sigma_{j+1}^\dagger + \sigma_j \sigma_{j+1}^\dagger \tau_{j+1}\right) \\
& - \left(\tau_j \tau_{j+1}^\dagger + \tau_j^\dagger \tau_{j+1} + \sigma_j^\dagger \sigma_{j+1}^\dagger \sigma_{j+2}^\dagger + \sigma_j \sigma_{j+1} \sigma_{j+2}\right)\Big],
\end{aligned}$$

where we have ignored a constant term. We see that, when $\beta = -1$, the first three lines do indeed correspond to $H(\theta_{\text{ff}})$, while the final line gives longer-range corrections.

To remove this final line and make the Hamiltonian nearest neighbour we consider

$$H = \sum_{m=1}^{3} H_m, \qquad H_m = \mathcal{Q}_m^3 + {\mathcal{Q}_m^\dagger}^3, \tag{4.47}$$

analogously to the sum over two supersymmetric Hamiltonians in the Ising case (3.52). We define

$$\mathcal{Q}_m = \sum_{a=1}^{2L} \left(\alpha_{m,a} \psi_a + \beta_{ma,} \psi_a^\dagger \psi_{a+1}^\dagger \right), \tag{4.48}$$

where

$$\alpha_{m,a} = \alpha e^{i\theta_m} e^{\frac{2\pi m a i}{3}}, \quad \beta_{m,a} = \beta e^{i\phi_m} e^{\frac{2\pi m a i}{3}}, \quad \mu_m = \theta_m + 2\phi_m. \tag{4.49}$$

Getting the self-dual Hamiltonian (4.38) then requires solving 8 equations for 8 unknowns:

$$\begin{aligned}
&2\cos\mu_1 + \cos\mu_2 - \sqrt{3}\sin\mu_2 = 0,\\
&\cos\mu_0 + \sqrt{3}\sin\mu_0 + 2\cos\mu_1 = \frac{\lambda_{\text{P}} - \lambda_1}{3\alpha\beta^2},\\
&\sin\mu_0 - \sqrt{3}\cos\mu_0 - 2\sin\mu_1 + \sin\mu_2 + \sqrt{3}\cos\mu_2 = 0,\\
&\cos\mu_0 + \sqrt{3}\sin\mu_0 - 2\cos\mu_1 + \cos\mu_2 - \sqrt{3}\sin\mu_2 = \frac{2\lambda_1}{3\alpha\beta^2},\\
&\cos 3\theta_0 + \cos 3\theta_1 + \cos 3\theta_2 = 0,\\
&\sin 3\theta_0 + \sin 3\theta_1 + \sin 3\theta_2 = 0,\\
&\cos 3\theta_1 - \cos 3\theta_2 = 0,\\
&\cos 3\theta_1 - \cos 3\theta_0 = \frac{\lambda_1}{6\beta^3}.
\end{aligned}$$

The last four equations can be solved easily and, for $\lambda_{\text{P}} \neq 0$, there are several solutions, all leading to equivalent $\mathcal{Q}_m$, with a few phases moved around. Picking one of these, we have $\lambda_1 = -9\beta^3$, $\theta_0 = 2\pi/3$, $\theta_1 = -2\pi/9$, $\theta_2 = 2\pi/9$.

The first four equations have different solutions depending on $\nu = 2\lambda_1/(\lambda_P - \lambda_1)$. All of these solutions are again equivalent, just with phases attached to different terms. One set of solutions, continuous except at $\nu = \infty$, is as follows. If $\nu < 1/2$,

$$\begin{aligned}
\alpha &= \beta\left(\frac{2}{\nu} - 1\right), \\
\mu_0 &= -\frac{2\pi}{3}, \\
\mu_1 &= \operatorname{atan}\left[\frac{1+\nu}{\nu-2}, \frac{\sqrt{3(1-2\nu)}}{2(2-\nu)}\right], \\
\mu_2 &= \operatorname{atan}\left[\frac{1+\nu-3\sqrt{1-2\nu}}{2(2-\nu)}, \sqrt{3}\,\frac{1+\nu+\sqrt{1-2\nu}}{2(2-\nu)}\right],
\end{aligned}$$

where $\operatorname{atan}[x, y]$ specifies the x and y coordinates and thus gives the angle unambiguously. For $\nu > 1/2$,

$$\begin{aligned}
\alpha &= -\beta\sqrt{\frac{4+\nu}{\nu}}, \\
\mu_0 &= \frac{\pi}{3} + \operatorname{atan}\left[\frac{\nu-2}{\sqrt{\nu(4+\nu)}}, -\frac{2\sqrt{2\nu-1}}{\sqrt{\nu(4+\nu)}}\right], \\
\mu_1 &= \operatorname{atan}\left[-\frac{1+\nu}{\sqrt{\nu(4+\nu)}}, \frac{\sqrt{2\nu-1}}{\sqrt{\nu(4+\nu)}}\right], \\
\mu_2 &= -\frac{\pi}{3} + \operatorname{atan}\left[\frac{1+\nu}{\sqrt{\nu(4+\nu)}}, \sqrt{3}\,\frac{\sqrt{2\nu-1}}{\sqrt{\nu(4+\nu)}}\right].
\end{aligned}$$

We can keep the Hamiltonian well-defined as $\nu \to 0$ by taking $\beta \to 0$, $\alpha \to \infty$, but $\alpha\beta^2 \to$ const. The only disagreement is then at $\nu \to -\infty$ and $\nu \to \infty$, where all μ pick up a minus sign.

In this language, we appear to have three special points in our phase diagram: $\nu = 0, 1/2, \infty$. $\nu = 0$ corresponds to the ferromagnetic and antiferromagnetic Potts points, depending of the sign of α, both of which are integrable. From Equation 4.48, we see that this is the limit where the two-parafermion term in $\mathcal{Q}_m$ vanishes, analogously to the Ising case. $\nu = \infty$ is the point $\lambda_P = \lambda_1$ and is where the $\tau_j + \sigma_j^\dagger\sigma_{j+1} + \text{h.c.}$ term completely vanishes from the Hamiltonian. $\nu = 1/2$ corresponds to $\lambda_P = 5\lambda_1$ and appears just to be a point in the ferromagnetic Potts phase.

4.7 The $U(1)$ point

We now continue around the phase diagram. Having seen how the Potts phase terminates when we increase θ from 0, we turn instead to decreasing θ from 0. To do this, we first revisit the point with $\theta = -\pi/2$, corresponding to $H(\theta) = -H_1$. In Chapter 5, when we deal with off-critical behaviour, we will study this point and the surrounding off-critical regions in more detail. For now, we will content ourselves with discussing the CFT of this point and how it leads to the phases on either side of it along the self-dual line.

As this point has a $U(1)$ charge (4.36) (and a dual $U(1)$ (4.37)), if its continuum limit is described by a CFT, it must have central charge $c \geq 1$. In fact, this point is given by a CFT with $c = 1$ and radius $R = \sqrt{3/2}$ in the conventions of Ginsparg [15, 52, 132, 133, 137], with the meaning of the radius as described in Section 2.5. While this central charge seems natural as it is the smallest allowed value, at first glance the radius appears somewhat arbitrary. In fact, the combination of the S_3 symmetry with self-duality constrains the boson to take exactly this radius.

As given in Equation 2.31, the free boson partition function is given by

$$Z(R) = \frac{1}{\eta\bar{\eta}} \sum_{m,n\in\mathbb{Z}} q^{\frac{1}{8R^2}\left(m+2R^2n\right)^2} \bar{q}^{\frac{1}{8R^2}\left(m-2R^2n\right)^2}, \tag{4.50}$$

where m denotes the "electric charge" and n the "magnetic charge". For $-H_1$, our $\mathbb{Z}_3$ symmetry is promoted to a $U(1)$ (4.36), while our dual $\mathbb{Z}_3$ is promoted to the dual $U(1)$ (4.37). We thus have two $U(1)$ symmetries on the lattice and two in the CFT, allowing us to identify the $U(1)$ on the lattice with the electric charge in the continuum and the dual $U(1)$ with the magnetic charge.[1]

Naïvely, we may now think that the lattice model is invariant under a duality mapping and so the partition function should be under exchange of electric and magnetic charges: $m \leftrightarrow n$. This is not true due to the non-trivial effect duality has on boundary conditions. For periodic boundary conditions, only the $\mathbb{Z}_3 = 0$ sector maps to itself under duality, with the $\mathbb{Z}_3 = 1, 2$ sectors mapping to twisted

[1] We could, of course, identify these the other way round, but this is just a redefinition of our boson radius from $R \to 1/(2R)$, as described by Ginsparg [15, 75].

boundary conditions [121, 138, 139]. To understand this, we consider what the $U(1)$ and dual $U(1)$ charges measure. The $U(1)$ (4.36) counts $N_{\hat{1}} - N_{\hat{2}}$, where $N_{\hat{1}}$ is the number of spins in the $|\hat{1}\rangle$ state, while $N_{\hat{2}}$ is the number in the $|\hat{2}\rangle$ state. The dual $U(1)$ (4.37) gives instead $N_\uparrow - N_\downarrow$, where $N_\uparrow$ gives the number of "kinks", where a kink is $|01\rangle$, $|12\rangle$ or $|20\rangle$, and $N_\downarrow$ is the number of antikinks ($|02\rangle$, $|10\rangle$ or $|21\rangle$). While $N_{\hat{1}} - N_{\hat{2}}$ can take any integer value between $-L$ and L, $N_\uparrow - N_\downarrow$ must be a multiple of 3 for periodic boundary conditions, or we would not return the same spin after going around the chain once, showing that the sectors with $\mathbb{Z}_3 = 1, 2$ must transform to sectors with different boundary conditions.

Using the results above, we see that we only require the $\mathbb{Z}_3 = 0$ part of our partition function to be invariant under duality. Thus

$$Z_{\mathbb{Z}_3=0}(R) = \frac{1}{\eta\bar{\eta}} \sum_{m',n\in\mathbb{Z}} q^{\frac{1}{8R^2}\left(3m'+2R^2n\right)^2} \bar{q}^{\frac{1}{8R^2}\left(3m'-2R^2n\right)^2} \tag{4.51}$$

should be invariant under $m' \leftrightarrow n$. This gives $3 = 2R^2$ and hence $R = \sqrt{3/2}$. If we had instead related the lattice $\mathbb{Z}_3$ charge to the magnetic field, we would have found $1 = 6\tilde{R}^2$ and hence $\tilde{R} = \sqrt{1/6} = 1/(2R)$, as expected.

As will be discussed in more detail in Chapter 5, this CFT has a single relevant operator, of conformal weights $(h, \bar{h}) = (3/4, 3/4)$, invariant under the Potts symmetry as well as duality. The flow caused by this operator was studied previously and is known to give a flow to the Potts CFT for either sign of the perturbation [118, 119]. This indicates that the Potts phase stretches all the way down to $\theta = -\pi/2$ and, more strangely, that perturbing from $-H_1$ by $-H_P$ gives a model described by the Potts CFT!

This second Potts phase will, again, be discussed in more detail in the next chapter. For now, we just state that it terminates at $\lambda_P/\lambda_1 \approx 0.67$ ($\theta \approx -0.69\pi$) via another point in the universality class of the TCP model, as illustrated in Figure 4.3.

4.8 The antiferromagnetic Potts phase

Beyond the second Potts region, we believe there is a second very small order-disorder coexistence region, followed by an incommensurate region. The size of

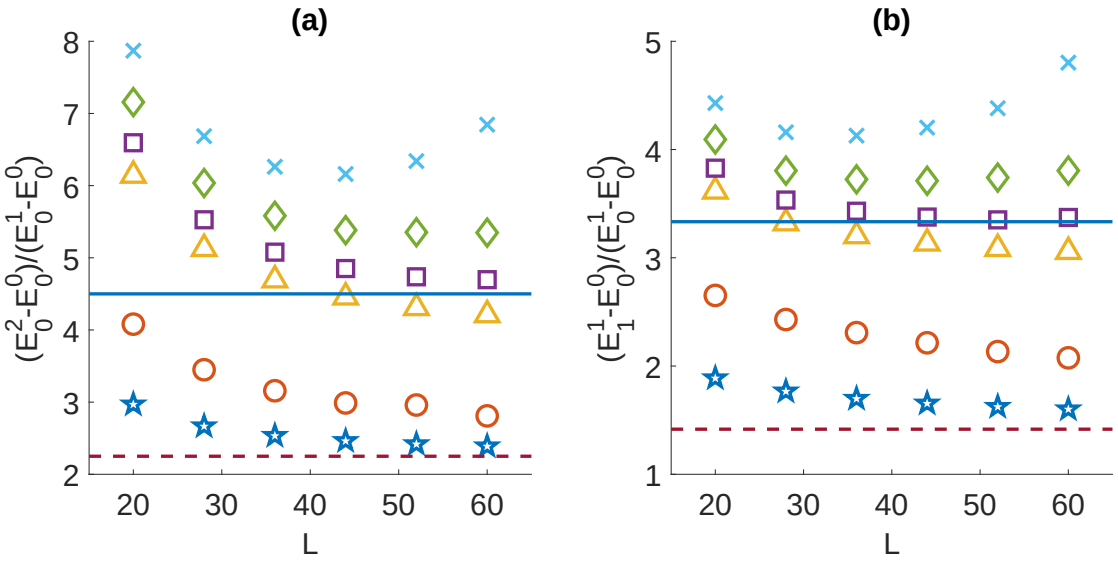

Figure 4.3: The ratios $(E_0^2 - E_0^0)/(E_0^1 - E_0^0)$ and $(E_1^1 - E_0^0)/(E_0^1 - E_0^0)$ are plotted against L for different values of λ_1/λ_P in (a) and (b), respectively. Values for $\lambda_1 = -1$, $\lambda_P = -0.6$ (blue stars), -0.65 (red circles), -0.67 (yellow triangles), -0.672 (purple squares), -0.674 (green diamonds) and -0.676 (teal crosses) are shown. The Potts and TCP lines are plotted in dashed red and solid blue at 9/4 and 9/2 in (a), and at 17/12 and 10/3 in (b), respectively.

this second order-disorder region has been difficult to determine numerically but should exist due to the symmetry with the first TCP point and order-disorder coexistence phase. The need for an incommensurate region will be explained at the end of this section. For now, we move past this region and instead focus on the next large, gapless region: the antiferromagnetic Potts phase.

At $\theta = -\pi$, Equation 4.38 reduces to $-H_P$. This is simply the antiferromagnetic Potts (AFP) model discussed in Subsection 4.2.2, where we saw the continuum limit was a CFT with $c = 1$ and radius $R = \sqrt{3/2}$ which, as explained in Section 4.7, is the only possible radius consistent with the Potts symmetry and self-duality. We find that this point extends to a whole phase, stretching from $\theta \approx -0.73\pi$ to $\theta \approx -1.07\pi$. The existence of a phase rather than just a point seems surprising – in Subsection 4.7 we claimed there was a relevant operator with weights $(h, \bar{h}) = (3/4, 3/4)$ that obeyed every symmetry of the Potts model and duality, so why does this operator not cause a transition?

The answer to this apparent conundrum can be found by looking at the low-lying

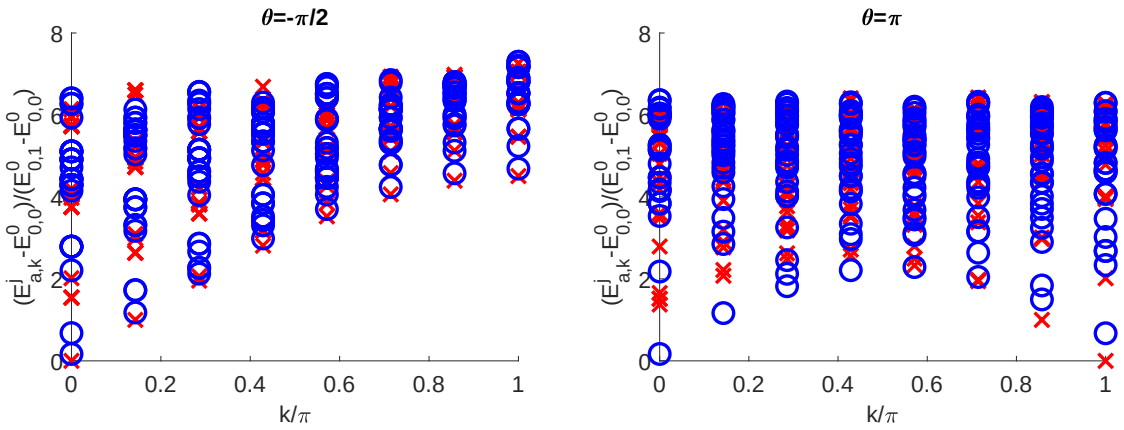

Figure 4.4: The gaps from the ground state to the 30 lowest energy levels are plotted in each $\mathbb{Z}_3$ r and momentum k sector for $H(-\pi/2)$ (left) and $H(\pi)$ (right) for $L = 14$. Red crosses denote $r = 0$ and blue circles $r = 1$, respectively. $H(-\pi/2)$ has large degeneracies and so several levels often lie on top of each other in the left-hand figure.

energy levels for $-H_1$ and $-H_{\mathrm{P}}$. In Figure 4.4 we plot the gaps from the ground state to the 30 lowest lying energy levels in each $\mathbb{Z}_3$ and momentum sector for $-H_1$ (left) and $-H_{\mathrm{P}}$ (right), respectively, for lattice length $L = 14$, as found using ED. We use the notation $E^j_{r,k}$ to represent the j^{th} excited state in the sector with $\mathbb{Z}_3$ charge r and momentum k. The gaps are normalised by dividing by the gap from the ground state energy to the lowest energy level in the $r = 0$ sector with momentum $\Delta k = 2\pi/L$ relative to the identity. For $\theta = -\pi/2$, the ground state is $E^0_{0,0}$, but for $\theta = \pi$ it is $E^0_{0,\pi}$. In fact, in the next chapter we will see that the momentum sector of the ground state in the AFP model depends on lattice length. As $E^1_{0,k_{\mathrm{GS}}+2\pi/L}$, where k_{GS} is the momentum of the ground state, corresponds to weights $(h, \bar{h}) = (1, 0)$ and hence dimension $\Delta = 1$ in the CFT, the values plotted are thus the approximate dimensions of the energy levels. We plot only $0 \leq k \leq \pi$ as, by parity, $E^j_{r,2\pi-k} = E^j_{r,k}$, and only $r = 0, 1$ as $E^j_{r,k} = E^j_{3-r,k}$ by charge conjugation.

From the left half of Figure 4.4, we see that all of the lowest lying states for $-H_1$ are close to $k = 0$, indicating that all conformal towers with primary operator of spin s are centred on $k = 2\pi s/L$. Looking instead at the right half, we see that there are low-lying states around both $k = 0$ and $k = \pi$, indicating that some conformal towers of spin s centre at $k = \pi + 2\pi s/L$ instead. In Chapter 5 we will see precisely which towers are close to $k = 0$ and which to $k = \pi$. For now, we

claim that our $(3/4, 3/4)$ perturbation has momentum π relative to the identity (in fact, for $L = 14$, (3/4, 3/4) has momentum 0 and the identity has momentum π) and hence it cannot be present in a translation invariant lattice perturbation, disallowing it from our perturbing Hamiltonian. As this was the only relevant self-dual operator obeying the symmetries of the Potts model, the antiferromagnetic Potts point is thus stable to perturbations and so extends to a phase.

The need for an incommensurate phase between the order-disorder phase and the AFP phase can now be explained by considering the energy levels. In the second Potts phase, all low-lying energy levels had momentum k close to 0, while for the AFP phase, there are many low-lying levels close to $k = \pi$. The most natural way of getting such a huge rearrangement of states without a point with enormous degeneracy (which does not seem to exist), is to have an intermediate incommensurate phase where many levels can cross each other.

4.9 The "c=3/2" phase

At $\theta \approx 0.93\pi$, the AFP phase terminates and a second incommensurate phase begins. At $\theta \approx 0.9\pi$ this phase ends and we transition to the final large phase marked in Figure 4.1. As with the other phases, we begin our analysis by studying a specific point, in this case $H(\pi/2) = H_1$. As this is just the negative of $H(-\pi/2)$, we would think that it must have exactly the same symmetries, including the non-commuting pair of $U(1)$ symmetries, Q (4.36) and $\hat{Q}$ (4.37). Indeed these are both symmetries and mean that the model again has large degeneracies and is integrable [52], but there is, in fact, one additional symmetry on top of these. At this point, the Hamiltonian can be written as $H_1 = \mathcal{Q}^2$ and thus it has lattice supersymmetry [96, 120, 140, 141]. Naïvely, we may think of supersymmetry as associating a fermion with the boson we know to be present due to the $U(1)$ symmetry, giving a central charge of $c = 1 + 1/2 = 3/2$ [140, 141].

Just as the $c = 1$ CFTs have been fully classified [75], the $c = 3/2$ SCFTs have also been [142]. Using duality and perturbing from an exactly solvable point

to be discussed in Chapter 5, we can again fix the SCFT exactly. The partition function is found to be $Z_{\text{s-a}}(\sqrt{3})$ [120, 142], where

$$Z_{\text{s-a}}(R) = \frac{1}{2}\left(\left|\frac{\theta_3}{\eta}\right| + \left|\frac{\theta_4}{\eta}\right|\right)\Gamma^+ + \frac{1}{2}\left(\left|\frac{\theta_3}{\eta}\right| - \left|\frac{\theta_4}{\eta}\right|\right)\Gamma^-_\delta + \frac{1}{2}\left|\frac{\theta_2}{\eta}\right|\left(\Gamma^- + \Gamma^+_\delta\right) \tag{4.52}$$

and, as in Equation 2.31,

$$\Gamma(R) = \frac{1}{\eta\bar{\eta}}\sum_{m,n} q^{\frac{1}{8R^2}\left(m+2R^2n\right)^2}\bar{q}^{\frac{1}{8R^2}\left(m-2R^2n\right)^2}, \tag{4.53}$$

but this time m and n may only take the values

$$\begin{aligned} &\Gamma^+ : m \in 2\mathbb{Z},\, n \in \mathbb{Z}; && \Gamma^- : m \in 2\mathbb{Z}+1,\, n \in \mathbb{Z}; \\ &\Gamma^+_\delta : m \in 2\mathbb{Z},\, n \in \mathbb{Z}+\frac{1}{2}; && \Gamma^-_\delta : m \in 2\mathbb{Z}+1,\, n \in \mathbb{Z}+\frac{1}{2}. \end{aligned}$$

While the Γ factors give the bosonic parts as before for $-H_1$, they are now non-trivially combined with the fermionic θ/η parts, where

$$\sqrt{\frac{\theta_2}{2\eta}} = q^{\frac{1}{24}}\prod_{r=1}^{\infty}\left(1+q^r\right), \sqrt{\frac{\theta_3}{\eta}} = q^{-\frac{1}{48}}\prod_{r=1}^{\infty}\left(1+q^{r-\frac{1}{2}}\right), \sqrt{\frac{\theta_4}{\eta}} = q^{-\frac{1}{48}}\prod_{r=1}^{\infty}\left(1-q^{r-\frac{1}{2}}\right).$$

Now that we know the continuum description at $\theta = \pi/2$, the next question is what happens when we perturb away from this point. For $\theta = -\pi/2$, perturbing infinitesimally in either direction led to a transition to the Potts CFT, as shown in Section 4.7. This time, however, it appears that we remain in a phase consistent with a central charge of $c = 3/2$. Looking at the scaling of the entanglement entropy with lattice length, as described in Subsection 2.3.3, we find the effective central charge as given in Figure 4.5.

These data are consistent with an effective central charge of $c \approx 3/2$ for a wide range of θ around $\theta = \pi/2$. The high amount of entanglement causes numerical problems and so reliable values for the entropy cannot be found for $L \gtrapprox 20$, meaning that the effective central charges are not as close to $3/2$ as we would like. Nonetheless, we are confident in this result as we will present a field theory argument in the next chapter to back it up.

While it appears that the model is consistent with a phase described by a CFT with $c = 3/2$, the ratios of gaps between energy levels do not agree with

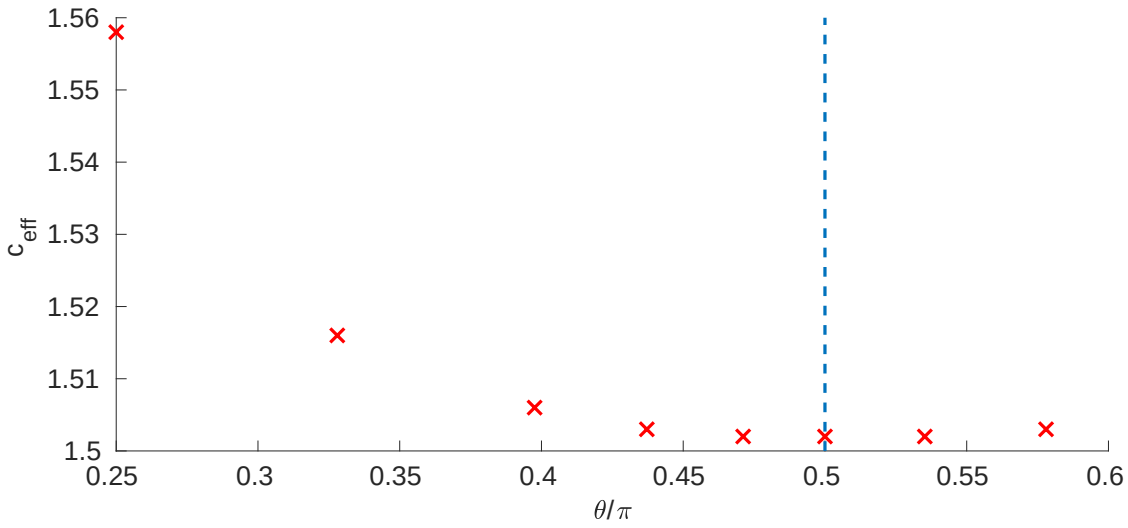

Figure 4.5: The effective central charge against θ. The blue dashed line marks $\theta = \pi/2$, where $H(\theta) = H_1$.

the partition function $Z_{\text{s-a}}(\sqrt{3})$ (4.52). Other logical options would be that it is described by $Z_{\text{s-a}}(R(\theta))$, where R depends on θ, or that the relative Fermi velocity between the boson and fermion changes from 1 (so the boson or fermion contributes more to the energy values), or a combination of these.

In fact, none of these is consistent with the energy ratios, meaning we have to dig a little deeper. Remarkably, it turns out that $Z_{\text{s-a}}(\sqrt{3})$ can be rewritten in terms of a Potts model and a TCI model non-trivially coupled [142]:

$$\begin{aligned} Z_{s-a}(\sqrt{3}) = &\left(\chi_0\bar{\chi}_0 + \chi_{\frac{7}{16}}\bar{\chi}_{\frac{7}{16}} + \chi_{\frac{3}{2}}\bar{\chi}_{\frac{3}{2}}\right)\left((\lambda_0+\lambda_3)(\bar{\lambda}_0+\bar{\lambda}_3) + 2\lambda_{\frac{2}{3}}\bar{\lambda}_{\frac{2}{3}}\right) \\ &+ \left(\chi_{\frac{3}{5}}\bar{\chi}_0 + \chi_{\frac{1}{10}}\bar{\chi}_{\frac{3}{2}} + \chi_{\frac{3}{80}}\bar{\chi}_{\frac{7}{16}}\right)\left((\lambda_{\frac{2}{5}}+\lambda_{\frac{7}{5}})(\bar{\lambda}_0+\bar{\lambda}_3) + 2\lambda_{\frac{1}{15}}\bar{\lambda}_{\frac{2}{3}}\right) \\ &+ \left(\chi_0\bar{\chi}_{\frac{3}{5}} + \chi_{\frac{3}{2}}\bar{\chi}_{\frac{1}{10}} + \chi_{\frac{7}{16}}\bar{\chi}_{\frac{3}{80}}\right)\left((\lambda_0+\lambda_3)(\bar{\lambda}_{\frac{2}{5}}+\bar{\lambda}_{\frac{7}{5}}) + 2\lambda_{\frac{2}{3}}\bar{\lambda}_{\frac{1}{15}}\right) \\ &+ \left(\chi_{\frac{1}{10}}\bar{\chi}_{\frac{1}{10}} + \chi_{\frac{3}{5}}\bar{\chi}_{\frac{3}{5}} + \chi_{\frac{3}{80}}\bar{\chi}_{\frac{3}{80}}\right)\left((\lambda_{\frac{2}{5}}+\lambda_{\frac{7}{5}})(\bar{\lambda}_{\frac{2}{5}}+\bar{\lambda}_{\frac{7}{5}}) + 2\lambda_{\frac{1}{15}}\bar{\lambda}_{\frac{1}{15}}\right), \end{aligned}$$

where χ and λ give the TCI and Potts characters [16], respectively. Being able to rewrite the partition function in a second form is highly unusual and does not happen for generic $c = 3/2$ SCFTs. It turns out that models with θ close to $\pi/2$ are consistent with this form of the partition function modified by changing the relative Fermi velocities, as shown in Figure 4.6. Here $v^j_{r,k}$ is the Fermi velocity of the TCI model found by comparing the energy gap of the j^{th} excited state in the $\mathbb{Z}_3 = r$

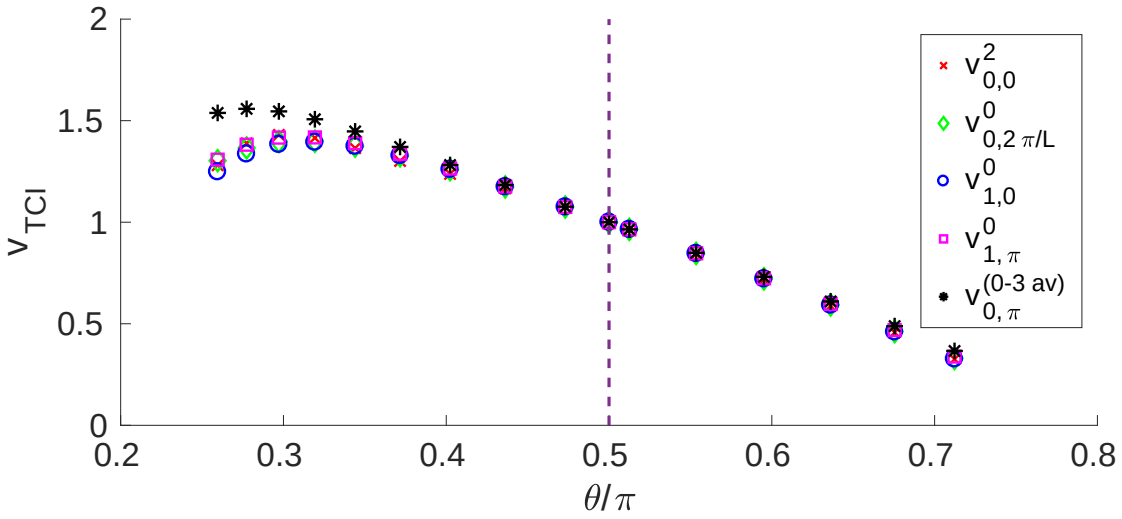

Figure 4.6: The effective Fermi velocities of the TCI model as calculated from different energy levels are plotted against θ with the Potts Fermi velocity set to 1.

and momentum k sector above the ground state energy $(E^j_{a,k} - E^0_{0,0})$, to the gap of the first excited state in the $\mathbb{Z}_3 = 0$ and momentum 0 sector above the ground state $(E^1_{0,0} - E^0_{0,0})$. We see that there is very good agreement close to $\theta = \pi/2$, indicating that this is the correct description, at least to leading order. The final set of points in the figure, $v^{(0-3\text{av})}_{0,\pi}$, are found using the average of the gaps to the lowest four energy levels in the $\mathbb{Z}_3 = 0$, $k = \pi$ sector. The average must be used as these points are degenerate at the integrable point and mix under the action of the marginal operator $(h_{\text{TCI}} + h_{\text{P}}, \bar{h}_{\text{TCI}} + \bar{h}_{\text{P}}) = (3/5 + 7/5, 0 + 0) + (0 + 0, 3/5 + 7/5)$, where h_{TCI} $(\bar{h}_{\text{TCI}})$ is the (anti)holomorphic weight of the TCI part and h_{P} $(\bar{h}_{\text{P}})$ is the (anti)holomorphic weight of the Potts part, and this marginal operator obeys the symmetries of the lattice model, as shown in Section 5.10.

Before moving on, we give an example of how to extract one of the Fermi velocities. Considering $v^2_{0,0}$, we are concerned with the gaps $g^2_{0,0} = E^2_{0,0} - E^0_{0,0}$ and $g^1_{0,0} = E^1_{0,0} - E^0_{0,0}$. The appropriate CFT fields to consider are

$$E^0_{0,0} : (0+0, 0+0)\,; \quad E^1_{0,0} : \left(\frac{1}{10} + \frac{2}{5}, \frac{1}{10} + \frac{2}{5}\right); \quad E^2_{0,0} : \left(\frac{3}{5} + \frac{2}{5}, \frac{3}{5} + \frac{2}{5}\right),$$

where the weights are expressed in the form $(h_{\text{TCI}} + h_{\text{P}}, \bar{h}_{\text{TCI}} + \bar{h}_{\text{P}})$, giving energies

$$g^1_{0,0} = \alpha \frac{v_{\text{TCI}} + 4}{5}, \quad g^2_{0,0} = \alpha \frac{6v_{\text{TCI}} + 4}{5} \tag{4.54}$$

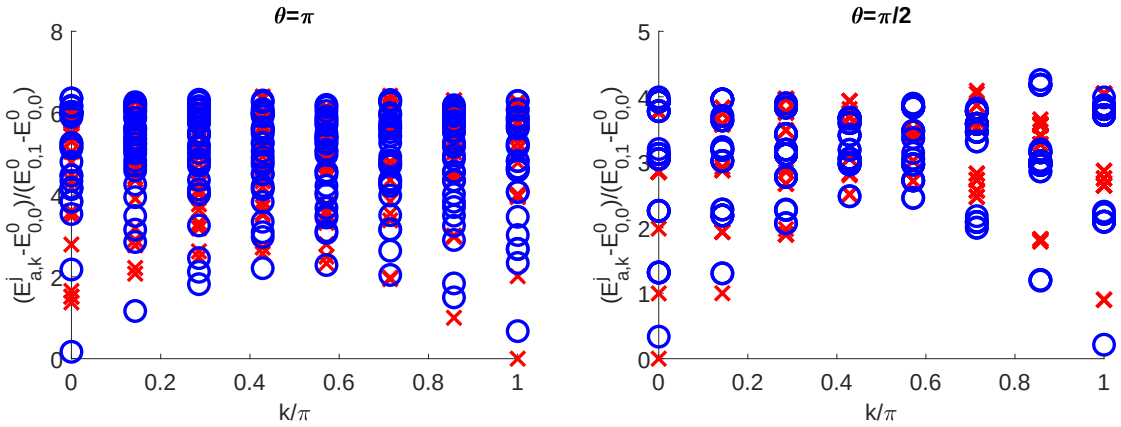

Figure 4.7: The gaps above the ground state to the low-lying energy levels for $-H_{\mathrm{P}}$ (left) and H_1 (right) at lattice length $L = 14$. Again, the energies are normalised such that the state corresponding to $(h, \bar{h}) = (1, 0)$ has energy 1.

for some constant of proportionality α. Rearranging, this gives

$$v_{\mathrm{TCI}} = 4\,\frac{g^2_{0,0} - g^1_{0,0}}{6g^1_{0,0} - g^2_{0,0}}. \tag{4.55}$$

We then help to correct for finite-size effects by dividing this by the value at $\theta = \pi/2$ (as we know here the true value is 1), and fit for lattice lengths L up to 16 to get the estimated value of $v^2_{0,0}$.

At the moment, the choice of fields corresponding to $E^1_{0,0}$ and $E^2_{0,0}$ may appear somewhat arbitrary. In Chapter 5 we will explain why these are correct by considering which fields in the boson + fermion partition function have to have which $\mathbb{Z}_3$ charges and momenta, and by requiring consistency between the two forms of the partition function.

This "$c = 3/2$" phase is believed to stretch from $\theta \approx 0.9\pi$ to $\theta \approx 0.19\pi$, where a third and final incommensurate region begins. The second and third incommensurate regions are again needed to shift the location of the low-lying states, as shown in Figures 4.7 and 4.8. Once more, the locations of the low-lying energy levels do not agree, requiring the presence of incommensurate regions. Which conformal towers are centred at k near 0 and which at k near π will be explained in Chapter 5.

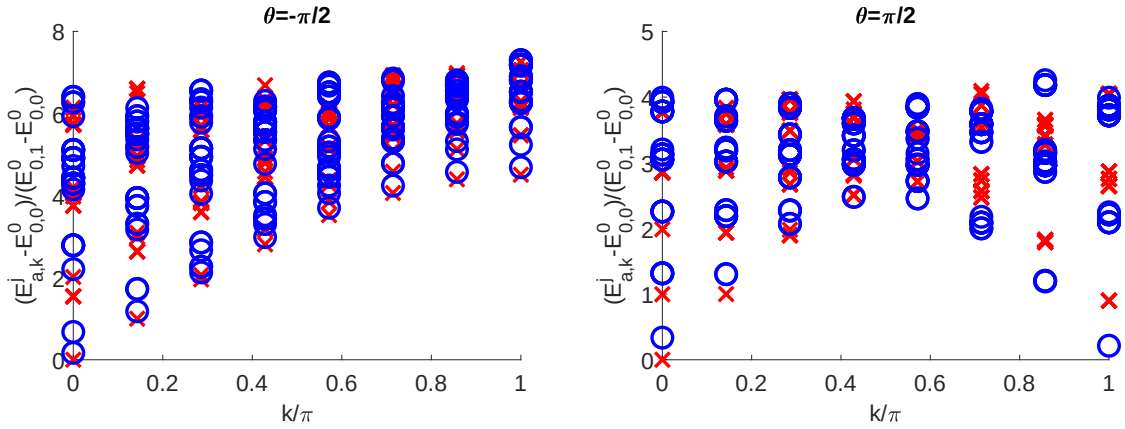

Figure 4.8: The gaps above the ground state to the low-lying energy levels for $-H_1$ (left) and H_1 (right) at lattice length $L = 14$. Again, the energies are normalised such that the state corresponding to $(h, \bar{h}) = (1, 0)$ has energy 1.

4.10 Conclusions and outlook

We have investigated the phase diagram of the two competing nearest-neighbour self-dual interactions obeying the symmetries of the 3-state Potts model. As well as the expected ferromagnetic and antiferromagnetic sections, we have found several more exotic phases. Firstly, we have an order-disorder coexistence phase, similar to that found in the perturbed Ising model of Chapter 3, separated from the Potts phase by a point in the universality class of the TCP CFT. We found a second Potts phase separating different ordered and disordered phases, to be discussed in Chapter 5, separated from the first by a point with $U(1)$ and dual $U(1)$ symmetries, resulting in an Onsager symmetry. There was also an extended AFP region, protected by the lattice momentum of certain CFT fields, as will be explained more fully in Chapter 5.

Perhaps most intriguingly of all, the second point with $U(1)$ and Onsager symmetry is supersymmetric and was found to be part of a broader phase with entanglement scaling consistent with at $c = 3/2$ CFT. Off this integrable point, to leading order, the theory appeared to split into two connected pieces with different Fermi velocities, one corresponding to a Potts CFT and the other to a TCI CFT.

While we have made significant progress in understanding this phase diagram, there are still several interesting questions to answer. Exactly how large are the incommensurate regions and how does the system transition into them? Due to

numerical roadblocks we have so far been unable to answer this, but we hope that improved numerical techniques in the future could lead to progress.

Another mystery is how the Onsager symmetry fits into the CFT at $\pm H_1$. The problem here is that the symmetries of the CFT are too big! The states degenerate due to the Onsager algebra, as given in Ref. [52], are degenerate in the CFT, but so are others which have different energies on the lattice. Some progress has been made in this area, but we have still not worked out the full story.

A third area to look at is the generalisation to higher q in the Potts model. We know that there are frustration-free points akin to those for $q = 3$ (4.39) for all $q \geq 3$ [127]. Likewise, we know that H_1 and $-H_1$ generalise to all $q \geq 2$, where the H_1 CFT can be written as a boson with radius $R = \sqrt{q(q-1)/2}$ combined with the $\mathbb{Z}_{q-1}$ parafermion model [52, 122, 143] (or alternatively the $\mathbb{Z}_q$ parafermion model combined with the $m = q$ minimal model), while $-H_1$ is described by a $c = 1$ bosonic CFT with radius $R = \sqrt{q/2}$. By adding different interactions to higher q Potts models (or, perhaps, parafermion models), what further exotic phases can we discover?

We also hope to make progress in understanding how the different expressions for the CFTs fit together at the $c = 3/2$ point, and how this generalises to the general q case [143]. As we mentioned in Section 4.9, being able to write this CFT in two different ways is highly non-trivial and could potentially lead to some new relations between CFT fields, or at least simpler ways to calculate them.

Finally, on the more practical side, we hope that the exotic phases explored here may prove of interest to experimentalists and especially those working on the interface between theory and experiment. As new materials with wonderful properties are being discovered all the time, it is useful to have underlying theory to explain the new phenomena encountered and to help in the design of new devices, whether they be quantum computers or something not yet even dreamt up!

5 Duality-breaking regions

Contents

5.1 Introduction

Throughout this thesis so far, we have focused on self-dual couplings. In this chapter we extend this to duality-breaking models around two points in the S_3-invariant model of Chapter 4.

The first half will focus on the region surrounding $H(-\pi/2) = -H_1$ from Equation 4.38. We have already seen in Section 4.7 that a self-dual perturbation preserving the Potts symmetries gives a transition to the Potts CFT, but we now extend this to duality-breaking perturbations. We will see that there are four gapped phases surrounding the $c = 1$ point, separated from each other by $c = 4/5$ lines. Each of these gapped phases has a frustration-free point with exact ground states, which is archetypal of the phase as a whole.

The first two phases are the mundane ordered and disordered Potts phases, as discussed in Section 4.2, while the two remaining phases are more novel. We have a "not-A" phase in which one spin direction is *dis*favoured and the other two are favoured. This is in sharp contrast to the ordered Potts model, where one direction is favoured and the other two are disfavoured. The final phase is the dual of this and corresponds to a "representation symmetry protected topological" (RSPT) phase. This is similar to a symmetry protected topological (SPT) phase [144–147], but with the phase protected by a doublet representation of a non-Abelian group (in this case S_3), rather than a projective representation. As we will see, this is a weaker condition than that of a normal SPT.

The archetypal point in the RSPT phase proves to be of even more interest. The ground state is given by a matrix product state (MPS) of a form very similar to that of the Affleck–Kennedy–Lieb–Tasaki (AKLT) model [148–150]. In fact, the Hamiltonians of both the AKLT model and at our special (MPS) point are part of a larger family of Hamiltonians with MPS ground states, first studied in Ref. [151]. This point is also found to have exact excited states, similar to the AKLT model [53, 152–154], showing its connection with quantum scars and violation of the strong Eigenstate Thermalization Hypothesis [155–157], currently very much in vogue due to their apparent appearance in a system of Rydberg atoms and its connection with the PXP model [158–161].

The second half of this chapter explains the momentum sectors of the different conformal towers in the AFP and "$c = 3/2$" phases. We do this by perturbing from an exactly solvable off-critical point and finding an effective XXZ model

there [3]. This model has a continuum limit given by a boson CFT with $c = 1$ [162]. By solving a limit of this model exactly, we can extract the momenta of the different states on the lattice. In the CFT, all relevant operators have momenta close to 0, but, on the lattice, the corresponding states for some of these pick up factors of π, disallowing them from translation-invariant perturbations, stabilising the AFP and "$c = 3/2$" phases. This analysis also allows us to determine the exact form of the supersymmetric CFT.

In Section 5.2 we introduce the off-critical Hamiltonian and give the phase diagram around $-H_1$. Sections 5.3 and 5.4 give the exact ground states at four special points and describe the phases surrounding them, while Section 5.5 is a brief aside on exact excited states at one of these points. The first half of this chapter then concludes in Section 5.6, where transitions between these phases are considered using a field theory argument. This half of the chapter is based predominantly on Ref. [50].

The second half of the chapter is a thesis exclusive. In section 5.7 we perform perturbation theory about an exactly solvable point and find the qualitative difference between momenta at the AFP and H_1 points. Section 5.8 solves the XX model and explains how lattice momenta and states correspond to fields in the CFT. Section 5.9 explains why we have the particular $c = 3/2$ CFT given by Equation 4.52 at H_1, while Section 5.10 looks at the operators in this CFT to determine the stability of the point. We wrap up the chapter as a whole with some conclusions and ideas for further study in Section 5.11.

5.2 The Hamiltonian

We begin by introducing the duality-broken Hamiltonian,

$$H_{\mathrm{DB}}(J, f, \lambda_1) = \lambda_1 H_1 - \sum_{j=1}^{L} \left[J\left(\sigma_j^\dagger \sigma_{j+1} + \sigma_j \sigma_{j+1}^\dagger\right) + f\left(\tau_j + \tau_j^\dagger\right) \right], \tag{5.1}$$

which corresponds to $H(\theta)$ from Equation 4.38 when $J = f = \cos\theta$ and $\lambda_1 = \sin\theta$.

The first half of this chapter is concerned with the phase diagram around the integrable point with Onsager symmetry and described by a CFT with $c = 1$:

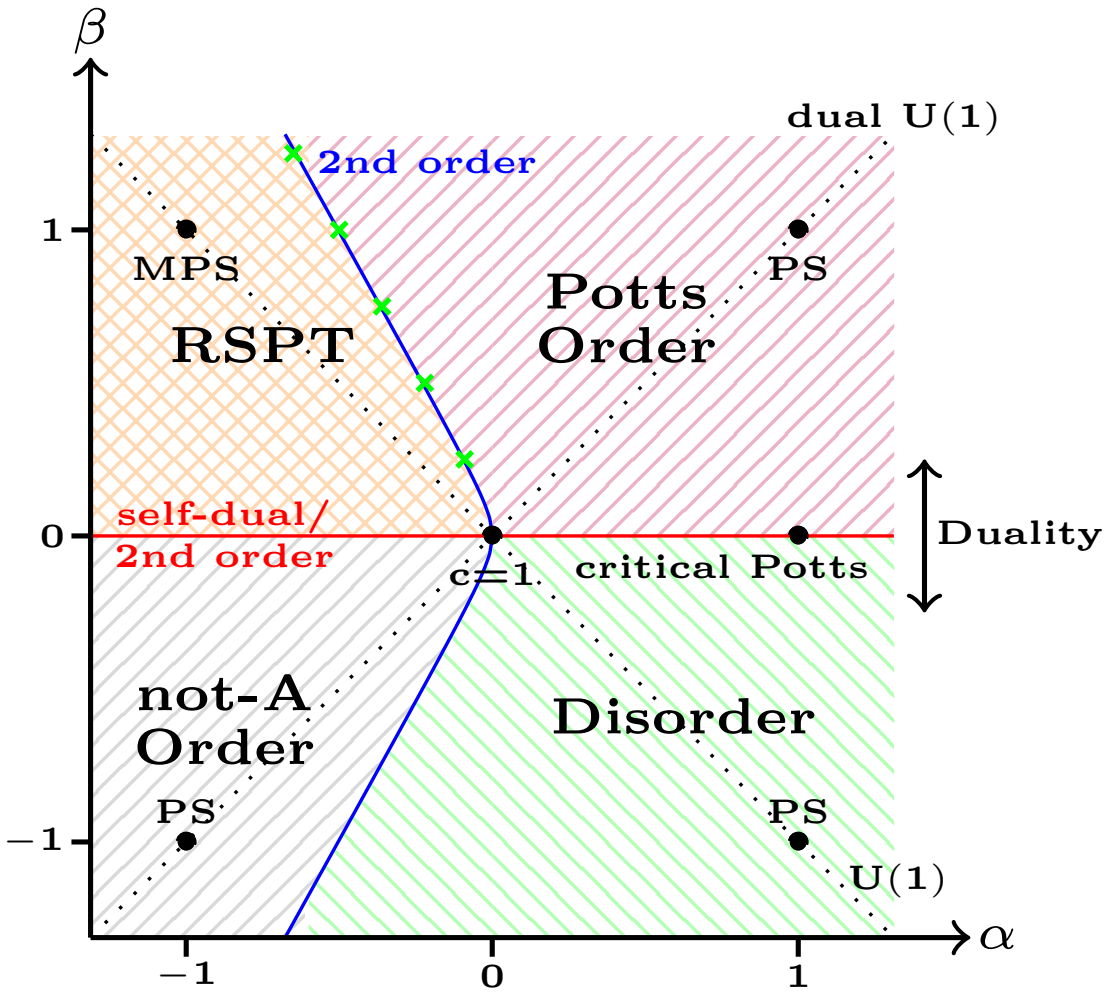

Figure 5.1: The phase diagram of the off critical model around the multicritical point $-H_1$, marked by $c = 1$. The axes are given by $J = \alpha + \beta$, $f = \alpha - \beta$ and $\lambda_1 = \alpha - 1$. The solid red horizontal line gives the self-dual line and marks Potts CFT transitions, as does the duality breaking solid blue line. The black dotted lines denote the $U(1)$ and dual $U(1)$ symmetric lines, with conserved charges Q (4.36) and $\hat{Q}$ (4.37), respectively. The four points with exact ground states are marked with black circles at $\alpha = \pm 1$, $\beta = \pm 1$, as is the critical Potts point at $\alpha = 1$, $\beta = 0$. A duality mapping ($J \leftrightarrow f$) corresponds to a reflection in $\beta = 0$.

$H_{\mathrm{DB}}(0, 0, -1) = -H_1 = H(-\pi/2)$ in the language of Equation 4.38. This phase diagram is given in Figure 5.1. In this chapter we will often use the alternative parameterization

$$J = \alpha + \beta, \quad f = \alpha - \beta, \quad \lambda_1 = \alpha - 1, \tag{5.2}$$

giving a more natural correspondence with the figure.

5.3 Exact ground states

5.3.1 The ordered and disordered Potts points

Around $-H_1$ there are four points with exact frustration-free ground states. The first two of these, at $H_{\mathrm{DB}}(1,0,0)$ and $H_{\mathrm{DB}}(0,1,0)$, are the completely ordered and disordered Potts model, with ground states $|AA...A\rangle$, where $A = 0, 1, 2$, and $\left|\hat{0}\hat{0}...\hat{0}\right\rangle$, respectively, with $\sigma |A\rangle = \omega^A |A\rangle$ and $\tau |\hat{n}\rangle = \omega^{\hat{n}} |\hat{n}\rangle$, as given in Equations 4.7 and 4.8. For later convenience we give these ground states again as

$$\left|\Psi_A^{\mathrm{OP}}\right\rangle = |AA...A\rangle\,, \tag{5.3}$$

$$\left|\Psi_{\hat{0}}^{\mathrm{DP}}\right\rangle = \left|\hat{0}\hat{0}...\hat{0}\right\rangle. \tag{5.4}$$

These points are part of larger ordered and disordered Potts phases, with the magnetisation order parameter

$$M_g = \langle g|\, \sigma_j\, |g\rangle \tag{5.5}$$

distinguishing between them, where $|g\rangle$ represents a ground state. This order parameter is non-vanishing in the ordered phase in an S_3-breaking ground state, while in the disordered phase it is 0. At the completely ordered Potts point, the three ground states have $M_0 = 1$, $M_1 = \omega$, $M_2 = \omega^2$, implying they all have the same value of $M^3 = 1$, where we define

$$M^3 \equiv \lim_{|j-k|,|k-l|,|j-l|\to\infty} G_{jkl}; \tag{5.6}$$

$$G_{jkl} \equiv \langle g|\, \sigma_j\sigma_k\sigma_l\, |g\rangle\,. \tag{5.7}$$

This order parameter will prove key in distinguishing between the ordered Potts phase and the "not-A" phase to be discussed later.

Before moving on, we note that, under the action of the S_3 symmetry, the ordered Potts ground states (5.3) transform between each other as

$$\mathcal{S}\left|\Psi_0^{\mathrm{OP}}\right\rangle = \left|\Psi_1^{\mathrm{OP}}\right\rangle, \quad \mathcal{S}\left|\Psi_1^{\mathrm{OP}}\right\rangle = \left|\Psi_2^{\mathrm{OP}}\right\rangle, \quad \mathcal{S}\left|\Psi_2^{\mathrm{OP}}\right\rangle = \left|\Psi_0^{\mathrm{OP}}\right\rangle, \tag{5.8}$$

$$\mathcal{C}\left|\Psi_0^{\mathrm{OP}}\right\rangle = \left|\Psi_0^{\mathrm{OP}}\right\rangle, \quad \mathcal{C}\left|\Psi_1^{\mathrm{OP}}\right\rangle = \left|\Psi_2^{\mathrm{OP}}\right\rangle, \tag{5.9}$$

where $\mathcal{S}$ and $\mathcal{C}$ are the $\mathbb{Z}_3$ and charge conjugation respectively. This will again prove important in distinguishing between the phases.

5.3.2 The "not-A" point

The ordered and disordered Potts points are completely trivial, and the full spectra can be written down there. The next two points we consider also have exact ground states, but generic states in the spectrum cannot be found exactly. We note though that certain exact excited states can be found, as will be explained in Section 5.5.

The Hamiltonian at $J = -2$, $f = 0$, $\lambda_1 = -2$ ($\alpha = \beta = -1$) can be written as

$$H_{\mathrm{DB}}(-2, 0, -2) = -6L + 9\sum_{j=1}^{L} P^{(l)}_{j,j+1} + P^{(r)}_{j,j+1}, \tag{5.10}$$

where $P^{(l)}_{j,j+1}$ projects onto the three states

$$|AA\rangle - |BA\rangle - |CA\rangle \tag{5.11}$$

and $P^{(r)}_{j,j+1}$ projects onto

$$|AA\rangle - |AB\rangle - |AC\rangle\,, \tag{5.12}$$

where the kets are on sites j and $j+1$, $A \neq B \neq C \neq A$ and $A = 0, 1, 2$. The three states

$$\left|\Psi^{\text{not-}A}_{\bar{A}}\right\rangle \equiv \left|\bar{A}\bar{A}...\bar{A}\right\rangle \tag{5.13}$$

are then exact ground states, where

$$\left|\bar{A}\right\rangle = \frac{1}{\sqrt{2}}\left(|B\rangle + |C\rangle\right) \tag{5.14}$$

and, again, $A \neq B \neq C \neq A$. Analogously to the ordered Potts case, the $\mathbb{Z}_3$ symmetry cycles through $\left|\Psi^{\text{not-}A}_{\bar{0}}\right\rangle$, $\left|\Psi^{\text{not-}A}_{\bar{1}}\right\rangle$ and $\left|\Psi^{\text{not-}A}_{\bar{2}}\right\rangle$ and charge conjugation leaves $\left|\Psi^{\text{not-}A}_{\bar{0}}\right\rangle$ invariant but exchanges $\left|\Psi^{\text{not-}A}_{\bar{1}}\right\rangle$ and $\left|\Psi^{\text{not-}A}_{\bar{2}}\right\rangle$, and so we see that the S_3 symmetry is again spontaneously broken. In this case, the magnetisations are

$$M_{\bar{A}} = -\frac{1}{2}\omega^A \tag{5.15}$$

and $M^3_{\bar{A}} = -1/8$.

5.3.3 The MPS ground state

The completely ordered Potts point is the dual of the completely disordered Potts point. We may then expect a special point at the dual of the "not-A" point as well: $H_{\mathrm{DB}}(0,-2,-2)$ ($\alpha=-1,\beta=1$), which we do indeed find. The Hamiltonian at this point becomes

$$H_{\mathrm{MPS}}=2\sum_{j=1}^{L}\left(S_j^{+2}S_{j+1}^{-2}-S_j^{+}S_{j+1}^{-}+\mathrm{h.c.}\right), \tag{5.16}$$

which has a unique ground state given by the MPS

$$|\Psi_{\mathrm{MPS}}\rangle=\mathrm{Tr}\left(R_1R_2...R_L\right), \tag{5.17}$$

where

$$R_j=\begin{pmatrix}|\hat{0}\rangle & |\hat{1}\rangle\\ |\hat{2}\rangle & |\hat{0}\rangle\end{pmatrix} \tag{5.18}$$

and all kets are on site j.

This state is again invariant under the S_3 symmetry, meaning the magnetisation M vanishes. For periodic boundary conditions (PBC) the ground state (5.17) is unique, while for open boundary conditions (OBC), where we take the sum to $L-1$ rather than L in H_{MPS} (5.16), there are four ground states, implying that it could be part of a symmetry protected topological (SPT) phase. In fact, we will see that the phase is not quite an SPT, but a related RSPT, which we describe in Subsection 5.4.2.

5.3.4 Conformal boundary conditions

As well as giving an archetypal point in each of the four phases, the exact ground states have an intriguing connection to conformal boundary conditions. In the critical two-dimensional classical Potts model there are eight different boundary conditions allowed by conformal invariance [163, 164]. The boundaries of two-dimensional surfaces are given by one-dimensional lines and it turns out that the allowed conformal boundary conditions of the two-dimensional Potts model are very strongly connected to the exact ground states at the four points $\alpha=\pm1$,

Phase	M^3	Degeneracy
Ordered Potts	>0	3
Disordered Potts	0	1
RSPT	0	4
not-A	<0	3

Table 5.1: The order parameter M^3 (5.7) and the ground-state degeneracy with OBC for each phase surrounding the $c = 1$ point, as given in Figure 5.1.

$\beta = \pm 1$ in Figure 5.1 described in the previous subsections, which, of course, live on one-dimensional chains!

The states $|AA...A\rangle$ for $A = 0, 1, 2$ correspond to the three fixed boundary conditions in the two-dimensional classical model, while $|\hat{0}\hat{0}...\hat{0}\rangle$ is analogous to free boundary conditions, where all spin directions are allowed. $|\bar{A}\bar{A}...\bar{A}\rangle$ correspond to the mixed boundary conditions in which two of the two-dimensional Potts states are allowed. The eighth and final conformal boundary condition is the strangest and was the last to be found [164], hence its name: the "new" boundary condition. This boundary condition is the dual of mixed though, and so we see that it corresponds to our MPS ground state as this is the dual of the "not-A" states.

5.4 The phases

Having found four points with exact ground states, we now expand our analysis to the phases surrounding them. The phases are distinguished by two criteria: their values of the M^3 order parameter (5.7) and their ground-state degeneracy for the model with OBC, as shown in Table 5.1. The rest of this section will be spent describing these phases.

Before getting on to a discussion of these phases, we demonstrate the numerical evidence supporting the values of M^3 and the degeneracy of the ground state with OBC in the different phases. In Figure 5.2 (a) we plot the value of M^3 from Equation 5.7 for the circle in Figure 5.1 with $\alpha^2 + \beta^2 = 1$ by setting $\alpha = \cos\phi$ and $\beta = \sin\phi$. The data were found using DMRG on a chain with OBC of length $L = 200$ and a bond dimension $\chi = 300$. We found that neither increasing L nor χ changed

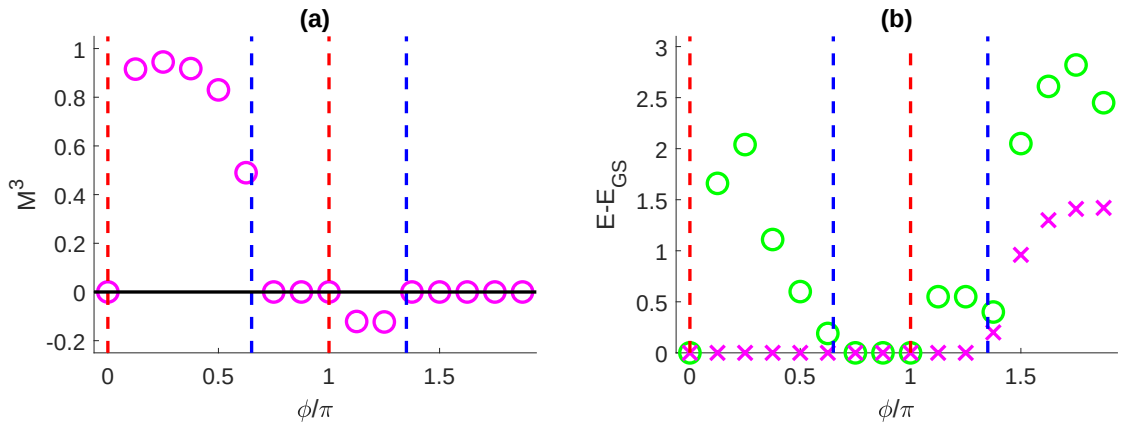

Figure 5.2: The order parameter M^3 is plotted against ϕ in (a), where $\alpha = \cos\phi$ and $\beta = \sin\phi$. In (b) the gaps from the ground state in the $\mathbb{Z}_3 = 0$ sector to the lowest energy level in the $\mathbb{Z}_3 = 1$ sector (purple crosses) and first excited level in the $\mathbb{Z}_3 = 0$ sector (green circles) are again plotted against ϕ.

the results, implying good convergence. The red and blue dashed lines represent the positions of the red and blue second order transitions in Figure 5.1. We see that $M^3 > 0$ between the first red and blue lines (the ordered Potts phase), before going to 0 in the RSPT phase. It then becomes negative in the not-A phase, before returning to 0 in the disordered Potts phase, as given in column 2 of Table 5.1.

In Figure 5.2 (b), we do the same but this time plot the gaps in the model with OBC from the ground state in the $\mathbb{Z}_3 = 0$ sector to the lowest energy level in the $\mathbb{Z}_3 = 1$ sector (purple crosses) and the first excited level in the $\mathbb{Z}_3 = 0$ sector (green circles). Again, we see that these data agree with column 3 of Table 5.1. To get these data we again performed DMRG for $L = 200$, but this time with $\chi = 800$.

5.4.1 The ordered phases

As we saw in Section 5.3, both the ordered Potts and not-A points had ordered ground states which transformed non-trivially under the S_3 symmetry and had $M^3 \neq 0$. As the Hamiltonian is S_3 invariant everywhere, this symmetry is expected to be spontaneously broken even as we perturb away from these points, giving extended ordered Potts and not-A phases.

As we deform the model away from these points, the ground states change and hence so does the value of M^3 but, as S_3 is a discrete group and the S_3 symmetry is

spontaneously broken in this phase, the three different ground states must transform into each other in the same way under its action unless there is a phase transition.[1] Taking $|\Psi_A\rangle$ to correspond to the continuation of $\left|\Psi_A^{\mathrm{OP}}\right\rangle$ as we perturb from the ordered Potts, we see that Equations 5.8 and 5.9 become

$$\mathcal{S}\,|\Psi_0\rangle = |\Psi_1\rangle\,, \quad \mathcal{S}\,|\Psi_1\rangle = |\Psi_2\rangle\,, \quad \mathcal{S}\,|\Psi_2\rangle = |\Psi_0\rangle\,, \tag{5.19}$$

$$\mathcal{C}\,|\Psi_0\rangle = |\Psi_0\rangle\,, \quad \mathcal{C}\,|\Psi_1\rangle = |\Psi_2\rangle\,, \tag{5.20}$$

with analogous relations holding for the ground states when we perturb from the not-A point. We then see that M^3 is the same for each $|\Psi_A\rangle$, although its value changes from that for $\left|\Psi_A^{\mathrm{OP}}\right\rangle$, and it remains real, with the same true for $|\Psi_{\bar{A}}\rangle$.

As M^3 remains real and is positive for the ordered Potts point and negative for the not-A point, the only way to get from one to the other is to go through a point where $M^3 = 0$, but here the magnetisation vanishes and so the S_3 is not spontaneously broken, indicating a phase transition. In fact, for the couplings allowed in our phase diagram, this happens precisely at the $c = 1$ point, $-H_1$, at the centre of Figure 5.1! As both the disordered Potts and RSPT phase have unique ground states with the S_3 not spontaneously broken, M^3 must be zero in both of these, leading to the second column in Table 5.1.

5.4.2 The disordered Potts and RSPT phases

The simplest of the four phases in our diagram is the disordered Potts phase. This phase is the dual of the ordered Potts phase and has $M^3 = 0$, along with a unique ground state with OBC.

The final phase surrounds the MPS point. As stated above, M^3 vanishes here, just as it does in the disordered Potts phase. The two are not in the same phase though, as a further analysis shows – the MPS point is part of a representation symmetry protected topological (RSPT) phase.

[1] Of course, were we to add an S_3-breaking interaction, this argument would no longer hold.

We begin by noting the similarity between our MPS ground state and the AKLT ground state of a spin-1 $SO(3)$ invariant chain [148, 149]. The difference between the two is the matrix building the MPS:

$$R_{\text{ours}} = \begin{pmatrix} |\hat{0}\rangle & |\hat{1}\rangle \\ |\hat{2}\rangle & |\hat{0}\rangle \end{pmatrix}, \quad R_{\text{AKLT}} = \begin{pmatrix} |\hat{0}\rangle & -\sqrt{2}\,|\hat{1}\rangle \\ \sqrt{2}\,|\hat{2}\rangle & -|\hat{0}\rangle \end{pmatrix}, \tag{5.21}$$

where the first is our matrix and the second is that for AKLT. Both our model at the MPS point and AKLT are part of a larger family of Hamiltonians [151, 165],

$$H_{\text{MPS}} = \sum_{j=1}^{L} \Big[h_j^2 + \beta\,(h_j g_j + g_j h_j) + \beta' g_j\,(1+g_j) + \alpha_2 g_j^2 \\ \alpha_3 h_j + \alpha_4\left(S_j^{z\,2} + S_{j+1}^{z\,2}\right) + \alpha_0 \Big], \tag{5.22}$$

where $h_j = S_j^+ S_{j+1}^- + S_j^- S_{j+1}^+$, $g_j = S_j^z S_{j+1}^z$, $\alpha_0 = a^2 - 2$, $\alpha_2 = a^2 - 2|\beta + a|$, $\alpha_3 = a + \beta$, and $\alpha_4 = |a+\beta| + 1 - a^2$. For all choices of a, β and β', this family of Hamiltonians has an exact zero-energy MPS ground state built from the matrix

$$R(a,\beta,\beta') = \begin{pmatrix} |\hat{0}\rangle & -\sqrt{a}\,|\hat{1}\rangle \\ \sqrt{a}\,|\hat{2}\rangle & -\text{sign}(\beta+a)\,|\hat{0}\rangle \end{pmatrix}. \tag{5.23}$$

Our Hamiltonian corresponds to $(a,\beta,\beta') = (-1,0,1/2)$, with the extra factors of i in the MPS cancelling in the product, while AKLT has $(a,\beta,\beta') = (2,1,3)$. The biggest difference between our ground state and AKLT is the presence of minus signs in the AKLT MPS, but the unitary transformation $U = \prod_j e^{ij\pi S_j^z}$ sends $(a,\beta,\beta') \to (-a,-\beta,\beta')$ and removes these.

Given the similarity between our ground state and AKLT, we consider the physics of AKLT to give us an insight into our model. One fascinating feature of AKLT is its status as the archetypal point of the classic symmetry protected topological (SPT) phase: the Haldane phase [144, 145]. This phase is stable as long as time-reversal, parity or a D_2 symmetry about all three orthogonal axes is preserved [145]. If time-reversal or the D_2 symmetry is preserved, there are four degenerate ground states for OBC. Unfortunately, the time-reversal symmetry in AKLT is not the same time-reversal as ours and is broken by the $\sigma_j^\dagger \sigma_{j+1} + \sigma_j \sigma_{j+1}^\dagger$ perturbation. Neither is the D_2 symmetry corresponding to charge conjugation and the $\mathbb{Z}_2 = \prod_j e^{i\pi S_j^z}$ preserved, and so we have to work a little harder.

The simplest way to demonstrate the existence of an SPT is to look at the ground states of the model with OBC. To get OBC, we simply change the upper limit of the sum in H_{MPS} (5.22) from L to $L-1$. At the MPS point, this Hamiltonian then has 4 ground states, given by the four entries of

$$\begin{pmatrix} |uu\rangle & |ud\rangle \\ |du\rangle & |dd\rangle \end{pmatrix} = R_1 R_2 ... R_L, \tag{5.24}$$

as in Equation 5.17, but where we now take the elements of the matrix individually, rather than the trace. As the system is gapped, the correlation length is finite and so the edges are uncorrelated in the infinite limit. Hence in the ground state each edge is in one of two states u and d, giving a degeneracy of $2 \times 2 = 4$. We now show how the S_3 symmetry protects this degeneracy.

Taking the $\mathbb{Z}_3$ and charge conjugation generators of the S_3 as $\mathcal{S}$ and $\mathcal{C}$ once more, these obey

$$\mathcal{S}^3 = 1, \quad \mathcal{C}^2 = 1, \quad \mathcal{C}\mathcal{S}^2 = \mathcal{S}\mathcal{C}, \quad \mathcal{S}^2\mathcal{C} = \mathcal{C}\mathcal{S}. \tag{5.25}$$

Looking at the ground state of our model, we find the action of the generators as

$$\mathcal{S}\begin{pmatrix} |\hat{0}\rangle & |\hat{1}\rangle \\ |\hat{2}\rangle & |\hat{0}\rangle \end{pmatrix} = \begin{pmatrix} |\hat{0}\rangle & \omega|\hat{1}\rangle \\ \omega^2|\hat{2}\rangle & |\hat{0}\rangle \end{pmatrix}, \quad \mathcal{C}\begin{pmatrix} |\hat{0}\rangle & |\hat{1}\rangle \\ |\hat{2}\rangle & |\hat{0}\rangle \end{pmatrix} = \begin{pmatrix} |\hat{0}\rangle & |\hat{2}\rangle \\ |\hat{1}\rangle & |\hat{0}\rangle \end{pmatrix}. \tag{5.26}$$

These are equivalent to the following unitaries acting on the auxiliary space of the MPS:

$$U_{\mathcal{S}} = \begin{pmatrix} \omega^2 & 0 \\ 0 & \omega \end{pmatrix}, \quad U_{\mathcal{C}} = \begin{pmatrix} 0 & 1 \\ 1 & 0 \end{pmatrix}, \tag{5.27}$$

where $R_j \to U_{\mathcal{S}/\mathcal{C}} R_j U_{\mathcal{S}/\mathcal{C}}^\dagger$ on every site gives the appropriate transformation.

Applying these unitaries to every site, they cancel everywhere other than sites 1 and L, thus transforming the edges:

$$\begin{pmatrix} |uu\rangle & |ud\rangle \\ |du\rangle & |dd\rangle \end{pmatrix} \to U_{\mathcal{S}} \begin{pmatrix} |uu\rangle & |ud\rangle \\ |du\rangle & |dd\rangle \end{pmatrix} U_{\mathcal{S}}^\dagger = \begin{pmatrix} |uu\rangle & \omega|ud\rangle \\ \omega^2|du\rangle & |dd\rangle \end{pmatrix}, \tag{5.28}$$

$$\begin{pmatrix} |uu\rangle & |ud\rangle \\ |du\rangle & |dd\rangle \end{pmatrix} \to U_{\mathcal{C}} \begin{pmatrix} |uu\rangle & |ud\rangle \\ |du\rangle & |dd\rangle \end{pmatrix} U_{\mathcal{C}}^\dagger = \begin{pmatrix} |uu\rangle & |du\rangle \\ |ud\rangle & |dd\rangle \end{pmatrix}. \tag{5.29}$$

As $U_{\mathcal{S}}$ and $U_{\mathcal{C}}$ obey the same relations as Equations 5.25, they from a representation of S_3. Clearly, they are not simultaneously diagonalisable and hence this is an

irreducible two-dimensional representation. Thus, each edge must transform as this representation.

As we perturb from our point with an exact bond dimension 2 MPS, the edges remain uncorrelated as long as the gap does not close. The S_3 symmetry remains preserved and is discrete, ensuring that both edges stay in their doublets and hence our four-fold degeneracy is maintained. This degeneracy will, in fact, be broken by a factor exponentially small in L due to the non-zero but finite correlation length, but this vanishes in the thermodynamic limit. This phase with four degenerate ground states for OBC will then survive as long as the gap does not close.

In fact, there is a small caveat to our statement above which should be addressed. The degeneracy *can* be broken without closing the gap or breaking the S_3 by adding a two-state system to one end of the chain. This can then transform as the doublet of the S_3 and so coupling it to the doublet of our original chain breaks the degeneracy on that edge. Defining

$$\sigma^+ = \begin{pmatrix} 0 & 1 \\ 0 & 0 \end{pmatrix}, \qquad \sigma^- = \begin{pmatrix} 0 & 0 \\ 1 & 0 \end{pmatrix}, \tag{5.30}$$

as the operators on the two-state system, adding the perturbation

$$H_{\text{break}} = \lambda_{\text{break}} \left(S_L^+ \sigma^- + S_L^- \sigma^+ \right) \tag{5.31}$$

preserves the S_3 but breaks the ground-state degeneracy down to 2. Coupling a second two-state system to the other end of the system then removes the ground state degeneracy completely.

Other than the doublet given above, all other irreducible representations of S_3 are one-dimensional. The three-state spin transforming under S_3 consists of a doublet and a one-dimensional representation, meaning that coupling an extra three-state spin to the end of the chain does not necessarily split the degeneracy, as the tensor product of a doublet with a one-dimensional representation is still a doublet. Thus, the phase is stable to S_3 invariant interactions preserving the Hilbert space and to those adding in one-dimensional representations.

From this we have seen that our phase is stable, but only when certain representations of S_3 are added. This is in contrast to an SPT phase, which is stable under all symmetry preserving perturbations. The difference comes from SPTs being protected by projective representations[2] [144, 145], which cannot be changed by local perturbations, whereas in our case a local perturbation can break the degeneracy, assuming it is in the correct representation. Because of this, we name this phase a representation symmetry protected topological (RSPT) phase.

5.5 Aside: exact excited states at the MPS point

The AKLT model has a number of exact excited states [152–154]. Of these, probably the most interesting correspond to a family of exact excited states obtained from the ground state by applying the operator

$$O^{+}_{\mathrm{AKLT}} = \sum_{j=1}^{L} (-1)^j {S^{+}_j}^2 \tag{5.32}$$

repeatedly to the AKLT ground state for even L (5.17), with matrix

$$R_{\mathrm{AKLT}} = \begin{pmatrix} |\hat{0}\rangle & -\sqrt{2}\,|\hat{1}\rangle \\ \sqrt{2}\,|\hat{2}\rangle & -|\hat{0}\rangle \end{pmatrix}, \tag{5.33}$$

as given in Equation 5.21. O^{+}_{AKLT} shifts the $U(1)$ charge by 2 and can be applied up to $L/2$ times before annihilating the ground state. Similarly, O^{-}_{AKLT}, found by replacing S^{+} by S^{-} in Equation 5.32, can be applied to lower the $U(1)$ charge. These states are exact eigenstates of the AKLT Hamiltonian [153, 154] and hence we have a tower of exact excited states. It should be noted though that O^{+}_{AKLT} applied to a generic eigenstate of the Hamiltonian does not give another eigenstate. Thus, the operator does not have a nice commutation relation with the Hamiltonian, i.e.

$$\left[H_{\mathrm{AKLT}}, O^{+}_{\mathrm{AKLT}}\right] \neq \alpha\, O^{+}_{\mathrm{AKLT}} \tag{5.34}$$

[2]The matrices $U(g_j)$ form a linear representation of the group G if $U(g_i)U(g_j) = U(g_i g_j)$ $\forall g_i, g_j \in G$. In a projective representation, the relation is changed to $U(g_i)U(g_j) = \omega(g_i, g_j)U(g_i g_j)$, where $\omega(g_i, g_j)$ is a phase factor. Projective representations related by $\tilde{U}(g_i) = \alpha(g_i)U(g_i)$, $\tilde{\omega}(g_i, g_j) = \alpha(g_i g_j)\omega(g_i, g_j)/(\alpha(g_i)\alpha(g_j))$, for a phase factor α_i are said to be in the same class. In different matrix product states, symmetry groups may have projective representations in different classes, leading to distinct phases as long as the symmetry is preserved and the gap does not close.

for a constant of proportionality α [53]. Instead it just acts as a ladder operator for this particular tower of eigenstates.

Due to the similarity of our MPS point and the AKLT model, it is perhaps unsurprising that there is an equivalent tower in our case. This time though the raising operator (again, only a raising operator within this tower) has $U(1)$ charge 3 and is given by

$$O^{+}_{\text{ours}} = \sum_{j=1}^{L} (-1)^j \left({S^{+}_j}^2 S^{+}_{j+1} + S^{+}_j {S^{+}_{j+1}}^2 \right). \tag{5.35}$$

Again, applying this operator repeatedly leads to a tower of exact eigenstates [53]. Once more, there is an equivalent $U(1)$ lowering operator O^{-}_{ours}.

Our model in fact has a family of exact excited states not present in AKLT. Taking the MPS

$$|\Psi_\alpha\rangle = \text{Tr}\left(A_1 B_2 A_3 B_4 ... A_{L-1} B_L\right), \tag{5.36}$$

where L is even and

$$A = \begin{pmatrix} |\hat{0}\rangle & \alpha\,|\hat{1}\rangle \\ \frac{1}{\alpha}\,|\hat{2}\rangle & |0\rangle \end{pmatrix}, \qquad B = \begin{pmatrix} |\hat{0}\rangle & -\frac{1}{\alpha}\,|\hat{2}\rangle \\ \alpha\,|\hat{1}\rangle & -|0\rangle \end{pmatrix}, \tag{5.37}$$

we have exact eigenstates for any choice of α, which are equivalent to those studied in Ref. [166], although they were discovered independently. While α can have any value, there are only $L+1$ independent eigenstates.

5.6 The phase transitions

After that brief interlude, we now return to the phase diagram. We have found the four duality breaking phases surrounding the $c = 1$ point, each with different values for M^3 and the OBC degeneracy, as in Table 5.1. To understand why we get these phases and to investigate the transitions between them, we turn to a field theory analysis. We have seen in Section 4.7 that the $c = 1$ point is described by a bosonic CFT with $c = 1$ and compactification radius $R = \sqrt{3/2}$, with partition function

$$Z\left(\sqrt{3/2}\right) = \frac{1}{\eta\bar{\eta}} \sum_{m,n\in\mathbb{Z}} q^{\frac{1}{12}(m+3n)^2} \bar{q}^{\frac{1}{12}(m-3n)^2}. \tag{5.38}$$

In terms of a bosonic field theory, the action is simply

$$S_0 = \frac{K}{2} \int d^2x \, (\nabla\Phi)^2 \,, \tag{5.39}$$

where the boson field, Φ, is compactified so that $\Phi \sim \Phi + 2\pi$ and the stiffness $K = 3/(2\pi)$ is forced by duality [119].[3] Perturbing by an S_3 invariant interaction then corresponds to amending the action to

$$S = \frac{K}{2} \int d^2x \left[(\nabla\Phi)^2 + v \cos 3\Phi + \hat{v} \cos 3\Theta \right] , \tag{5.40}$$

where Θ is the field dual to Φ. In our original language the $\cos 3\Phi$ term corresponds to perturbing by the $(3/4, 3/4)$ operator $[3, 0] + [-3, 0]$, while $\cos 3\Theta$ is $[0, 1] + [0, -1]$, where $[m, n]$ denotes the field with electric charge m and magnetic charge n. Terms of the form $\sin 3\Phi$ and $\sin 3\Theta$ are forbidden by charge conjugation, while $\cos n\Phi$ and $\cos n\Theta$ for n not a multiple of 3 are disallowed by the $\mathbb{Z}_3$. Of course, $\cos 6\Phi$, $\cos 15\Theta$, etc. would be allowed, but these perturbations are irrelevant.

In our phase diagram (Figure 5.1), setting v to 0 preserves the $U(1)$ symmetry and hence corresponds to perturbing along the line $\alpha = -\beta$, while setting $\hat{v}$ to 0 preserves the dual $U(1)$ and corresponds to perturbing along $\alpha = \beta$. Both of these lead to the well-known sine-Gordon model, which is integrable and gapped [54].

Focusing on $\hat{v} = 0$, we now pay attention to the two signs of v. For $v > 0$, the minima in the potential occur at $\Phi = 0,\ 2\pi/3,\ 4\pi/3$ and these correspond to the three directions of the Potts spin, giving the ordered Potts phase. Taking instead $v < 0$, $\Phi = 0,\ 2\pi/3,\ 4\pi/3$ are now *maxima* of the potential and hence are avoided, showing that now we have one direction not favoured and enter the not-A phase. Thus, we have recovered these two phases, at least along the $\hat{v} = 0$ line. The disordered Potts and RSPT phases are simply the duals of these two phases and so must occur along the $v = 0$ line.

Keeping $|v| \neq |\hat{v}|$, we remain in the gapped phase determined by whichever of v and $\hat{v}$ has the larger magnitude [119], but $v = \hat{v}$ is a more interesting scenario. Here Refs. [118, 119] showed that we instead get a flow to the 3-state Potts CFT,

[3] In fact, generally, $R^2 = K\pi$.

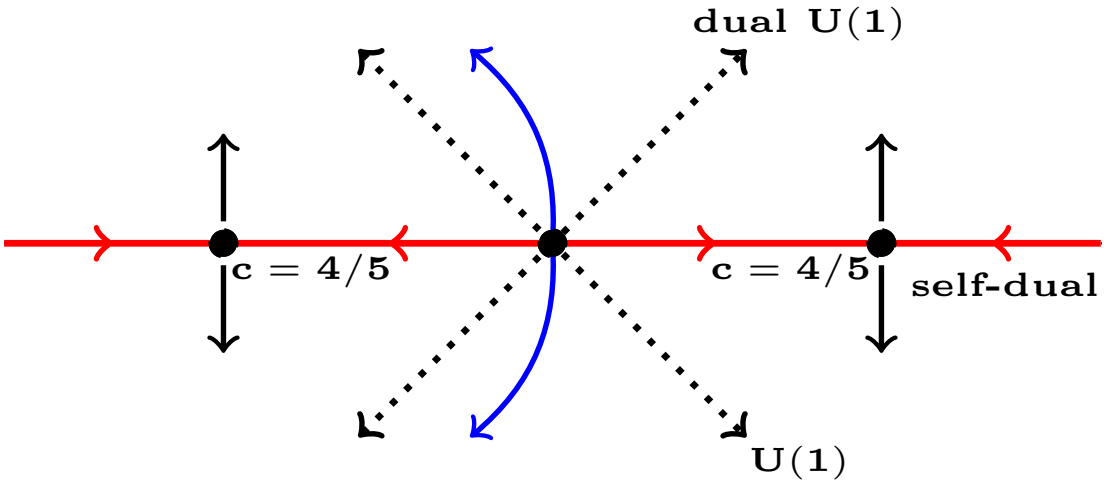

Figure 5.3: The Renormalization Group flow around $-H_1$. The red critical line is constrained to lie along the self-dual line, but the blue line cannot be determined without numerics.

regardless of the sign of v. That the flow in the field theory is independent of direction can be seen from the redefinition $\Phi \to \Phi + \pi$, $\Theta \to \Theta + \pi$, which flips v and $\hat{v}$ but leaves the kinetic term invariant.

Even more surprisingly, taking $\Phi \to \Phi + \pi$ but leaving Θ invariant flips the sign of v, but not $\hat{v}$. This is again just a redefinition and should not affect the field theory, implying that we should get flows to Potts CFTs for $v = -\hat{v}$ as well. On the lattice there is a fundamental difference between the cases $v = \hat{v}$ and $v = -\hat{v}$ though, due to their behaviours under duality. As the point we are perturbing from, $-H_1$, is self-dual, adding a self-dual interaction still leaves the model invariant under duality, and so the Potts CFT line is constrained to stay on the self-dual line. As $-H_1$ is not anti-self-dual, "anti-self-duality" is not preserved and so the flow does not have to remain perpendicular to the self-dual flow, as shown in Figure 5.3.

While we know the blue second-order transition lines in Figures 5.1 and 5.3 must be vertical infinitesimally close to $\alpha = \beta = 0$, we have to rely on numerics to locate the transition away from this point due to it not being protected by a lattice symmetry, as explained above. To do this, we work out the effective central charge c_{eff} for different α, β by using DMRG and the entanglement entropy at different lattice lengths, as explained in Subsection 2.3.3. In the gapped region,

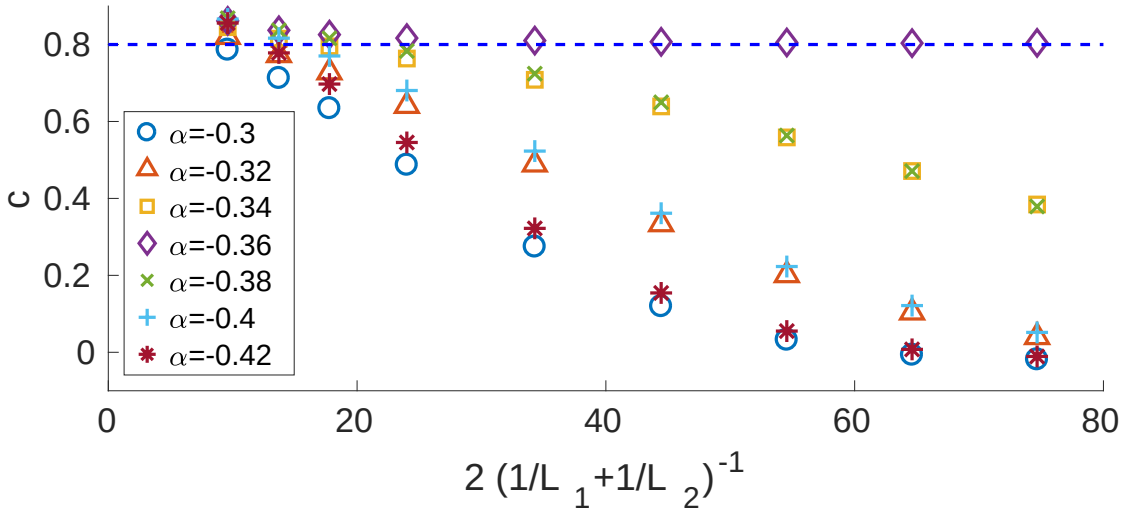

Figure 5.4: The effective central charge is plotted for $\beta = 0.75$ and different α. Convergence to $c_{\text{eff}} = 0.8$ appears to occur at $\alpha \approx -0.36$, implying that the transition line passes close to the point $\alpha = -0.36$, $\beta = 0.75$. L_1 and L_2 are the two values of L the entanglement entropy S is found for from which c_{eff} is extracted.

we should find $c_{\text{eff}} = 0$, while exactly on the transition lines $c_{\text{eff}} = 4/5$. Close to the transitions, the correlation length will increase and the c_{eff} calculated for small lattice lengths L will appear close to $4/5$, before falling to 0 as L is increased, thus allowing us to locate the second-order line. In Figure 5.4, we see that, for $\beta = 0.75$, the transition occurs at $\alpha \approx -0.36$.

Finding the approximate values of α for which transitions occur at different β allows us to locate the off-critical second order line, as indicated in Figure 5.1. The green crosses give the locations determined numerically, with the blue line interpolating between them. Finally, we note that the line for $\beta < 0$ is just the reflection of that for $\beta > 0$ in the $\beta = 0$ line by duality.

5.7 The ADP point and XXZ

In Chapter 4 we discovered that different regions of the phase diagram of Figure 4.1 had conformal towers centred at different momenta. In the rest of this chapter we will explain this, along with showing why the particular partition function of Equation 4.52 has to describe the continuum limit of H_1.

To find the answers to both of these questions, we consider perturbing from a trivially solvable point. Considering Equation 5.1, this corresponds to $H_{\mathrm{DB}}(0,-1,0)$, which has the simple Hamiltonian

$$H_{\mathrm{ADP}} = \sum_{j=1}^{L} \left(\tau_j + \tau_j^\dagger\right), \tag{5.41}$$

where we name this point the "anti-disordered Potts" (ADP) point. In the τ-diagonal basis,

$$\tau + \tau^\dagger = \begin{pmatrix} 2 & 0 & 0 \\ 0 & -1 & 0 \\ 0 & 0 & -1 \end{pmatrix} \tag{5.42}$$

and hence we have 2^L exactly degenerate ground states, corresponding to either $\left|\hat{1}\right\rangle$ or $\left|\hat{2}\right\rangle$ at each site, where $\tau\left|\hat{n}\right\rangle = \omega^{\hat{n}}\left|\hat{n}\right\rangle$. There is then a gap of size 3 to the first excited states.

While this point is exactly solvable, this is no longer true when we perturb away from it by $H_{\mathrm{DB}}(J,0,\lambda_1)$. Instead, we use perturbation theory to approximate the model. As there are 2^L degenerate ground states at the unperturbed point, we find an effective Hamiltonian with two states per site. To see how this works, we first perturb $H_{\mathrm{DB}}(0,f,0)$ by $H_{\mathrm{DB}}(J,0,0)$, where $f<0$ and $|J/f| \ll 1$:

$$H = \sum_{j=1}^{L} -f\left(\tau_j + \tau_j^\dagger\right) - J\left(\sigma_j^\dagger\sigma_{j+1} + \sigma_j\sigma_{j+1}^\dagger\right). \tag{5.43}$$

We now consider the action of the perturbation on each set of ground states of H_{ADP}. The two-site perturbation to the Hamiltonian obeys

$$\left(\sigma_j^\dagger\sigma_{j+1} + \sigma_j\sigma_{j+1}^\dagger\right)\left|\hat{1}\hat{1}\right\rangle = \left|\hat{0}\hat{2}\right\rangle + \left|\hat{2}\hat{0}\right\rangle, \tag{5.44}$$

$$\left(\sigma_j^\dagger\sigma_{j+1} + \sigma_j\sigma_{j+1}^\dagger\right)\left|\hat{1}\hat{2}\right\rangle = \left|\hat{0}\hat{0}\right\rangle + \left|\hat{2}\hat{1}\right\rangle, \tag{5.45}$$

and the analogous relations with $\left|\hat{1}\right\rangle \leftrightarrow \left|\hat{2}\right\rangle$. We see that only the second term on the second line remains in the Hilbert space of ground states at the unperturbed point. We can thus convert this to the first-order two-state per site Hamiltonian

$$H_{\mathrm{eff}} = fL - J\sum_{j=1}^{L}\left(\sigma_j^+\sigma_{j+1}^- + \sigma_j^-\sigma_{j+1}^+\right), \tag{5.46}$$

where

$$\sigma^+ = \begin{pmatrix} 0 & 1 \\ 0 & 0 \end{pmatrix}, \quad \sigma^- = \begin{pmatrix} 0 & 0 \\ 1 & 0 \end{pmatrix}, \tag{5.47}$$

act on the two-state Hilbert space given by

$$|\uparrow\rangle = \begin{pmatrix} 1 \\ 0 \end{pmatrix}, \qquad |\downarrow\rangle = \begin{pmatrix} 0 \\ 1 \end{pmatrix}. \tag{5.48}$$

We choose $|\uparrow\rangle$ in the two-state model to correspond to $\left|\hat{2}\right\rangle$ in the three-state model and $|\downarrow\rangle$ to $\left|\hat{1}\right\rangle$ for later convenience. Equation 5.46 is simply the XX model, which can be solved exactly in terms of free fermions and corresponds to a CFT of central charge $c = 1$ with boson radius $R = 1$ [162].

Going to second order and considering the general Hamiltonian $H_{\mathrm{DB}}(J, f, \lambda_1)$, where $f < 0$ and $|J/f|, |\lambda_1/f| \ll 1$, we find

$$\begin{aligned} \frac{H^{(2)}}{-\tilde{f}} =& -L\left(1 + \frac{5\tilde{J}^2 + 4\tilde{J}\lambda_1 + 8\lambda_1^2}{12\tilde{f}^2}\right) \\ &- \sum_{j=1}^{L}\Bigg[\left(\frac{\tilde{J} + 4\lambda_1}{-\tilde{f}} + \frac{(\tilde{J} - 2\lambda_1)^2}{6\tilde{f}^2}\right)\left(\sigma_j^+\sigma_{j+1}^- + \sigma_j^-\sigma_{j+1}^+\right) + \frac{\tilde{J}^2 + 4\tilde{J}\lambda_1}{4\tilde{f}^2}\sigma_j^z\sigma_{j+1}^z \\ &\quad + \frac{\left(\tilde{J} + \lambda_1\right)^2}{3\tilde{f}^2}\left(\sigma_j^+\sigma_{j+2}^- + \sigma_j^-\sigma_{j+2}^+ + 2\sigma_j^+\sigma_{j+1}^+\sigma_{j+2}^+ + 2\sigma_j^-\sigma_{j+1}^-\sigma_{j+2}^-\right)\Bigg], \end{aligned} \tag{5.49}$$

where $\tilde{J} = J - \lambda_1$, $\tilde{f} = f - \lambda_1$ and

$$\sigma^z = \begin{pmatrix} 1 & 0 \\ 0 & -1 \end{pmatrix}.$$

The first line is just a constant, while the second is the XXZ model [3], and the third contains longer-range corrections. The XXZ model has Hamiltonian

$$H_{\mathrm{XXZ}} = -\sum_{j=1}^{L}\left(\sigma_j^+\sigma_{j+1}^- + \sigma_j^-\sigma_{j+1}^+ + \frac{\Delta}{2}\sigma_j^z\sigma_{j+1}^z\right) \tag{5.50}$$

and has a $U(1)$ symmetry corresponding to

$$Q_{\mathrm{XXZ}} = -\sum_{j=1}^{L}\sigma_j^z, \tag{5.51}$$

where the minus sign is chosen for later convenience. By considering the relation between the three-state and two-state models, we see that this is precisely the

negative of the $U(1)$ charge of $\pm H_1$, as given in Equation 4.36. The only difference is that flipping a spin in the XXZ language changes the charge by 2. To understand this, we consider the allowed states in both the 2- and 3-state models. In the 2-state model, the smallest increase in Q_{XXZ} corresponds to flipping a single $|\uparrow\rangle \to |\downarrow\rangle$, which in the 3-state model is $\left|\hat{2}\right\rangle \to \left|\hat{1}\right\rangle$, giving a change in Q of 2. To get a change in Q of 1, we would need $\left|\hat{2}\right\rangle \to \left|\hat{0}\right\rangle$ or $\left|\hat{0}\right\rangle \to \left|\hat{1}\right\rangle$, both of which involve $\left|\hat{0}\right\rangle$, and so are not present in the two state model. This shows that, around H_{ADP}, all low-lying states must have even charge Q in the 3-state model (for even lattice length L), with all odd Q states gapped. This fact will prove to be key to our analysis of the $c = 3/2$ point later.

Returning to the XXZ model, for $-1 \leq \Delta < 1$, the continuum limit is described by a CFT with $c = 1$ and radius given by

$$\Delta = \cos\left(\frac{\pi}{2R^2}\right), \tag{5.52}$$

where we take $R \geq 1/\sqrt{2}$ [162]. We see that, for the XX model, corresponding to $\Delta = 0$, we recover $R = 1$.

To see if the terms in the final line of Equation 5.49 destabilise the XXZ phase, we consider the boson partition function again (2.31):

$$Z(R) = \frac{1}{\eta\bar{\eta}} \sum_{m,n\in\mathbb{Z}} q^{\frac{1}{8R^2}\left(m+2R^2n\right)^2} \bar{q}^{\frac{1}{8R^2}\left(m-2R^2n\right)^2}.$$

The first two terms of the third line of Equation 5.49 are symmetric under the $U(1)$ of the XXZ model (5.51). These terms were not found to cause a phase transition for small perturbations in Ref. [167]. The final two terms in the third line are more problematic. They have $U(1)$ charge ± 3 and so the most relevant operators consistent with this have $m = \pm 3$, $n = 0$, leading to weights

$$\left(h, \bar{h}\right) = \left(\frac{9}{8R^2}, \frac{9}{8R^2}\right). \tag{5.53}$$

Hence these are irrelevant for $R^2 < 9/8$, meaning the XXZ phase survives for a finite region.

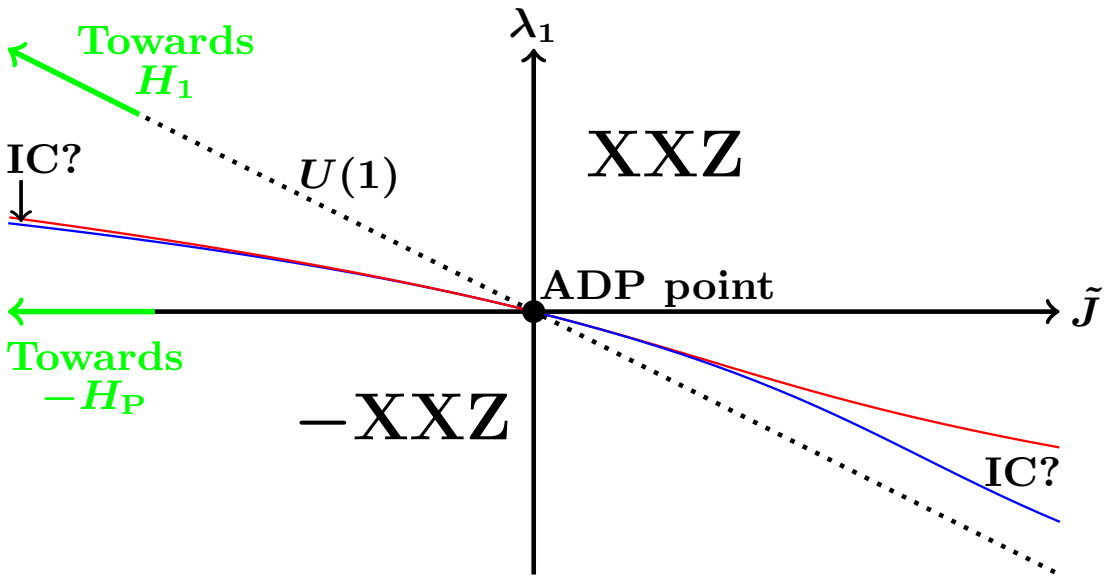

Figure 5.5: The heuristic phase diagram around the ADP point (5.41). The system is in the XXZ phase above the red line and in the $-$XXZ phase below the blue line. In between we believe there are incommensurate (IC) regions. The black dotted line denotes the line where the $U(1)$ charge is preserved.

We now claim that the XXZ region extends all the way down to the antiferromagnetic Potts phase on the self-dual line. There appears to be a problem with this argument though – the AFP phase has $R^2 = 3/2 > 9/8$! To resolve this, we take a closer look at Equations 5.49 and 5.50. We see that the XXZ Hamiltonian has a negative coefficient for its $\sigma_j^\dagger\sigma_{j+1} + \sigma_j\sigma_{j+1}^\dagger$ term, but our Hamiltonian can have either a positive or a negative coefficient, depending on the values of $\tilde{J}$ and λ_1. Indeed, the AFP model has $\tilde{J} < 0$ and $\lambda_1 = 0$, meaning that the coefficient of the $\sigma_j^\dagger\sigma_{j+1} + \sigma_j\sigma_{j+1}^\dagger$ part is negative.

The heuristic phase diagram surrounding the ADP point is presented in Figure 5.5. The "XXZ" phase has a negative coefficient for $\sigma_j^\dagger\sigma_{j+1} + \sigma_j\sigma_{j+1}^\dagger$ and is found to extend all the way to the "$c = 3/2$" phase on the self-dual line, while the "$-$XXZ" phase has a positive coefficient for $\sigma_j^\dagger\sigma_{j+1} + \sigma_j\sigma_{j+1}^\dagger$ and is found to extend to the antiferromagnetic Potts phase on the self-dual line.[4] As the low-lying states of the XXZ phase try to maximise the eigenvalue of the hopping term $(\sigma_j^\dagger\sigma_{j+1} + \sigma_j\sigma_{j+1}^\dagger)$ and the low-lying states of the $-$XXZ phase try to minimise

[4]Note that the phases extend to the self-dual line, but the second-order XXZ Hamiltonian (5.49) is not a good approximation here as $\tilde{J}$ and λ_1 are the same order of magnitude as $\tilde{f}$.

it, their forms change abruptly as we move from one to the other, causing the transition. The incommensurate phases in between, in which the hopping term becomes small, account for this transition and allow the eigenstates to reshuffle.

To analyse the "−XXZ" phase and understand how it survives to the self-dual line, we consider the unitary transformation

$$U_1 = \prod_{j=1}^{L/2} \sigma^z_{2j-1}, \tag{5.54}$$

which takes $H_{\mathrm{XXZ}}(\Delta) \to -H_{\mathrm{XXZ}}(-\Delta)$, and so we can map it onto an XXZ model with which we are familiar. This unitary takes Equation 5.49 to

$$\begin{aligned}\frac{\tilde{H}^{(2)}}{-\tilde{f}} =& -L\left(1+\frac{5\tilde{J}^2+4\tilde{J}\lambda_1+8\lambda_1^2}{12\tilde{f}^2}\right) \\ &-\sum_{j=1}^{L}\Bigg[-\left(\frac{\tilde{J}+4\lambda_1}{-\tilde{f}}+\frac{(\tilde{J}-2\lambda_1)^2}{6\tilde{f}^2}\right)\left(\sigma_j^+\sigma_{j+1}^- + \sigma_j^-\sigma_{j+1}^+\right)+\frac{\tilde{J}^2+4\tilde{J}\lambda_1}{4\tilde{f}^2}\sigma_j^z\sigma_{j+1}^z \\ &\quad+\frac{\left(\tilde{J}+\lambda_1\right)^2}{3\tilde{f}^2}(\sigma_j^+\sigma_{j+2}^- + \sigma_j^-\sigma_{j+2}^+) \\ &\quad+\frac{\left(\tilde{J}+\lambda_1\right)^2}{3\tilde{f}^2}(-1)^j(2\sigma_j^+\sigma_{j+1}^+\sigma_{j+2}^+ + 2\sigma_j^-\sigma_{j+1}^-\sigma_{j+2}^-)\Bigg].\end{aligned} \tag{5.55}$$

The terms in the last line of this Hamiltonian now have momentum π. These are the only terms which break the $U(1)$ (at least to this order in perturbation theory), indicating that states differing by $U(1)$ charge 3 may also differ in momentum by π, as we will see next.

As we just hinted, the second interesting effect of this unitary transformation is on the states. Considering the line $J = 0$ ($\tilde{J} = -\lambda_1$), we know that we have a $U(1)$ symmetry. All states should then be eigenstates of the $U(1)$ operator. They are thus eigenfunctions of the operator

$$U = \prod_{j=1}^{L} \sigma_j^z, \tag{5.56}$$

with eigenvalue equation

$$U\left|\psi\right\rangle = (-1)^{L/2+m}\left|\psi\right\rangle, \tag{5.57}$$

where m is the $U(1)$ charge and we are still assuming L is even. But note that

$$U = U_1 U_2, \tag{5.58}$$

where

$$U_2 = \prod_{j=1}^{L/2} \sigma_{2j}^z \tag{5.59}$$

is just U_1 translated by one site and an equally valid transformation from $H_{\mathrm{XXZ}}(\Delta)$ to $-H_{\mathrm{XXZ}}(-\Delta)$. It is then simple to see that doing this transformation changes the momentum by an amount

$$\Delta k = \left(\frac{L}{2} + m\right)\pi \tag{5.60}$$

to

$$\tilde{k} = [k + \Delta k] \text{ modulo } (2\pi), \tag{5.61}$$

where k is the momentum on the XXZ side, $\tilde{k}$ is the momentum on the $-$XXZ side, and momentum is only defined modulo 2π. Even when we break the $U(1)$, we expect the states to be continuous and so they should remain in the same momentum sectors, meaning that, when we change the sign of the $\sigma_j^+\sigma_{j+1}^- + \sigma_j^-\sigma_{j+1}^+$ term, the states should change momentum by the same amount. This explains why the identity (and all other states) shift momentum sectors at the AFP point for different L. We have now found the change in momentum when we go from XXZ to $-$XXZ, but we still do not know the momentum of each tower, as we have not worked out their values in the XXZ model. We will do this in the next section by taking a closer look at the exactly solvable XX model.

Before moving to the XX model, we consider the case $\tilde{J}+4\lambda_1 \sim \mathcal{O}(\tilde{J}^2/\tilde{f}^2, \lambda_1^2/f^2)$. Here the model becomes second order and the analysis is complicated by the other perturbations being the same order as the $\sigma_j^+\sigma_{j+1}^- + \sigma_j^-\sigma_{j+1}^+$ term. A simple analysis shows that, for a constant $\lambda_1 \approx -\tilde{J}/4$, the size of this region grows as

$$\delta\tilde{J} \sim \frac{\tilde{J}^2}{-f} \tag{5.62}$$

and vanishes to a point at $\tilde{J} = 0$, as expected. This is the region of transition between the XXZ and $-$XXZ models and involves many states of different momenta crossing. We thus expect it to be incommensurate. As a sanity check, we have verified numerically that for small couplings along the line $\tilde{J} = -4\lambda_1$, the gaps do indeed grow as $\tilde{J}^2$, consistent with the second-order Hamiltonian. We suggest that this region survives all the way to the two incommensurate phases on the left-hand side of Figure 4.1, explaining both their existence and the transition between phases with conformal towers centred on different momenta.

5.8 The XX model

To understand the momentum sectors at the AFP and supersymmetric points, we first study the XX model in detail. Taking the XX Hamiltonian (5.46),

$$H_{\mathrm{XX}} = -J \sum_{j=1}^{L} \left(\sigma_j^+ \sigma_{j+1}^- + \sigma_j^- \sigma_{j+1}^+ \right), \tag{5.63}$$

we can rewrite this as

$$H_{\mathrm{XX}} = -\frac{J}{2} \sum_{j=1}^{L} \left(\sigma_j^x \sigma_{j+1}^x + \sigma_j^y \sigma_{j+1}^y \right), \tag{5.64}$$

where

$$\sigma_x = \begin{pmatrix} 0 & 1 \\ 1 & 0 \end{pmatrix}, \quad \sigma_y = \begin{pmatrix} 0 & -i \\ i & 0 \end{pmatrix}. \tag{5.65}$$

Defining the Majorana operators

$$\gamma_{2j-1} = \left(\prod_{k<j} \sigma_j^z \right) \sigma_j^y, \quad \gamma_{2j} = i \left(\prod_{k<j} \sigma_k^z \right) \sigma_j^y \sigma_j^z, \tag{5.66}$$

obeying $\{\gamma_a, \gamma_b\} = 2\,\delta_{a,b}$, the Hamiltonian becomes

$$H_{\mathrm{XX}} = -\frac{iJ}{2} \sum_{j=1}^{L} \left(\gamma_{2j-1} \gamma_{2j+2} - \gamma_{2j} \gamma_{2j+1} \right). \tag{5.67}$$

We now define complex fermions as these will make the momenta clearer:

$$c_j = \frac{1}{2} \left(\gamma_{2j-1} + i \gamma_{2j} \right), \quad c_j^\dagger = \frac{1}{2} \left(\gamma_{2j-1} - i \gamma_{2j} \right), \tag{5.68}$$

which obey $\{c_j, c_{j'}\} = \{c_j^\dagger, {c_{j'}}^\dagger\} = 0$, $\left\{{c_j}^\dagger, c_{j'}\right\} = \delta_{j,j'}$. This turns the Hamiltonian into

$$H_{\mathrm{XX}} = -J \sum_{j=1}^{L} \left(c_j^\dagger c_{j+1} - c_j c_{j+1}^\dagger \right). \tag{5.69}$$

We Fourier transform to the momentum basis by defining

$$c_j \equiv \frac{1}{\sqrt{L}} \sum_k e^{ikj} c_k, \tag{5.70}$$

where k takes the values allowed by the boundary conditions in the fermion model. With a little algebraic manipulation, the Hamiltonian is rewritten as

$$H_{\mathrm{XX}} = -2J \sum_k \cos(k) n_k, \tag{5.71}$$

where $n_k \equiv c_k^\dagger c_k$ is the fermion number operator at momentum k. The ground state of a sector will then have all fermions with $|k| < \pi/2$ present and all with $|k| > \pi/2$ absent for $J > 0$, and the reverse for $J < 0$. Low-lying states have excitations corresponding to extra particles or holes around $k = \pm\pi/2$.

In this language, the $U(1)$ is simply

$$Q_{\mathrm{XX}} = -\sum_j \sigma_j^z = -L + 2\sum_k n_k, \tag{5.72}$$

where $n_k = c_k^\dagger c_k$ expresses whether there is a fermion of momentum k ($n_k = 1$) or not ($n_k = 0$). The state with no fermions, i.e. annihilated by $c_k \,\forall\, k$, has $Q_{\mathrm{XX}} = -L$, while the state with fermions everywhere, i.e. annihilated by $c_k^\dagger \,\forall\, k$, has $Q_{\mathrm{XX}} = L$.

To obtain the spectrum of the model, we first need to find the appropriate momentum sectors now we have transformed to the fermion basis. As we saw in Section 3.5, to match periodic boundary conditions (PBC) in the spin language, for even fermion number we need antiperiodic boundary conditions (APBC) in the fermion language, while for odd fermion number we need PBC. We will see that the solution in fact depends on the number of sites modulo 4. We will only analyse L even here as this is sufficient for our explanation of the different phases of the 3-state model on the self-dual line, but odd L can be considered analogously.

j	E	E_g	Degeneracy	(Q_{XX}, k)	$\mathbb{Z}_2$
0	$-2\,\mathrm{cosec}\left(\frac{\pi}{L}\right)$	0	1	$(0,0)$	0
1	$-2\cot\left(\frac{\pi}{L}\right)$	$\frac{1}{4}$	2	$(\pm\frac{1}{2},0)$	1
2	$-2\,\mathrm{cosec}\left(\frac{\pi}{L}\right)+8\sin\left(\frac{\pi}{L}\right)$	1	6	$(\pm1,0)$, $2\times(0,\pi)$, $(0,\pm2\pi/L)$	0
3	$-2\cot\left(\frac{\pi}{L}\right)+4\sin\left(\frac{2\pi}{L}\right)$	$\frac{5}{4}$	8	$(\pm\frac{1}{2},\pm\frac{2\pi}{L})$, $(\pm\frac{1}{2},\pi\pm\frac{2\pi}{L})$	1

Table 5.2: The lowest energy states in the XX model for lattice length $L=4l$ and $J=1$. j specifies the j^{th} excited level, E the exact energy, and E_g the gap from the ground-state energy, normalised by dividing by $8\frac{\pi}{L}$ and ignoring corrections at $\mathcal{O}(1/L)$. The degeneracy of each level is given, along with the $U(1)$ charge and momentum (Q_{XX},k) and the fermion parity $\mathbb{Z}_2$. For $J=-1$ and $L=4l$ the results are identical. For $L=4l+2$ and $J=1$, $\mathbb{Z}_2$ is reversed, while for $L=4l+2$ and $J=-1$, $\mathbb{Z}_2$ is reversed and the resulting $\mathbb{Z}_2=1$ states pick up a change in momentum $\Delta k=\pi$.

Focusing on even L, we start with the case of an even number of fermions and hence $k=\pm\pi/L,\pm3\pi/L,...,\pm(\pi-\pi/L)$. For $L=4l$, $\pm\pi/2$ are not allowed values and hence there is a unique ground state. For both $J>0$ and $J<0$, this ground state has momentum 0 and energy

$$E^0_{L=4l,\mathbb{Z}_2=0} = -2J\sum_{n=-\frac{L}{4}+\frac{1}{2}}^{\frac{L}{4}-\frac{1}{2}}\cos\left(\frac{2n\pi}{L}\right) \tag{5.73}$$

$$= -2|J|\mathrm{cosec}\,(\pi/L), \tag{5.74}$$

where $\mathbb{Z}_2$ measures the fermion number parity modulo 2. Taking $J>0$, the lowest single-particle energy excitations are fermions at $k=\pm(\pi/2+\pi/L)$ or holes at $k=\pm(\pi/2-\pi/L)$. As we must retain an even number of fermions, there are 6 first-excited states, corresponding to choosing 2 of the 4 possible excitations. Each of these has energy

$$E^1_{L=4l,\mathbb{Z}_2=0} = -2|J|\,\mathrm{cosec}\,(\pi/L)+8\sin(\pi/L). \tag{5.75}$$

We see that there are states with $Q_{\mathrm{XX}}=\pm1$ and $k=0$, along with a pair with $Q_{\mathrm{XX}}=0$ and $k=\pi$, and states with $Q_{\mathrm{XX}}=0$ and $k=\pm2\pi/L$. Repeating this for $J<0$, we find exactly the same results due to the symmetry of the spectrum under $k\to\pi-k$.

Considering instead $L=4l+2$, the same no longer holds. We now have two ground states in the $\mathbb{Z}_2=0$ sector as we have a pair of fermions with $k=\pm\pi/2$.

In the ground state, we either have both of these or neither of these, and so have degenerate ground states of energy

$$E^0_{L=4l+2,\mathbb{Z}_2=0} = -2|J|\cot(\pi/L) \tag{5.76}$$

and $k = 0$. We can find excited states in the same way as for $L = 4l$, by considering adding/removing pairs of particles.

So far we have only looked at even fermion number. Switching to odd fermion number, we have PBC in fermions, giving momenta $k = 0, \pm 2\pi/L, ..., \pm(\pi - 2\pi/L), \pi$. Doing the analogous calculation to the one for even fermion number, we find that the momenta and energies of the low-lying excitations just swap from $L = 4l \leftrightarrow L = 4l + 2$. There is one key difference though: the presence of the $k = 0$ and $k = \pi$ fermions. Unlike every other fermion, these are unpaired with a corresponding fermion with the opposite momentum, giving a shift of $\Delta k = 0$ and $\Delta k = \pi$ to the total momentum of every state, respectively. This is no problem for $J > 0$ as here this just gives a shift of $\Delta k = 0$, but for $J < 0$ it results in a shift of $\Delta k = \pi$. These results are summarised in Table 5.2.

The final task is to find how these fields fit into the CFT. At the XX point the boson radius is 1 and the partition function is

$$Z_{\mathrm{XX}} = \frac{1}{\eta\bar{\eta}} \sum_{m,n\in\mathbb{Z}} q^{\frac{1}{8}(m+2n)^2} \bar{q}^{\frac{1}{8}(m-2n)^2}. \tag{5.77}$$

We know that m corresponds to Q_{XX} and so, to make the partition function consistent with the momenta of the states on the lattice, we see that states pick up momentum $\Delta k \approx n\pi$, with momentum again defined modulo 2π. To understand where this fits in, we consider Figure 5.6, which shows the energies of the different fermions for $L = 4l$ with an even number of fermions. The ground state is shown in (a) and has all levels filled up to the Fermi surface, with none filled above it. The lowest energy state with electric charge m and magnetic charge n in the CFT can then be thought of as the state with the $m + n$ lowest levels with $k > \pi/2$ filled above the Fermi sea and $m - n$ for $k < -\pi/2$. If $m + n$ is negative, this corresponds to making holes at the $-(m + n)$ levels closest to $k = \pi/2$ with $k < \pi/2$, and

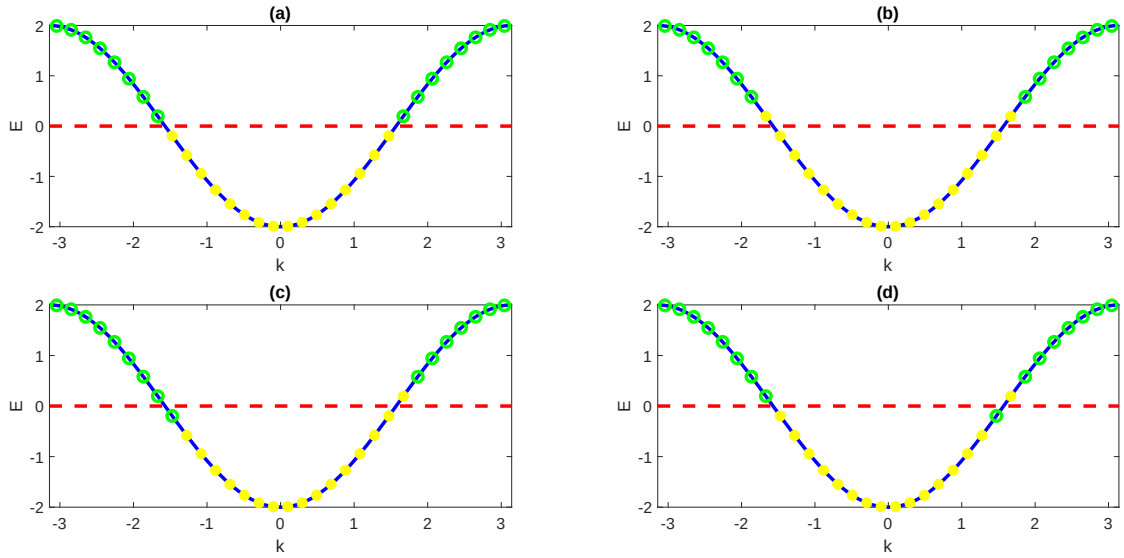

Figure 5.6: The fermion energy levels of the XX model with $J = 1$ and $L = 4l$ are plotted against the momentum, k. A full yellow circle denotes a fermion, while an empty green circle is an absent fermion. The red dashed line denotes the Fermi energy of 0. In (a), the ground state is shown, where all levels below the Fermi surface are filled and none above it. In (b) a further two fermions have been added in the lowest energy states, corresponding to $m = 2$, $n = 0$ and giving momentum $k = 0$. In (c) one fermion has been taken from the left-hand side to the right, corresponding to $m = 0$, $n = 1$ and $k = \pi$. In (d) one fermion has moved to a higher energy state on its own side, corresponding to L_{-1} acting on the identity in the CFT and $k = 2\pi/L$.

analogously for $m - n$ around $k = -\pi/2$. This can be interpreted as increasing m by 2 adds two fermions, while increasing n by 1 moves one fermion from $k < 0$ to $k > 0$. Thus, we see where the factor of $\Delta k \approx n\pi$ appears from – moving n fermions from $k \approx -\pi/2$ to $k \approx \pi/2$ increases the momentum by $\Delta k \approx n\pi$.

The locations of the conformal towers are summarised in Table 5.3, explaining the momenta of the towers at the AFP point. We also see where the factor of $k = (L/2 + m)\pi$ in doing the transformation from $J > 0$ to $J < 0$ appears from. This is necessary to ensure the sector with an odd number of fermions (m even for $L = 4l$ and m odd for $L = 4l + 2$) picks up the appropriate factor of π.

We see that, for $J < 0$, as is the case for the AFP point, there is a factor of $(m + n)\pi$. As the $(3/4, 3/4)$ operators have $m = \pm 3$, $n = 0$ or $m = 0$, $n = \pm 1$, they always have momentum π relative to the identity, showing that they are disallowed from the perturbation, thus stabilising the phase along the self-dual line around the AFP point in Figure 4.1.

L modulo 4	$J > 0$	$J < 0$
0	$n\pi$	$(m+n)\pi$
2	$n\pi$	$(m+n+1)\pi$

Table 5.3: The "centre" of momentum for each of the towers for L even, with all momenta defined modulo 2π. The highest weight state does not have the momentum given as it has spin mn, but the towers will be close to these values.

The final task we have is to address the CFT at the supersymmetric point H_1 and its stability, which we do next.

5.9 Why this particular $c = 3/2$ theory?

In Section 4.9 we claimed that the integrable point H_1 was described by a CFT of central charge $c = 3/2$ with radius $R = \sqrt{3}$ on the self-affine line in Ginsparg's conventions [75]. While the value of c is natural given the underlying supersymmetry and the $U(1)$ symmetry ($U(1)$ implies a boson and coupled with supersymmetry this suggests a fermion too, giving $c = 1 + 1/2$), this radius and orbifold seem more arbitrary. We will see though, using an argument similar to that at the $c = 1$ point presented in Section 4.7, that this is in fact the only possible theory.

Under duality, the boson partition function exchanges $m \leftrightarrow n$, as at the $c = 1$ point. The duality of the fermion manifests itself as the Ising duality to be explained now. The Ising CFT is normally described as having three primary fields with weights 0, 1/16 and 1/2, respectively, giving a partition function of

$$Z_{\text{Ising}} = |\chi_0|^2 + |\chi_{1/16}|^2 + |\chi_{1/2}|^2. \tag{5.78}$$

The $(0,0)$ and $(1/2,1/2)$ operators transform into themselves under duality (up to a relative sign), but the $(1/16,1/16)$ operator transforms to another $(1/16,1/16)$ operator which is non-local and hence not in the partition function [16]. For the partition function of the combined boson and fermion to be well behaved under duality, a second $(1/16,1/16)$ field will thus have to be introduced.

The situation is further complicated by the off-dual behaviour of the model. As we have seen, the model around $H_{\text{ADP}} = \sum_j (\tau_j + \tau_j^\dagger)$ is described by a bosonic CFT

of central charge $c = 1$, but along the $U(1)$ line those states with $U(1)$ charge Q (4.36) odd are gapped (at least for L even).[5] This continues until the $c = 3/2$ point. On the other side of the $c = 3/2$ point we have another $c = 1$ CFT, but this time all $U(1)$ sectors are gapless. We must somehow explain this behaviour.

We start by considering the boson partition function

$$\Gamma(R) = \frac{1}{\eta\bar{\eta}} \sum_{m,n} q^{\frac{1}{8R^2}\left(m+2R^2n\right)^2} \bar{q}^{\frac{1}{8R^2}\left(m-2R^2n\right)^2}, \tag{5.79}$$

where m and n are integers. As Dixon, Ginsparg and Harvey showed [142], when we consider supersymmetric CFTs with $c = 3/2$, the possible bosonic parts generalise to $\Gamma^{\pm}$, $\Gamma^{\pm}_{\delta}$, where $+$ indicates $m \in 2\mathbb{Z}$, $-$ indicates $m \in 2\mathbb{Z}+1$ and δ means $n \in \mathbb{Z} + 1/2$, rather than $\mathbb{Z}$, as is the case for $\Gamma^{\pm}$. The different Γ pair with different parts of the fermion partition function, hence why $n \in \mathbb{Z} + 1/2$ is now allowed, as non-integer bosonic spin can be cancelled by non-integer fermionic spin. Expanding them explicitly, we find

$$\Gamma(R) = \Gamma^{+}(R) + \Gamma^{-}(R), \tag{5.80}$$

$$\Gamma(R/2) = \Gamma^{+}(R) + \Gamma^{+}_{\delta}(R). \tag{5.81}$$

This is a particularly useful pair of relations as we require a lattice charge of 2 to correspond to $m = 1$ on one side of the self-dual line (the side connected to $H = \sum_j (\tau_j + \tau_j^\dagger)$) and to $m = 2$ on the other (the side connected to $H = \sum_j (\sigma_j^\dagger \sigma_{j+1} + \sigma_j \sigma_{j+1}^\dagger)$). This works for $\Gamma(R/2)$ on the $H = \sum_j (\tau_j + \tau_j^\dagger)$ side and $\Gamma(R)$ on the other.

We can set the value of R as we did on the $c = 1$ side by requiring invariance of the $\mathbb{Z}_3 = 0$ sector. From

$$\Gamma_{\mathbb{Z}_3=0}(R/2) = \frac{1}{\eta\bar{\eta}} \sum_{m',n} q^{\frac{1}{8R^2}\left(6m'+R^2n\right)^2} \bar{q}^{\frac{1}{8R^2}\left(6m'-R^2n\right)^2}, \tag{5.82}$$

$$\widetilde{\Gamma}_{\mathbb{Z}_3=0}(R) = \frac{1}{\eta\bar{\eta}} \sum_{m',n} q^{\frac{1}{8R^2}\left(3n+2R^2m'\right)^2} \bar{q}^{\frac{1}{8R^2}\left(3n-2R^2m'\right)^2}, \tag{5.83}$$

where $\widetilde{\Gamma}$ is the dual of Γ, we see that $\Gamma_{\mathbb{Z}_3=0}(R/2) = \widetilde{\Gamma}_{\mathbb{Z}_3=0}(R)$ sets $R = \sqrt{3}$.

[5] This can be understood as an odd Q (for L even) requires an odd number of states in the $|\hat{0}\rangle$ state, but these are gapped for H_{ADP}. By continuity, these states remain gapped until a phase transition occurs.

We now need to work out how to use the fermion to stitch the two boson partition functions (5.80 and 5.81) together. In particular, we need $\Gamma^{-}(R)$ present on one side and $\Gamma^{+}_{\delta}(R)$ on the other. The answer comes by coupling one to the $(1/16, 1/16)$ field and the other to its dual. Taking one of the $(1/16, 1/16)$ fields to be the physical field on one side of the self-dual line, this removes the other from the CFT. As they are duals of each other, the role of the physical field switches under the action of duality, i.e. going from one side of the self-dual line to the other.

Requiring all of the above and comparing with the complete classification of Dixon, Ginsparg and Harvey [142], leaves us with a single superconformal field theory with $c = 3/2$, $Z_{\text{s-a}}\left(\sqrt{3}\right)$, as given in Equation 4.52 and repeated here:

$$Z_{\text{s-a}}(R) = \frac{1}{2}\left(\left|\frac{\theta_3}{\eta}\right| + \left|\frac{\theta_4}{\eta}\right|\right)\Gamma^{+} + \frac{1}{2}\left(\left|\frac{\theta_3}{\eta}\right| - \left|\frac{\theta_4}{\eta}\right|\right)\Gamma^{-}_{\delta} + \frac{1}{2}\left|\frac{\theta_2}{\eta}\right|\left(\Gamma^{-} + \Gamma^{+}_{\delta}\right).$$

In terms of the fermion fields, the theta functions correspond to

$$\frac{1}{2}\left(\left|\frac{\theta_3}{\eta}\right| + \left|\frac{\theta_4}{\eta}\right|\right) : \quad \left(0,0\right) + \left(\frac{1}{2},\frac{1}{2}\right) \text{ and descendents,} \tag{5.84}$$

$$\frac{1}{2}\left(\left|\frac{\theta_3}{\eta}\right| - \left|\frac{\theta_4}{\eta}\right|\right) : \quad \left(\frac{1}{2},0\right) + \left(0,\frac{1}{2}\right) \text{ and descendents,} \tag{5.85}$$

$$\frac{1}{2}\left|\frac{\theta_2}{\eta}\right| \quad : \quad \left(\frac{1}{16},\frac{1}{16}\right) \text{ and descendents.} \tag{5.86}$$

All fields in the free-fermion CFT can be found by considering fermion modes acting on either $(0,0)$ or $(1/16, 1/16)$, the ground states of the model with antiperiodic and periodic boundary conditions in the fermion model, respectively [15, 16]. For $(0,0)$, half-odd-integer modes $\psi_{-(n-1/2)}$ can be applied, for $n = 1, 2, ...$, increasing the holomorphic weight by $n+1/2$, while $\bar{\psi}_{-(n-1/2)}$ does the same for the antiholomorphic part. Applying an even number of modes to the ground state gives a state in Equation 5.84, while an odd number gives a state in Equation 5.85.

For $(1/16, 1/16)$, the modes have integer values instead: ψ_{-n}, for $n = 1, 2, ...$ (and the same for $\bar{\psi}_{-n}$). The tower generated by these modes then corresponds to Equation 5.86. There is an additional zero mode ψ_0 which maps between the two $(1/16, 1/16)$ towers.

We then have the interpretation that, off the self-dual line, the fermion gaps out and applying any fermion mode to the ground state in either of the fermion

sectors gaps the system. This completely removes Γ_δ^- from the partition function and takes us down to a single copy of Γ^+, along with either Γ^- or Γ_δ^+. If we perturb towards $H_{\text{ADP}} = \sum_j(\tau_j + \tau_j^\dagger)$, we take the $(1/16, 1/16)$ ground state to be the one coupled to Γ_δ^+ and the fermion zero mode gaps out Γ^-, while perturbing towards $H = \sum_j(\sigma_j^\dagger\sigma_{j+1} + \sigma_j\sigma_{j+1}^\dagger)$ takes the other $(1/16, 1/16)$ field to be the ground state by duality and gaps out Γ_δ^+ instead.

5.10 Perturbing from the $c = 3/2$ point

Now that we have found the partition function of the CFT at the supersymmetric point H_1, we can find the momenta of the states on the lattice corresponding to the different fields. As mentioned in the previous section and indicated in Figure 5.5, this point is connected to the XXZ model found by perturbing from $H_{\text{ADP}} = \sum_j(\tau_j + \tau_j^\dagger)$ and so we might expect the momentum dependence to be as in the second column of Table 5.3. This is not quite the case and is explained by noting that the boson in the supersymmetric theory has radius $R = \sqrt{3}$, while the one in the infinitesimally off-critical theory has radius $R = \sqrt{3}/2$, from Equation 5.81. This has the effect of taking $n \to n/2$ and $m \to 2m$, meaning that we now have a factor of $2n\pi$ in the momentum, where again the momentum is only defined modulo 2π. On top of this, duality requires us to get a factor of $m\pi$ from the electric charge as can be seen from approaching the supersymmetric point from the other direction. Combining these, we see that conformal towers will be based at momentum $k \approx ([m+2n] \text{ modulo } 2)\pi$.

Now that we know the momenta of the states, our next task is to find which relevant operators can contribute to perturbations of the supersymmetric Hamiltonian. Before addressing the fields themselves, we first list the symmetries and how each exhibits itself in the CFT. The $\mathbb{Z}_3$ charge, r, is the value of m modulo 3 in the boson + fermion (B + F) picture, and is the $\mathbb{Z}_3$ charge of the Potts field in the TCI + Potts (TCI + P) language. The only fields with non-zero r in the Potts picture are $(1/15, 1/15)$ and $(2/3, 2/3)$, along with their descendants, each of which can have $r = 1$ or 2.

Next, we have the momentum, k, as we discussed above. For a field of spin $s = 0$, this is $k = 0$ or π. In the B + F picture, $k = (m + 2n)\pi$, while, for consistency, it is specified by the $\mathbb{Z}_2$ charge of the TCI field in the TCI + Potts language. If the TCI field is $(3/80, 3/80)$ or $(7/16, 7/16)$, or a descendant of either of them, $k = \pi$, otherwise $k = 0$. Fields of spin s then have momentum differing by $2\pi s/L$ from $k = 0$ or $k = \pi$, depending on where the tower they are part of is centred.

Finally, we have duality. Throughout this thesis we have talked about a duality between operators. In fact, as well as the duality we have mentioned before,

$$\mathcal{D} : \tau_j \to \sigma_j^\dagger \sigma_{j+1}, \quad \sigma_j^\dagger \sigma_{j+1} \to \tau_{j+1}, \tag{5.87}$$

there is a second duality, related by parity symmetry to the first [125]. This is

$$\mathcal{D}' : \tau_{j+1} \to \sigma_j^\dagger \sigma_{j+1}, \quad \sigma_j^\dagger \sigma_{j+1} \to \tau_j. \tag{5.88}$$

As duality takes the $r = 1, 2$ sectors to twisted sectors [139], we only consider duality for $r = 0$.

To determine the action of duality, we rely on numerical data. Taking the boson and fermion picture first, we see that it must act on both parts. From the duality breaking model, we know it must act on the boson, and if it did not act on the fermion then the fermion bilinear $(1/2, 1/2)$ would be relevant and cause a transition as we vary θ from $\pi/2$. In fact, this is the very perturbation that gaps out the fermion when we break duality, as it adds an $M\psi\bar{\psi}$ fermion mass term to the action, and causes a transition to the $c = 1$ model.[6]

There is, of course, ambiguity as to which way round we label $\mathcal{D}$ and $\mathcal{D}'$, so we choose

$$\mathcal{D} : \ m \leftrightarrow -n, \quad \left(0, \frac{1}{2}\right) \to \left(0, \frac{1}{2}\right), \quad \left(\frac{1}{2}, 0\right) \to -\left(\frac{1}{2}, 0\right); \tag{5.89}$$

$$\mathcal{D}' : \ m \leftrightarrow n, \quad \left(0, \frac{1}{2}\right) \to -\left(0, \frac{1}{2}\right), \quad \left(\frac{1}{2}, 0\right) \to \left(\frac{1}{2}, 0\right); \tag{5.90}$$

where the final two expressions on each line ignore the bosonic parts of the weights. Both dualities exchange the electric and magnetic fields, with the extra minus sign

[6] If perturbed in the direction of the ADP model (5.41), this $c = 1$ model is the continuation of the XXZ phase, as indicated in Figure 5.5.

in $\mathcal{D}$ present due to the ambiguity of the sign of the charge, while $\mathcal{D}$ gives the fermion $\psi = (1/2, 0)$ a minus sign but leaves $\bar{\psi} = (0, 1/2)$ invariant, and $\mathcal{D}'$ does the reverse. Both dualities then give the fermion energy field $\psi\bar{\psi} = (1/2, 1/2)$ a minus sign, agreeing with it being a forbidden perturbation along the self-dual line. For consistency between the B + F and TCI + P pictures, we see that duality affects only the Potts part in the TCI + P language. Neither duality changes 0 or 7/5, but $(2/5, 0)$ and $(3, 0)$ are odd under $\mathcal{D}$, while $(0, 2/5)$ and $(0, 3)$ are even, with the reverse true for $\mathcal{D}'$.

We now use these symmetries to find which of these operators are allowed relevant perturbations. Each relevant and marginal field that appears in the partition function (4.52) (or, equivalently, 4.54) is listed in Table 5.4, along with its eigenvalues for different symmetries. The spin, s, and $\mathbb{Z}_3$ charge, r, are not listed as they can be determined from the momentum k and duality behaviour $(\mathcal{D}, \mathcal{D}')$ respectively: $s = (L/2\pi) \times (k \text{ modulo } \pi)$, and $r = 0$ if duality is well-defined, while it is $r = 1, 2$ for duality unspecified. For each duality, "+" means the field is even, while "−" denotes it is odd, and "·" it is unspecified under both dualities and hence has $r = 1, 2$. In the table, h' corresponds to the Virasoro generator L_{-1} acting on h ($h' \equiv L_{-1}h$), while $h'' \equiv L_{-2}h$, with analogous definitions for the antiholomorphic parts.

As stated earlier, ignoring the identity, the most relevant field obeying every symmetry, but not duality, is the field $(0 + 1/2, 0 + 1/2)$ in the B + F picture, corresponding to adding a mass to the fermion and breaking the $c = 3/2$ CFT down to a $c = 1$ CFT. This field is odd under both dualities and so the allowed fields with the lowest dimension all have $\Delta = 2$. Imposing parity symmetry, there are then 3 marginal operators with weights $(2, 0) + (0, 2)$. In the B + F picture, these are the boson stress-energy tensor combined with the fermion identity, $(0''+0, 0+0)+(0+0, 0''+0)$, the fermion stress-energy tensor combined with the boson identity, $(0+0'', 0+0)+(0+0, 0+0'')$, and $(3/2+1/2, 0+0)+(0+0, 3/2+1/2)$. In the TCI + P language, these are the TCI stress-energy tensor combined with the Potts identity $(0''+0, 0+0)+(0+0, 0''+0)$, the Potts stress-energy tensor combined with the

Δ	k	TCI + P	B + F	$[m,n]$	$(\mathcal{D},\mathcal{D}')$
0	0	(0+0,0+0)	(0+0,0+0)	[0,0]	(+,+)
$\frac{5}{24}$	π	$(\frac{3}{80}+\frac{1}{15},\frac{3}{80}+\frac{1}{15})$	$(\frac{1}{24}+\frac{1}{16},\frac{1}{24}+\frac{1}{16})$	[1,0]	·
$\frac{1}{3}$	0	$(\frac{1}{10}+\frac{1}{15},\frac{1}{10}+\frac{1}{15})$	$(\frac{1}{6}+0,\frac{1}{6}+0)$	[−2,0]	·
$\frac{7}{8}$	π	$(\frac{7}{16}+0,\frac{7}{16}+0)$	$(\frac{3}{8}+\frac{1}{16},\frac{3}{8}+\frac{1}{16})$	$[3,0]+[0,\frac{1}{2}]+[-3,0]+[0,-\frac{1}{2}]$	(+,+)
		$(\frac{7}{16}+0,\frac{3}{80}+\frac{2}{5})$	$(\frac{3}{8}+\frac{1}{16},\frac{3}{8}+\frac{1}{16})$	$[3,0]-[0,\frac{1}{2}]-[-3,0]+[0,-\frac{1}{2}]$	(+,−)
		$(\frac{3}{80}+\frac{2}{5},\frac{7}{16}+0)$	$(\frac{3}{8}+\frac{1}{16},\frac{3}{8}+\frac{1}{16})$	$[3,0]+[0,\frac{1}{2}]-[-3,0]-[0,-\frac{1}{2}]$	(−,+)
		$(\frac{3}{80}+\frac{2}{5},\frac{3}{80}+\frac{2}{5})$	$(\frac{3}{8}+\frac{1}{16},\frac{3}{8}+\frac{1}{16})$	$[3,0]-[0,\frac{1}{2}]+[-3,0]-[0,-\frac{1}{2}]$	(−,−)
1	0	$(\frac{1}{10}+\frac{2}{5},\frac{1}{10}+\frac{2}{5})$	$(0+\frac{1}{2},0+\frac{1}{2})$	[0,0]	(−,−)
1	$\frac{2\pi}{L}$	$(\frac{3}{5}+\frac{2}{5},0+0)$	(1+0,0+0)	[0,0]	(−,+)
$\frac{29}{24}$	$\pi+\frac{2\pi}{L}$	$(\frac{7}{16}+\frac{2}{3},\frac{3}{80}+\frac{1}{15})$	$(\frac{1}{24}'+\frac{1}{16},\frac{1}{24}+\frac{1}{16})$	[1,0]	·
		$(\frac{3}{80}'+\frac{1}{15},\frac{3}{80}+\frac{1}{15})$	$(\frac{1}{24}+\frac{1}{16}',\frac{1}{24}+\frac{1}{16})$	[1,0]	·
		$(\frac{3}{80}+\frac{1}{15}',\frac{3}{80}+\frac{1}{15})$	$(\frac{25}{24}+\frac{1}{16},\frac{1}{24}+\frac{1}{16})$	$[-2,-\frac{1}{2}]$	·
$\frac{4}{3}$	0	$(0+\frac{2}{3},0+\frac{2}{3})$	$(\frac{1}{6}+\frac{1}{2},\frac{1}{6}+\frac{1}{2})$	[−2,0]	·
		$(\frac{3}{5}+\frac{1}{15},0+\frac{2}{3})$	$(\frac{1}{6}+\frac{1}{2},\frac{2}{3}+0)$	$[1,-\frac{1}{2}]$	·
		$(0+\frac{2}{3},\frac{3}{5}+\frac{1}{15})$	$(\frac{2}{3}+0,\frac{1}{6}+\frac{1}{2})$	$[1,\frac{1}{2}]$	·
		$(\frac{3}{5}+\frac{1}{15},\frac{3}{5}+\frac{1}{15})$	$(\frac{2}{3}+0,\frac{2}{3}+0)$	[4,0]	·
$\frac{15}{8}$	$\pi+\frac{2\pi}{L}$	$(\frac{7}{16}'+0,\frac{7}{16}+0)$	$(\frac{3}{8}'+\frac{1}{16},\frac{3}{8}+\frac{1}{16})$	$[3,0]+[0,\frac{1}{2}]+[-3,0]+[0,-\frac{1}{2}]$	(+,+)
		$(\frac{3}{80}+\frac{7}{5},\frac{7}{16}+0)$	$(\frac{3}{8}+\frac{1}{16}',\frac{3}{8}+\frac{1}{16})$	$[3,0]+[0,\frac{1}{2}]+[-3,0]+[0,-\frac{1}{2}]$	(+,+)
		$(\frac{7}{16}'+0,\frac{3}{80}+\frac{2}{5})$	$(\frac{3}{8}'+\frac{1}{16},\frac{3}{8}+\frac{1}{16})$	$[3,0]-[0,\frac{1}{2}]-[-3,0]+[0,-\frac{1}{2}]$	(+,−)
		$(\frac{3}{80}+\frac{7}{5},\frac{3}{80}+\frac{2}{5})$	$(\frac{3}{8}+\frac{1}{16}',\frac{3}{8}+\frac{1}{16})$	$[3,0]-[0,\frac{1}{2}]-[-3,0]+[0,-\frac{1}{2}]$	(+,−)
		$(\frac{3}{80}+\frac{2}{5}',\frac{7}{16}+0)$	$(\frac{3}{8}'+\frac{1}{16},\frac{3}{8}+\frac{1}{16})$	$[3,0]+[0,\frac{1}{2}]-[-3,0]-[0,-\frac{1}{2}]$	(−,+)
		$(\frac{3}{80}'+\frac{2}{5},\frac{7}{16}+0)$	$(\frac{3}{8}+\frac{1}{16}',\frac{3}{8}+\frac{1}{16})$	$[3,0]+[0,\frac{1}{2}]-[-3,0]-[0,-\frac{1}{2}]$	(−,+)
		$(\frac{3}{80}+\frac{2}{5}',\frac{3}{80}+\frac{2}{5})$	$(\frac{3}{8}'+\frac{1}{16},\frac{3}{8}+\frac{1}{16})$	$[3,0]-[0,\frac{1}{2}]+[-3,0]-[0,-\frac{1}{2}]$	(−,−)
		$(\frac{3}{80}'+\frac{2}{5},\frac{3}{80}+\frac{2}{5})$	$(\frac{3}{8}+\frac{1}{16}',\frac{3}{8}+\frac{1}{16})$	$[3,0]-[0,\frac{1}{2}]+[-3,0]-[0,-\frac{1}{2}]$	(−,−)
2	0	$(\frac{3}{5}+\frac{2}{5},\frac{3}{5}+\frac{2}{5})$	(1+0,1+0)	[0,0]	(−,−)
2	$\frac{2\pi}{L}$	$(\frac{3}{2}+0,\frac{1}{10}+\frac{2}{5})$	$(\frac{3}{2}+0,0+\frac{1}{2})$	$[3,\frac{1}{2}]+[-3,-\frac{1}{2}]$	(+,−)
		$(\frac{1}{10}+\frac{7}{5},\frac{1}{10}+\frac{2}{5})$	$(1+\frac{1}{2},0+\frac{1}{2})$	[0,0]	(+,−)
		$(\frac{1}{10}+\frac{2}{5}',\frac{1}{10}+\frac{2}{5})$	$(\frac{3}{2}+0,0+\frac{1}{2})$	$[3,\frac{1}{2}]-[-3,-\frac{1}{2}]$	(−,−)
		$(\frac{1}{10}'+\frac{2}{5},\frac{1}{10}+\frac{2}{5})$	$(0+\frac{1}{2}',0+\frac{1}{2})$	[0,0]	(−,−)
2	$\frac{4\pi}{L}$	$(0''+0,0+0)$	$(0''+0,0+0)$	[0,0]	(+,+)
		$(0+0'',0+0)$	$(0+0'',0+0)$	[0,0]	(+,+)
		$(\frac{3}{5}+\frac{7}{5},0+0)$	$(\frac{3}{2}+\frac{1}{2},0+0)$	$[3,\frac{1}{2}]-[-3,-\frac{1}{2}]$	(+,+)
		$(\frac{3}{5}'+\frac{2}{5},0+0)$	$(\frac{3}{2}+\frac{1}{2},0+0)$	$[3,\frac{1}{2}]+[-3,-\frac{1}{2}]$	(−,+)
		$(\frac{3}{5}+\frac{2}{5}',0+0)$	$(1'+0,0+0)$	[0,0]	(−,+)

Table 5.4: The relevant and marginal fields for H_1 with spin $s \geq 0$. The dimension, Δ, and momentum, k, are given along with the behaviour under the dualities of Equations 5.87 and 5.88. Each field is given in terms of its TCI + Potts (TCI + P) fields, along with its Boson + Fermion (B + F) fields and the bosonic electric and magnetic charges [m,n]. If duality is well-defined, the $\mathbb{Z}_3$ charge is $r = 0$, otherwise there are fields with both $r = 1, 2$. The spin, s, is given by k modulo π.

TCI identity, $(0+0'',0+0)+(0+0,0+0'')$, and $(3/5+7/5,0+0)+(0+0,3/5+7/5)$. The representation of these TCI + P fields in terms of the B + F fields is an interesting question and will be studied in a future work [143].

Perturbing along the self-dual line, we can add in the three marginal operators described above. The Potts and TCI stress-energy tensors will just change the relative Fermi velocities of the two parts. The third operator is presumably the reason why the lattice model is not fully described by a change in Fermi velocity between the Potts and TCI parts. The precise behaviour of this operator will be investigated in a future work [143].

As we perturb along the self-dual line, we could expect the dimensions of fields to change. Indeed, for generic fields this will be the case, but as the spin s is fixed to take integer values, it must stay constant along the flow. As all the allowed marginal operators have $s = 2$, they can never become relevant. The least irrelevant allowed operators with spin $s < 2$ are a pair of $s = 0$ fields with dimension $\Delta = 3$: $(3/2 + 0, 3/2 + 0)$ and $(1/10 + 7/5, 1/10 + 7/5)$ in the TCI + P language. When these (or any other allowed irrelevant operators) flow to have dimension $\Delta < 2$, we would expect a transition and the phase to end, but this will not happen in a finite region around the supersymmetric point.

5.11 Conclusions and outlook

In this chapter we have investigated some off-critical properties of the 3-state model. In the first half, we perturbed around the multicritical point $-H_1$ and found four gapped phases, each with a frustration-free point. Along with the well-known ordered and disordered Potts phases, there were not-A and RSPT phases. We then used a field theory analysis to determine the transitions between these phases to be second order and in the universality class of the Potts CFT.

The not-A phase is particularly interesting. It has the same degeneracy as the ordered Potts phase, suggesting it could be useful in the description of topological parafermion phases [47]. Whether this not-A behaviour is present in any physical materials is an interesting question going into the future.

The connection between the frustration-free points and the conformal boundary conditions of the critical two-dimensional classical Potts model is another fascinating question [163, 164]. Clearly this is no coincidence, but precisely what the significance of this result is escapes us for the moment. Hopefully, future work will enlighten us on this.

The second half focused on perturbing from the exactly solvable point $H_{\mathrm{ADP}} = \sum_j (\tau_j + \tau_j^\dagger)$. We found an XXZ description around this point, allowing us to explain the momenta of different states in the AFP and "$c = 3/2$" phases of Chapter 4. This description also explained the CFT description at H_1 and the behaviour as we perturb from this point.

The XXZ picture breaks down in the incommensurate regions separating the XXZ models with positive and negative XX parts, but we hope that improved numerical techniques in the future may lead to a better understanding of these phases and, hopefully, their extensions to the self-dual line. There are other regions of the off-critical diagram not yet fully explained either – for example, how does the RSPT phase transition to the XXZ phase (or is there some intermediate phase)? Once again, this has proved to be too numerically challenging a problem to solve at the moment.

6 Conclusions

Contents

6.1 Conclusions

In this thesis we have considered short-range interactions obeying the symmetries of the Ising and three-state Potts models, the natural playgrounds for Majorana fermions and parafermions, respectively. In these very simple models, we have found many exotic phases displaying a huge range of properties, from the standard Ising and Potts critical phases, to order-disorder coexistence, RSPT order, and many more.

CFT has played a vital role throughout in explaining our numerical results, but a key point of this thesis has also been finding lattice models which have particular CFTs as their continuum limits, allowing us to understand the field theories themselves better. The point H_1 (4.34) in particular has proved enlightening for this, giving us a lattice realisation of the highly unusual CFT with two different representations, $Z_{\text{s-a}}(\sqrt{3})$ [142].

Perhaps the biggest take-away from this work is the importance of duality. Not only does it allow us to locate the positions of transitions between duality-

breaking phases as mentioned in the introduction, but it also allows us to constrain the very transitions these can be, as shown in Chapters 4 and 5. In terms of Majoranas and parafermions this mapping becomes even more significant, demonstrating the complex behaviour expected from these emergent degrees of freedom in physical systems.

Throughout this thesis we have mentioned the open questions still left by this work and the potential future directions others could take. There are certainly practical applications of these results, potentially in the field of quantum computation [41], but there are also many theoretical problems unsolved. Firstly, what else can we learn about CFTs from these results? We have solved some mysteries, but many still remain, such as how the Onsager symmetry fits into the conformal group and how the fields for $Z_{\text{s-a}}(\sqrt{3})$ match up between the different representations.

We could also ask what happens for q-state Potts models with $q > 3$. Having seen such rich structure for $q = 2$ and 3, it seems difficult to believe that even more exotic phases do not exist as we take more states per site. We do not know exactly what happens for arbitrary off-critical points of $H_{\text{DB}}(J, f, \lambda_1)$ (5.1) either, or in the incommensurate regions of Figure 4.1.

Some of these problems have not been solved due to a lack of time, while for others the available computational power is not yet up to the task. We hope that in the future all of these mysteries will be solved, and yet more weird and wonderful physics will be discovered in these models.

Appendices

A

TCI transitions for different perturbations

We now return to the mystery mentioned earlier: why does the Rahmani model (3.10) have its TCI transition at a ratio of couplings three orders of magnitude larger than our model (3.11)? To gain some intuition as to which of these is the "odd one out" we consider the other four-Majorana interaction which is just next-nearest-neighbour in terms of spins. Recalling that the Rahmani and our perturbations were, respectively,

$$H_R = \sum_a \gamma_{a-1}\gamma_a\gamma_{a+1}\gamma_{a+2}, \tag{A.1}$$

$$H_3 = -\sum_a \gamma_{a-2}\gamma_{a-1}\gamma_{a+1}\gamma_{a+2}, \tag{A.2}$$

we consider the perturbation

$$\begin{aligned} H_y &= \sum_a \left(\gamma_{a-2}\gamma_a\gamma_{a+1}\gamma_{a+2} - \gamma_{a-2}\gamma_{a-1}\gamma_a\gamma_{a+2}\right) \\ &= \sum_j \left(\sigma^z_{j-1}\sigma^y_j\sigma^x_{j+1} + \sigma^x_{j-1}\sigma^y_j\sigma^z_{j+1} - \sigma^y_{j-1}\sigma^z_{j+1} - \sigma^z_{j-1}\sigma^y_{j+1}\right). \end{aligned} \tag{A.3}$$

Recalling our Ising Hamiltonian,

$$H_I = \sum_a i\gamma_a\gamma_{a+1}, \tag{A.4}$$

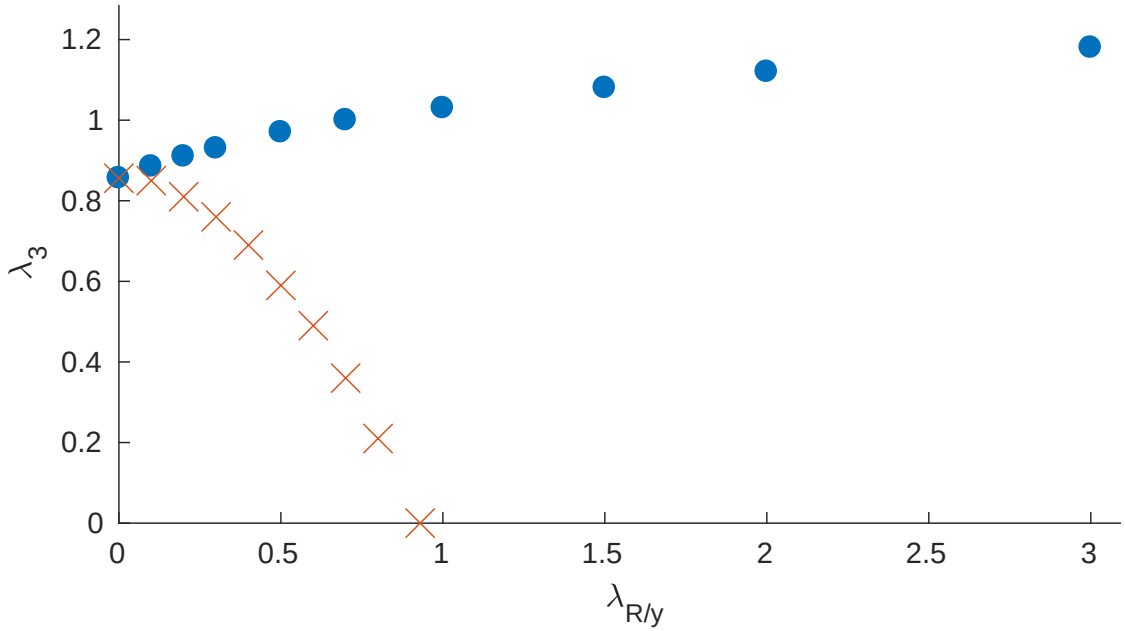

Figure A.1: Locations of the TCI transition for λ_3 as a function of λ_R (blue dots) or λ_y (orange crosses), with the other coupling set to 0.

we write down the full Hamiltonian of the Ising model perturbed by its next-nearest-neighbour (in spins), $\mathbb{Z}_2$ and chirally symmetric Hamiltonian as

$$H(\lambda_I, \lambda_3, \lambda_R, \lambda_y) = 2\lambda_I H_I + \lambda_3 H_3 + \lambda_R H_R + \lambda_y H_y. \tag{A.5}$$

To demonstrate the effect of adding H_R and H_y, we plot the location of the TCI transition for different couplings in Figure A.1. The position of the TCI transition is given as a function of λ_3 versus λ_R (blue dots) or λ_y (orange crosses), with the other of λ_R or λ_y set to 0. As can be seen, increasing λ_R in fact increases the value of λ_3 needed for the transition (at least for λ_3 of $\mathcal{O}(1)$), while increasing λ_y decreases the necessary λ_3. The transition with $\lambda_3 = 0$ is again at λ_y of $\mathcal{O}(1)$, showing that H_3 and H_y behave qualitatively similarly, while H_R appears to be the anomalous one.

Why H_R should behave differently was an unsolved question until recently when Aasen *et al.* came up with a beautiful explanation [41], which we now summarise briefly. They first went to momentum space, writing

$$\gamma_a = \frac{\sqrt{2}}{\sqrt{N}} \sum_k e^{ika} \gamma_k, \tag{A.6}$$

where $\{\gamma_k, \gamma'_k\} = \delta_{k,-k'}$, $\gamma_k = \gamma^\dagger_{-k}$ and N is the number of Majoranas. This transforms H_I into

$$H_I = \sum_{-\pi<k<0} \epsilon_0(k)\gamma^\dagger_k\gamma_k, \tag{A.7}$$

where $\epsilon_0(k) = 4|\sin(k)|$ is the energy cost of a single particle excitation at momentum k ($\gamma^\dagger_k\gamma_k = 1$, rather than 0 for $-\pi < k < 0$).

To take account of the interactions H_R, H_3 and H_y, Aasen *et al.* studied the kinetic energy renormalisation through a rewriting of the interactions, similar to normal ordering. To do this, they rewrote the four-fermion interaction terms such that all terms other than constants and Majorana number operators ($\gamma^\dagger_k\gamma_k$) have vanishing matrix elements on the subspace of zero- and one-particle excitations. For a general translation invariant interaction with four fermions, the calculation is

$$\begin{aligned}
\delta H &= U\sum_a \gamma_{a+\mu}\gamma_{a+\nu}\gamma_{a+\sigma}\gamma_{a+\rho} \\
&= \frac{4U}{N^2}\sum_a \sum_{k_1,\ldots,k_4} e^{i(k_1(a+\mu)+k_2(a+\nu)+k_3(a+\sigma)+k_4(a+\rho))}\gamma_{k_1}\gamma_{k_2}\gamma_{k_3}\gamma_{k_4} \\
&= \frac{4U}{N^2}\sum_a \sum_{-\pi<k_1,\ldots,k_4<0} \left(e^{ik_1(a+\mu)}\gamma_{k_1} + e^{-ik_1(a+\mu)}\gamma^\dagger_{k_1}\right)\left(e^{ik_2(a+\nu)}\gamma_{k_2} + e^{-ik_2(a+\nu)}\gamma^\dagger_{k_2}\right) \\
&\qquad \times \left(e^{ik_3(a+\sigma)}\gamma_{k_3} + e^{-ik_3(a+\sigma)}\gamma^\dagger_{k_3}\right)\left(e^{ik_4(a+\rho)}\gamma_{k_4} + e^{-ik_4(a+\rho)}\gamma^\dagger_{k_4}\right) \\
&= \frac{4U}{N^2}\sum_a \sum_{-\pi<k_1,\ldots,k_4<0} \Big[e^{i(k_1+k_2-k_3-k_4)a}e^{i(\mu k_1+\nu k_2-\sigma k_3-\rho k_4)}\gamma_{k_1}\gamma_{k_2}\gamma^\dagger_{k_3}\gamma^\dagger_{k_4} \\
&\qquad + e^{i(k_1-k_2+k_3-k_4)a}e^{i(\mu k_1-\nu k_2+\sigma k_3-\rho k_4)}\gamma_{k_1}\gamma^\dagger_{k_2}\gamma_{k_3}\gamma^\dagger_{k_4} \\
&\qquad + e^{i(k_1-k_2-k_3+k_4)a}e^{i(\mu k_1-\nu k_2-\sigma k_3+\rho k_4)}\gamma_{k_1}\gamma^\dagger_{k_2}\gamma^\dagger_{k_3}\gamma_{k_4} \\
&\qquad + e^{i(-k_1+k_2+k_3-k_4)a}e^{i(-\mu k_1+\nu k_2+\sigma k_3-\rho k_4)}\gamma^\dagger_{k_1}\gamma_{k_2}\gamma_{k_3}\gamma^\dagger_{k_4} \\
&\qquad + e^{i(-k_1+k_2-k_3+k_4)a}e^{i(-\mu k_1+\nu k_2-\sigma k_3+\rho k_4)}\gamma^\dagger_{k_1}\gamma_{k_2}\gamma^\dagger_{k_3}\gamma_{k_4} \\
&\qquad + e^{i(-k_1-k_2+k_3+k_4)a}e^{i(-\mu k_1-\nu k_2+\sigma k_3+\rho k_4)}\gamma^\dagger_{k_1}\gamma^\dagger_{k_2}\gamma_{k_3}\gamma_{k_4} + \ldots \Big] \\
&= \frac{4U}{N^2}\sum_a \sum_{-\pi<p,q,r<0} \Big[-e^{-i(p-r)a}e^{i(\mu p+\nu q-\sigma q-\rho r)}\gamma^\dagger_r\gamma_p + e^{i(q-r)a}e^{i(\mu p+\nu q-\sigma p-\rho r)}\gamma^\dagger_r\gamma_q \\
&\qquad + e^{i(p-r)a}e^{i(\mu p+\nu q-\sigma r-\rho q)}\gamma^\dagger_r\gamma_p - e^{i(q-r)a}e^{i(\mu p+\nu q-\sigma r-\rho p)}\gamma^\dagger_r\gamma_q \\
&\qquad - e^{i(q-r)a}e^{i(\mu p-\nu p+\sigma q-\rho r)}\gamma^\dagger_r\gamma_q - e^{i(p-q)a}e^{i(\mu p-\nu q+\sigma r-\rho r)}\gamma^\dagger_q\gamma_p
\end{aligned}$$

$$
\begin{aligned}
&+ e^{i(r-q)a} e^{i(\mu p - \nu q + \sigma r - \rho p)} \gamma_q^\dagger \gamma_r + e^{i(r-q)a} e^{i(\mu p - \nu p - \sigma q + \rho r)} \gamma_q^\dagger \gamma_r \\
&- e^{i(r-q)a} e^{i(\mu p - \nu q - \sigma p + \rho r)} \gamma_q^\dagger \gamma_r + e^{i(q-p)a} e^{i(-\mu p + \nu q + \sigma r - \rho r)} \gamma_p^\dagger \gamma_q \\
&- e^{i(r-p)a} e^{i(-\mu p + \nu q + \sigma r - \rho q)} \gamma_p^\dagger \gamma_r + e^{i(r-p)a} e^{i(-\mu p + \nu q - \sigma q + \rho r)} \gamma_p^\dagger \gamma_r \Big] + ... \\
= \frac{4U}{N} \sum_{-\pi<s,t<0} \Big[& e^{i((\mu-\rho)s+(\nu-\sigma)t)} + e^{i((\nu-\rho)s+(\mu-\sigma)t)} + e^{i((\mu-\sigma)s+(\nu-\rho)t)} \\
&- e^{i((\nu-\sigma)s+(\mu-\rho)t)} - e^{i((\sigma-\rho)s+(\mu-\nu)t)} - e^{i((\mu-\nu)s+(\sigma-\rho)t)} \\
&+ e^{i((\sigma-\nu)s+(\mu-\rho)t)} + e^{i((\rho-\sigma)s+(\mu-\nu)t)} - e^{i((\rho-\nu)s+(\mu-\sigma)t)} \\
&+ e^{i((\nu-\mu)s+(\sigma-\rho)t)} - e^{i((\sigma-\mu)s+(\nu-\rho)t)} + e^{i((\rho-\mu)s+(\nu-\sigma)t)} \Big] \gamma_s^\dagger \gamma_s + ... \\
\equiv \sum_{-\pi<s<0} & \delta\epsilon(s) \gamma_s^\dagger \gamma_s + ...,
\end{aligned}
$$

The first line is just the expression for the interaction. The second line rewrites this in terms of momentum space fermions, as defined in Equation A.6. The third line moves everything into Majoranas and conjugates with negative momenta. The fourth line expands this out, keeping only the terms with two Majoranas and two conjugates as all other terms will vanish on the subspace of zero- and one-particle excitations. The fifth line moves all conjugates to the left and drops constant terms and those that vanish in the subspace of zero- and one-particle excitations. The sixth line performs the sum over a. The seventh line gives the definition of $\delta\epsilon(k)$.

To make further progress we note that, if our k values, and hence our s and t, can be $k = -\pi + \pi/N, \pi + 3\pi/N, ..., -3\pi/N, -\pi/N$, as expected for antiperiodic boundary conditions in fermions,

$$
\sum_k e^{ink} = \frac{i\left(1-(-1)^n\right)}{2\sin\left(\frac{n\pi}{N}\right)}. \tag{A.8}
$$

We can then perform the sums over t and arrive at our final answers.

Starting with the easiest case of the Ising interaction, we have $\mu = 0$, $\nu = 1$, $\sigma = \rho = 2$. With $U = i$, this gives

$$
\delta\epsilon_I(k) = -4\sin k = -4k + \mathcal{O}\left(k^3\right), \tag{A.9}
$$

where in the final equality we have taken k close to 0. If k is near π instead, replacing k by $\pi - k$ produces the correct result.[1]

Turning now to the Rahmani interaction, we have $\mu = -1$, $\nu = 0$, $\sigma = 1$, $\rho = 2$, giving

$$\delta\epsilon_R(k) = -\frac{4U_R}{N}\left[\left(\frac{4}{\sin(\pi/N)} + \frac{2}{\sin(3\pi/N)}\right)\right)\sin k + \frac{2}{\sin(\pi/N)}\sin(3k)\right] \quad \text{(A.10)}$$

$$= -\frac{128}{3\pi}U_R\left[k + \mathcal{O}\left(k^3, \frac{k}{N^2}\right)\right], \quad \text{(A.11)}$$

We see that there is a strong correction to the velocity from the Rahmani interaction.

Considering instead our interaction, we have $\mu = -2$, $\nu = -1$, $\sigma = 1$, $\rho = 2$, resulting in

$$\delta\epsilon_3(k) = -\frac{16U_3}{N}\left[\frac{1}{\sin(\pi/N)}\sin k - \frac{1}{\sin(3\pi/N)}\sin(3s)\right] \quad \text{(A.12)}$$

$$= -\frac{64U_3}{3\pi}k\left[\left(\frac{\pi^2}{N^2} - k^2\right) + \mathcal{O}(N^{-4}, N^{-2}k^2, k^{-4})\right], \quad \text{(A.13)}$$

showing that the linear term is suppressed by a factor of $1/N^2$ and the largest terms are of size k^3.

Due to the minus sign in the final interaction, H_y, $\delta\epsilon_y(k)$ vanishes at all orders in this approximation.

We now see the difference between the Rahmani interaction and the other two - it boosts the low energy Ising terms as well as providing other effective couplings. This explains why the transition needs such a strong λ_R relative to λ_3 and λ_y.

[1] Of course, in the Ising case this is exact and the lengthy calculation was not needed, but we include it to show consistency!

References

[1] W. Lenz, "Beiträge zum Verständnis der magnetischen Eigenschaften in festen Körpern," Physikalische Zeitschrift **21**, 613–615 (1920).

[2] E. Ising, "Beitrag zur Theorie des Ferromagnetismus," Zeitschrift für Physik **31**, 253–258 (1925).

[3] W. Heisenberg, "Zur Theorie des Ferromagnetismus," Zeitschrift für Physik **49**, 619–636 (1928).

[4] V. L. Berezinskii, "Destruction of long-range order in one-dimensional and two-dimensional systems having a continuous symmetry group. I. Classical systems," Sov. Phys. JETP **32**, 493–500 (1971), [Zh. Eksp. Teor. Fiz. 59, 907 (1971)].

[5] V. L. Berezinskii, "Destruction of long-range Order in One-dimensional and Two-dimensional Systems Possessing a Continuous Symmetry Group. II. Quantum Systems." Sov. Phys. JETP **34**, 610–616 (1972), [Zh. Eksp. Teor. Fiz. 61, no.3, 1144 (1972)].

[6] J. M. Kosterlitz and D. J. Thouless, "Ordering, metastability and phase transitions in two-dimensional systems," Journal of Physics C: Solid State Physics **6**, 1181–1203 (1973).

[7] H. A. Kramers and G. H. Wannier, "Statistics of the Two-Dimensional Ferromagnet. Part I," Phys. Rev. **60**, 252–262 (1941).

[8] L. D. Landau, "On the theory of phase transitions," Zh. Eksp. Teor. Fiz. **7**, 19–32 (1937), [Phys. Z. Sowjetunion 11, 26 (1937); Ukr. J. Phys. 53, 25 (2008)].

[9] K. G. Wilson, "Renormalization Group and Critical Phenomena. I. Renormalization Group and the Kadanoff Scaling Picture," Phys. Rev. B **4**, 3174–3183 (1971).

[10] K. G. Wilson and J. Kogut, "The renormalization group and the ϵ expansion," Physics Reports **12**, 75 – 199 (1974).

[11] K. G. Wilson, "The renormalization group: Critical phenomena and the Kondo problem," Rev. Mod. Phys. **47**, 773–840 (1975).

[12] A. A. Belavin, A. M. Polyakov, and A. B. Zamolodchikov, "Infinite conformal symmetry in two-dimensional quantum field theory," Nuclear Physics B **241**, 333 – 380 (1984).

[13] R. B. Potts, "Some generalized order-disorder transformations," Mathematical Proceedings of the Cambridge Philosophical Society **48**, 106–109 (1952).

[14] V. Dotsenko, "Critical behaviour and associated conformal algebra of the Z_3 Potts model," Nuclear Physics B **235**, 54 – 74 (1984).

[15] P. Ginsparg, "Applied Conformal Field Theory," (1988), arXiv:hep-th/9108028v1 .

[16] P. D. Francesco, P. Mathieu, and D. Senechal, *Conformal Field Theory* (Springer, 1997).

[17] X. G. Wen, "Vacuum degeneracy of chiral spin states in compactified space," Phys. Rev. B **40**, 7387–7390 (1989).

[18] D. C. Tsui, H. L. Stormer, and A. C. Gossard, "Two-Dimensional Magnetotransport in the Extreme Quantum Limit," Phys. Rev. Lett. **48**, 1559–1562 (1982).

[19] R. B. Laughlin, "Anomalous Quantum Hall Effect: An Incompressible Quantum Fluid with Fractionally Charged Excitations," Phys. Rev. Lett. **50**, 1395–1398 (1983).

[20] F. Verstraete, J. I. Cirac, J. I. Latorre, E. Rico, and M. M. Wolf, "Renormalization-group transformations on quantum states," Phys. Rev. Lett. **94**, 140601 (2005).

[21] M. den Nijs and K. Rommelse, "Preroughening transitions in crystal surfaces and valence-bond phases in quantum spin chains," Phys. Rev. B **40**, 4709–4734 (1989).

[22] F. Haldane, "Continuum dynamics of the 1-d Heisenberg antiferromagnet: Identification with the O(3) nonlinear sigma model," Physics Letters A **93**, 464 – 468 (1983).

[23] F. D. M. Haldane, "Nonlinear field theory of large-spin Heisenberg antiferromagnets: Semiclassically quantized solitons of the one-dimensional easy-axis Néel state," Phys. Rev. Lett. **50**, 1153–1156 (1983).

[24] R. P. Feynman, "Simulating physics with computers," International Journal of Theoretical Physics **21**, 467–488 (1982).

[25] D. Deutsch, "Quantum theory, the Church–Turing principle and the universal quantum computer," Proceedings of the Royal Society A **400** (1985), https://doi.org/10.1098/rspa.1985.0070.

[26] A. Kitaev, "Fault-tolerant quantum computation by anyons," Annals of Physics **303**, 2 – 30 (2003).

[27] C. Nayak, S. H. Simon, A. Stern, M. Freedman, and S. Das Sarma, "Non-Abelian anyons and topological quantum computation," Rev. Mod. Phys. **80**, 1083–1159 (2008).

[28] P. W. Shor, "Algorithms for quantum computation: discrete logarithms and factoring," in *Proceedings 35th Annual Symposium on Foundations of Computer Science* (1994) pp. 124–134.

[29] P. W. Shor, "Polynomial-Time Algorithms for Prime Factorization and Discrete Logarithms on a Quantum Computer," SIAM Journal on Computing **26**, 1484–1509 (1997), https://doi.org/10.1137/S0097539795293172 .

[30] L. K. Grover, "A Fast Quantum Mechanical Algorithm for Database Search," in *Proceedings of the Twenty-Eighth Annual ACM Symposium on Theory of Computing*, STOC '96 (Association for Computing Machinery, New York, NY, USA, 1996) p. 212–219.

[31] L. K. Grover, "Quantum Mechanics Helps in Searching for a Needle in a Haystack," Phys. Rev. Lett. **79**, 325–328 (1997).

[32] W. K. Wootters and W. H. Zurek, "A single quantum cannot be cloned," Nature **299**, 802–803 (1982).

[33] D. Dieks, "Communication by EPR devices," Physics Letters A **92**, 271 – 272 (1982).

[34] E. Majorana, "Teoria simmetrica dell'elettrone e del positrone," Il Nuovo Cimento **14** (1937), 10.1007/bf02961314.

[35] A. Y. Kitaev, "Unpaired Majorana fermions in quantum wires," Phys. Usp. **44**, 131–136 (2001).

[36] N. Read and D. Green, "Paired states of fermions in two dimensions with breaking of parity and time-reversal symmetries and the fractional quantum hall effect," Phys. Rev. B **61**, 10267–10297 (2000).

[37] A. Kitaev, "Anyons in an exactly solved model and beyond," Annals of Physics **321**, 2 – 111 (2006), January Special Issue.

[38] G. Jackeli and G. Khaliullin, "Mott Insulators in the Strong Spin-Orbit Coupling Limit: From Heisenberg to a Quantum Compass and Kitaev Models," Phys. Rev. Lett. **102**, 017205 (2009).

[39] K. W. Plumb, J. P. Clancy, L. J. Sandilands, V. V. Shankar, Y. F. Hu, K. S. Burch, H.-Y. Kee, and Y.-J. Kim, "$\alpha - RuCl_3$: A spin-orbit assisted Mott insulator on a honeycomb lattice," Phys. Rev. B **90**, 041112 (2014).

[40] H.-S. Kim, V. S. V., A. Catuneanu, and H.-Y. Kee, "Kitaev magnetism in honeycomb $RuCl_3$ with intermediate spin-orbit coupling," Phys. Rev. B **91**, 241110 (2015).

[41] D. Aasen, R. S. K. Mong, B. M. Hunt, D. Mandrus, and J. Alicea, "Electrical probes of the non-Abelian spin liquid in Kitaev materials," (2020), arXiv:2002.01944 .

[42] E. Fradkin and L. Kadanoff, "Disorder variables and para-fermions in two-dimensional statistical mechanics," Nuclear Physics B **170**, 1–15 (1980).

[43] F. Y. Wu, "The Potts model," Rev. Mod. Phys. **54**, 235–268 (1982).

[44] D. J. Clarke, J. Alicea, and K. Shtengel, "Exotic non-Abelian anyons from conventional fractional quantum Hall states," Nature Communications **4** (2013), https://doi.org/10.1038/ncomms2340.

[45] M. H. Freedman, L. Michael, and W. Zhenghan, "A Modular Functor Which is Universal for Quantum Computation," Communications in Mathematical Physics **227**, 605–622 (2002).

[46] M. H. Freedman, L. Michael, and W. Zhenghan, "The Two-Eigenvalue Problem and Density of Jones Representation of Braid Groups," Communications in Mathematical Physics **228**, 177–199 (2002).

[47] J. Alicea and P. Fendley, "Topological Phases with Parafermions: Theory and Blueprints," Annual Review of Condensed Matter Physics **7**, 119–139 (2016), https://doi.org/10.1146/annurev-conmatphys-031115-011336 .

[48] D. Aasen, R. S. K. Mong, and P. Fendley, "Topological defects on the lattice: I. The Ising model," Journal of Physics A: Mathematical and Theoretical **49**, 354001 (2016).

[49] E. O'Brien and P. Fendley, "Lattice Supersymmetry and Order-Disorder Coexistence in the Tricritical Ising Model," Phys. Rev. Lett. **120**, 206403 (2018).

[50] E. O'Brien, E. Vernier, and P. Fendley, ""Not-A", representation symmetry-protected topological, and Potts phases in an S_3-invariant chain," Phys. Rev. B **101**, 235108 (2020).

[51] E. O'Brien and P. Fendley, "Self-dual S_3-invariant quantum chains," (2019), arXiv:1912.09464 .

[52] E. Vernier, E. O'Brien, and P. Fendley, "Onsager symmetries in $U(1)$ -invariant clock models," Journal of Statistical Mechanics: Theory and Experiment **2019**, 043107 (2019).

[53] S. Moudgalya, E. O'Brien, B. A. Bernevig, P. Fendley, and N. Regnault, "Large Classes of Quantum Scarred Hamiltonians from Matrix Product States," arXiv:2002.11725 .

[54] G. Mussardo, *Statistical field theory* (Oxford Univ. Press, New York, NY, 2010).

[55] L. Onsager, "Crystal Statistics. I. A Two-Dimensional Model with an Order-Disorder Transition," Phys. Rev. **65**, 117–149 (1944).

[56] S. El-Showk, M. F. Paulos, D. Poland, S. Rychkov, D. Simmons-Duffin, and A. Vichi, "Solving the 3d Ising Model with the Conformal Bootstrap II. c-Minimization and Precise Critical Exponents," Journal of Statistical Physics **157**, 869–914 (2014).

[57] P. W. Kasteleyn, "Dimer Statistics and Phase Transitions," Journal of Mathematical Physics **4**, 287–293 (1963), https://doi.org/10.1063/1.1703953 .

[58] S. Samuel, "The use of anticommuting variable integrals in statistical mechanics. I. The computation of partition functions," Journal of Mathematical Physics **21**, 2806–2814 (1980), https://doi.org/10.1063/1.524404 .

[59] S. R. White, "Density matrix formulation for quantum renormalization groups," Phys. Rev. Lett. **69**, 2863–2866 (1992).

[60] U. Schollwöck, "The density-matrix renormalization group," Rev. Mod. Phys. **77**, 259–315 (2005).

[61] U. Schollwöck, "The density-matrix renormalization group in the age of matrix product states," Annals of Physics **326**, 96 – 192 (2011), january 2011 Special Issue.

[62] M. B. Hastings, "An area law for one-dimensional quantum systems," Journal of Statistical Mechanics: Theory and Experiment **2007**, P08024 (2007).

[63] G. Vidal, "Class of Quantum Many-Body States That Can Be Efficiently Simulated," Phys. Rev. Lett. **101**, 110501 (2008).

[64] B. Pirvu, F. Verstraete, and G. Vidal, "Exploiting translational invariance in matrix product state simulations of spin chains with periodic boundary conditions," Phys. Rev. B **83**, 125104 (2011).

[65] "iTensor," `http://itensor.org/`.

[66] D. Friedan, Z. Qiu, and S. Shenker, "Conformal Invariance, Unitarity, and Critical Exponents in Two Dimensions," Phys. Rev. Lett. **52**, 1575–1578 (1984).

[67] D. Friedan, Z. Qiu, and S. Shenker, "Details of the nonunitarity proof for highest weight representations of the Virasoro algebra," Comm. Math. Phys. **107**, 535–542 (1986).

[68] A. Cappelli, C. Itzykson, and J. B. Zuber, "The A-D-E classification of minimal and $A_1^{(1)}$ conformal invariant theories," Communications in Mathematical Physics **113**, 1–26 (1987).

[69] H. W. J. Blöte, J. L. Cardy, and M. P. Nightingale, "Conformal invariance, the central charge, and universal finite-size amplitudes at criticality," Phys. Rev. Lett. **56**, 742–745 (1986).

[70] I. Affleck, "Universal term in the free energy at a critical point and the conformal anomaly," Phys. Rev. Lett. **56**, 746–748 (1986).

[71] P. Calabrese and J. Cardy, "Entanglement entropy and quantum field theory," Journal of Statistical Mechanics: Theory and Experiment **2004**, P06002 (2004).

[72] D. Friedan, Z. Qiu, and S. H. Shenker, "Superconformal Invariance in Two-Dimensions and the Tricritical Ising Model," Phys. Lett. **151B**, 37–43 (1985).

[73] P. Ramond, "Dual Theory for Free Fermions," Phys. Rev. D **3**, 2415–2418 (1971).

[74] A. Neveu and J. Schwarz, "Factorizable dual model of pions," Nuclear Physics B **31**, 86 – 112 (1971).

[75] P. Ginsparg, "Curiosities at $c = 1$," Nuclear Physics B **295**, 153 – 170 (1988).

[76] L. Dixon, J. Harvey, C. Vafa, and E. Witten, "Strings on orbifolds," Nuclear Physics B **261**, 678 – 686 (1985).

[77] L. Dixon, J. Harvey, C. Vafa, and E. Witten, "Strings on orbifolds (II)," Nuclear Physics B **274**, 285 – 314 (1986).

[78] R. Coldea, D. A. Tennant, E. M. Wheeler, E. Wawrzynska, D. Prabhakaran, M. Telling, K. Habicht, P. Smeibidl, and K. Kiefer, "Quantum Criticality in an Ising Chain: Experimental Evidence for Emergent E8 Symmetry," Science **327**, 177–180 (2010), https://science.sciencemag.org/content/327/5962/177.full.pdf .

[79] A. Zamolodchikov, "Integrals of Motion and S Matrix of the (Scaled) T=T(c) Ising Model with Magnetic Field," Int. J. Mod. Phys. A **4**, 4235 (1989).

[80] J. Alicea, "New directions in the pursuit of Majorana fermions in solid state systems," Reports on Progress in Physics **75**, 076501 (2012).

[81] M. Blume, V. J. Emery, and R. B. Griffiths, "Ising Model for the λ Transition and Phase Separation in He^3-He^4 mixtures," Phys. Rev. A **4**, 1071–1077 (1971).

[82] M. Blume, "Theory of the First-Order Magnetic Phase Change in UO_2," Phys. Rev. **141**, 517–524 (1966).

[83] H. Capel, "On the possibility of first-order phase transitions in Ising systems of triplet ions with zero-field splitting," Physica **32**, 966 – 988 (1966).

[84] F. C. Alcaraz, J. R. Drugowich de Felício, R. Köberle, and J. F. Stilck, "Hamiltonian studies of the Blume-Emery-Griffiths model," Phys. Rev. B **32**, 7469–7475 (1985).

[85] A. Rahmani, X. Zhu, M. Franz, and I. Affleck, "Phase diagram of the interacting Majorana chain model," Phys. Rev. B **92**, 235123 (2015).

[86] A. Rahmani, X. Zhu, M. Franz, and I. Affleck, "Emergent supersymmetry from strongly interacting majorana zero modes," Physical review letters **115**, 166401 (2015).

[87] T. Grover, D. N. Sheng, and A. Vishwanath, "Emergent Space-Time Supersymmetry at the Boundary of a Topological Phase," Science **344**, 280–283 (2014), http://science.sciencemag.org/content/344/6181/280.full.pdf .

[88] P. Fendley, K. Schoutens, and J. de Boer, "Lattice Models with $\mathcal{N} = 2$ Supersymmetry," Phys. Rev. Lett. **90**, 120402 (2003).

[89] P. Fendley, B. Nienhuis, and K. Schoutens, "Lattice fermion models with supersymmetry," Journal of Physics A: Mathematical and General **36**, 12399–12424 (2003).

[90] L. Huijse, "Detailed analysis of the continuum limit of a supersymmetric lattice model in 1D," J. Stat. Mech. **1104**, P04004 (2011).

[91] B. Bauer, L. Huijse, E. Berg, M. Troyer, and K. Schoutens, "Supersymmetric multicritical point in a model of lattice fermions," Phys. Rev. B **87**, 165145 (2013).

[92] N. Sannomiya and H. Katsura, "Supersymmetry breaking and Nambu-Goldstone fermions in interacting Majorana chains," Phys. Rev. D **99**, 045002 (2019).

[93] D. A. Kastor, E. J. Martinec, and S. H. Shenker, "RG Flow in N=1 Discrete Series," Nucl. Phys. **B316**, 590–608 (1989).

[94] M. Lässig, G. Mussardo, and J. L. Cardy, "The scaling region of the tricritical Ising model in two dimensions," Nuclear Physics B **348**, 591 – 618 (1991).

[95] Z. Qiu, "Supersymmetry, two-dimensional critical phenomena and the tricritical Ising model," Nuclear Physics B **270**, 205 – 234 (1986).

[96] E. Witten, "Constraints on supersymmetry breaking," Nuclear Physics B **202**, 253 – 316 (1982).

[97] P. Fendley, "Free fermions in disguise," Journal of Physics A: Mathematical and Theoretical **52**, 335002 (2019).

[98] Y. A. Gol'fand and E. P. Likhtman, "Extension of the algebra of poincare group generators and violation of p invariance," JETP Letters **13**, 323 (1971).

[99] D. Volkov and V. Akulov, "Is the neutrino a goldstone particle?" Physics Letters B **46**, 109 – 110 (1973).

[100] J. Wess and B. Zumino, "Supergauge transformations in four dimensions," Nuclear Physics B **70**, 39 – 50 (1974).

[101] E. Gildener, "Gauge-symmetry hierarchies," Phys. Rev. D **14**, 1667–1672 (1976).

[102] S. Weinberg, "Implications of dynamical symmetry breaking," Phys. Rev. D **13**, 974–996 (1976).

[103] S. Dimopoulos and H. Georgi, "Softly broken supersymmetry and SU(5)," Nuclear Physics B **193**, 150 – 162 (1981).

[104] N. Sannomiya, H. Katsura, and Y. Nakayama, "Supersymmetry breaking and Nambu-Goldstone fermions in an extended Nicolai model," Phys. Rev. D **94**, 045014 (2016).

[105] H. Nicolai, "Supersymmetry and spin systems," Journal of Physics A: Mathematical and General **9**, 1497 (1976).

[106] N. Sannomiya, H. Katsura, and Y. Nakayama, "Supersymmetry breaking and Nambu-Goldstone fermions with cubic dispersion," Phys. Rev. D **95**, 065001 (2017).

[107] R. S. K. Mong, D. J. Clarke, J. Alicea, N. H. Lindner, and P. Fendley, "Parafermionic conformal field theory on the lattice," Journal of Physics A: Mathematical and Theoretical **47**, 452001 (2014).

[108] C. Li, E. Lantagne-Hurtubise, and M. Franz, "Supersymmetry in an interacting Majorana model on the kagome lattice," Phys. Rev. B **100**, 195146 (2019).

[109] A. Rahmani and M. Franz, "Interacting Majorana fermions," Reports on Progress in Physics **82**, 084501 (2019).

[110] C. Li and M. Franz, "Majorana-Hubbard model on the honeycomb lattice," Phys. Rev. B **98**, 115123 (2018).

[111] Y. Zou, A. Milsted, and G. Vidal, "Conformal Data and Renormalization Group Flow in Critical Quantum Spin Chains Using Periodic Uniform Matrix Product States," Phys. Rev. Lett. **121**, 230402 (2018).

[112] W. Li, S. Yang, H.-H. Tu, and M. Cheng, "Criticality in translation-invariant parafermion chains," Phys. Rev. B **91**, 115133 (2015).

[113] V. A. Fateev and A. B. Zamolodchikov, "Representations of the Algebra of 'Parafermion Currents' of Spin 4/3 in Two-dimensional Conformal Field Theory. Minimal Models and the Tricritical Potts $Z(3)$ Model," Theor. Math. Phys. **71**, 451–462 (1987), [Teor. Mat. Fiz. 71, 163 (1987)].

[114] V. A. Fateev and A. B. Zamolodchikov, "Conformal field theory and purely elastic S matrices," Int. J. Mod. Phys. **A5**, 1025–1048 (1990).

[115] H. J. de Vega and V. A. Fateev, "Factorizable S matrices from nonlocal Z(N) charges," J. Phys. **A25**, 2693–2710 (1992).

[116] R. J. Baxter and S. F. Edwards, "Critical antiferromagnetic square-lattice Potts model," Proceedings of the Royal Society. Series A, Mathematical and Physical Sciences (1982), 10.1098/rspa.1982.0119.

[117] H. Saleur, "The antiferromagnetic Potts model in two dimensions: Berker-Kadanoff phase, antiferromagnetic transition, and the role of Beraha numbers," Nuclear Physics B **360**, 219–263 (1991).

[118] G. Delfino, "Field theory of scaling lattice models. The Potts antiferromagnet," Statistical Field Theories. NATO SCIENCE SERIES II **73**, 3–12 (2002), arXiv:hep-th/01101811 .

[119] P. Lecheminant, A. O. Gogolin, and A. A. Nersesyan, "Criticality in self-dual sine-Gordon models," Nuclear Physics B **639**, 502 – 523 (2002).

[120] C. Hagendorf, "Spin Chains with Dynamical Lattice Supersymmetry," Journal of Statistical Physics **150**, 609–657 (2013).

[121] R. J. Baxter, *Exactly Solved Models in Statistical Mechanics* (Harcourt Brace Jovanovich, 1982).

[122] A. B. Zamolodchikov and V. A. Fateev, "Nonlocal (parafermion) currents in two-dimensional conformal quantum field theory and self-dual critical points in Z_n-symmetric statistical systems," Zh. Eksp. Teor. Fiz. **89**, 380–399 (1985).

[123] J. L. Cardy, "Operator content of two-dimensional conformally invariant theories," Nuclear Physics B **270**, 186 – 204 (1986).

[124] A. Cappelli, "Modular invariant partition functions of superconformal theories," Physics Letters B **185**, 82 – 88 (1987).

[125] J. L. Cardy, "Critical exponents of the chiral potts model from conformal field theory," Nuclear Physics B **389**, 577 – 586 (1993).

[126] N. Temperley and E. H. Lieb, "Relations between the 'Percolation' and 'Colouring' Problem and other Graph-Theoretical Problems Associated with Regular Planar Lattices: Some Exact Results for the 'Percolation' Problem," Proc. R. Soc. A. **322**, 251–280 (1971).

[127] Y. Ikhlef, J. L. Jacobsen, and H. Saleur, "A Temperley–Lieb quantum chain with two- and three-site interactions," Journal of Physics A: Mathematical and Theoretical **42**, 292002 (2009).

[128] A. Nichols, "The Temperley–Lieb algebra and its generalizations in the Potts and XXZ models," Journal of Statistical Mechanics: Theory and Experiment **2006**, P01003 (2006).

[129] L. Dolan and M. Grady, "Conserved charges from self-duality," Phys. Rev. D **25**, 1587–1604 (1982).

[130] B. Davies, "Onsager's algebra and superintegrability," Journal of Physics A: Mathematical and General **23**, 2245–2261 (1990).

[131] B. Davies, "Onsager's algebra and the Dolan–Grady condition in the non-self-dual case," Journal of Mathematical Physics **32**, 2945–2950 (1991), https://doi.org/10.1063/1.529036 .

[132] F. C. Alcaraz, M. N. Barber, M. T. Batchelor, R. Baxter, and G. Quispel, "Surface exponents of the quantum XXZ, Ashkin-Teller and Potts models," Journal of Physics A: mathematical and general **20**, 6397 (1987).

[133] H. Frahm, N.-C. Yu, and M. Fowler, "The integrable XXZ Heisenberg model with arbitrary spin: Construction of the Hamiltonian, the ground-state configuration and conformal properties," Nuclear Physics B **336**, 396 – 434 (1990).

[134] M. Batchelor and C. Yung, "q-deformations of quantum spin chains with exact valence-bond ground states," International Journal of Modern Physics B **08**, 3645–3654 (1994).

[135] B. Nienhuis, *in Phase Transitions and Critical Phenomena, vol. 11*, edited by C. Domb and J. L. Lebowitz (1987).

[136] A. W. W. Ludwig and J. L. Cardy, "Perturbative Evaluation of the Conformal Anomaly at New Critical Points with Applications to Random Systems," Nucl. Phys. **B285**, 687–718 (1987).

[137] A. B. Zamolodchikov and V. A. Fateev, "Model factorized S-matrix and an integrable Heisenberg chain with spin 1. (In Russian)," Sov. J. Nucl. Phys. **32**, 298–303 (1980), [Yad. Fiz. 32, 581 (1980)].

[138] B. Nienhuis, "Critical behavior of two-dimensional spin models and charge asymmetry in the Coulomb gas," J. Statist. Phys. **34**, 731–761 (1984).

[139] G. Schutz, "'Duality twisted' boundary conditions in n-state Potts models," Journal of Physics A: Mathematical and General **26**, 4555 (1993).

[140] F. C. Alcaraz and M. J. Martins, "Conformal anomaly for the exactly integrable SU(n) magnets," Journal of Physics A: Mathematical and General **22**, L865–L870 (1989).

[141] F. C. Alcaraz and M. J. Martins, "The spin-s XXZ quantum chain with general toroidal boundary conditions," Journal of Physics A: Mathematical and General **23**, 1439–1451 (1990).

[142] L. Dixon, P. Ginsparg, and J. Harvey, "$\hat{c} = 1$ superconformal field theory," Nuclear Physics B **306**, 470 – 496 (1988).

[143] P. Fendley, (2020), to appear.

[144] Z.-C. Gu and X.-G. Wen, "Tensor-entanglement-filtering renormalization approach and symmetry-protected topological order," Phys. Rev. B **80**, 155131 (2009).

[145] F. Pollmann, A. M. Turner, E. Berg, and M. Oshikawa, "Entanglement spectrum of a topological phase in one dimension," Phys. Rev. B **81**, 064439 (2010).

[146] X. Chen, Z.-C. Gu, and X.-G. Wen, "Classification of gapped symmetric phases in one-dimensional spin systems," Phys. Rev. B **83**, 035107 (2011).

[147] F. Pollmann, E. Berg, A. M. Turner, and M. Oshikawa, "Symmetry protection of topological phases in one-dimensional quantum spin systems," Phys. Rev. B **85**, 075125 (2012).

[148] I. Affleck, T. Kennedy, E. H. Lieb, and H. Tasaki, "Rigorous results on valence-bond ground states in antiferromagnets," Phys. Rev. Lett. **59**, 799–802 (1987).

[149] I. Affleck, T. Kennedy, E. H. Lieb, and H. Tasaki, "Valence bond ground states in isotropic quantum antiferromagnets," Comm. Math. Phys. **115**, 477–528 (1988).

[150] F. Verstraete, V. Murg, and J. Cirac, "Matrix product states, projected entangled pair states, and variational renormalization group methods for quantum spin systems," Advances in Physics **57**, 143–224 (2008).

[151] A. Klümper, A. Schadschneider, and J. Zittartz, "Matrix Product Ground States for One-Dimensional Spin-1 Quantum Antiferromagnets," Europhysics Letters (EPL) **24**, 293–297 (1993).

[152] D. P. Arovas, "Two exact excited states for the S = 1 AKLT chain," Physics Letters A **137**, 431 – 433 (1989).

[153] S. Moudgalya, S. Rachel, B. A. Bernevig, and N. Regnault, "Exact excited states of nonintegrable models," Phys. Rev. B **98**, 235155 (2018).

[154] S. Moudgalya, N. Regnault, and B. A. Bernevig, "Entanglement of exact excited states of Affleck-Kennedy-Lieb-Tasaki models: Exact results, many-body scars, and violation of the strong eigenstate thermalization hypothesis," Phys. Rev. B **98**, 235156 (2018).

[155] N. Shiraishi and T. Mori, "Systematic Construction of Counterexamples to the Eigenstate Thermalization Hypothesis," Phys. Rev. Lett. **119**, 030601 (2017).

[156] J. M. Deutsch, "Quantum statistical mechanics in a closed system," Phys. Rev. A **43**, 2046–2049 (1991).

[157] M. Srednicki, "Chaos and quantum thermalization," Phys. Rev. E **50**, 888–901 (1994).

[158] H. Bernien, S. Schwartz, A. Keesling, H. Levine, A. Omran, H. Pichler, S. Choi, A. S. Zibrov, M. Endres, M. Greiner, V. Vuletić, and M. D. Lukin, "Probing many-body dynamics on a 51-atom quantum simulator," Nature **551**, 579–584 (2017).

[159] P. Fendley, K. Sengupta, and S. Sachdev, "Competing density-wave orders in a one-dimensional hard-boson model'," Phys. Rev. B **69**, 075106 (2004).

[160] C. J. Turner, A. A. Michailidis, D. A. Abanin, M. Serbyn, and Z. Papić, "Weak ergodicity breaking from quantum many-body scars," Nature Physics **14**, 745–749 (2018).

[161] C. J. Turner, A. A. Michailidis, D. A. Abanin, M. Serbyn, and Z. Papić, "Quantum scarred eigenstates in a Rydberg atom chain: Entanglement, breakdown of thermalization, and stability to perturbations," Phys. Rev. B **98**, 155134 (2018).

[162] F. C. Alcaraz, M. N. Barber, and M. T. Batchelor, "Conformal invariance, the XXZ chain and the operator content of two-dimensional critical systems," Annals of Physics **182**, 280 – 343 (1988).

[163] J. L. Cardy, "Boundary conditions, fusion rules and the Verlinde formula," Nuclear Physics B **324**, 581 – 596 (1989).

[164] I. Affleck, M. Oshikawa, and H. Saleur, "Boundary critical phenomena in the three-state Potts model," Journal of Physics A: Mathematical and General **31**, 5827–5842 (1998).

[165] C. Lange, A. Klümper, and J. Zittartz, "Exact groundstates for antiferromagnetic spin-one chains with nearest and next-nearest neighbour interactions," Zeitschrift für Physik B Condensed Matter **96**, 267–270 (1994).

[166] S. Chattopadhyay, H. Pichler, M. D. Lukin, and W. W. Ho, "Quantum many-body scars from virtual entangled pairs," (2019), arXiv:1910.08101 .

[167] R. Jafari and A. Langari, "Second order quantum renormalisation group of XXZ chain with next-nearest neighbour interactions," Physica A: Statistical Mechanics and its Applications **364**, 213 – 222 (2006).